DESIGN CHEMISTRY FOR THE ENVIRONMENT: FROM PROCESSING FLUOROPOLYMERS IN SUPERCRITICAL CARBON DIOXIDE TO NEW NONBIOPERSISTENT FLUORINATED COATING MATERIALS

Ji Guo

A dissertation submitted to the faculty of the University of North Carolina at Chapel Hill in partial fulfillment of the requirements for the degree of Doctor of Philosophy in the Department of Chemistry

Chapel Hill
2006

Approved By

Advisor: Joseph M. DeSimone

Reader: Michael Rubinstein

Reader: Valerie S. Ashby

Reader: John M. Papanikolas

Reader: Paul Resnick

ABSTRACT

JI GUO: Designing Chemistry for the Environment: From Processing Fluoropolymers Solutions in Supercritical Carbon Dioxide to New Nonbiopersistent Fluorinated Coating Materials (Under the direction of Dr. Joseph M. DeSimone)

The solution properties of a fluorinated alkyl methacrylate, poly(1,1,2,2-tetrahydro perfluorooctyl methacrylate) (PFOMA) in carbon dioxide (CO_2) were studied by static and dynamic light scattering. The solvent quality of CO_2 was found to improve with increasing temperature and CO_2 density as exhibited by an increase of the second virial coefficient. Both the hydrodynamic radius expansion factor and the second virial coefficient of PFOMA solution were found to be functions of a single interaction parameter that can be independently changed by either temperature or density variations. Furthermore, we demonstrate that the relationship between two directly measurable quantities, the second virial coefficient and the hydrodynamic expansion ratio, is the same for both temperature-induced and CO_2 density-induced variations of solvent quality.

The degradation of coating materials that contain long perfluoro chains leads to the release of biopersistent perfluorooctanoic acid (PFOA) into the environment. In order to find environmentally friendly substitutes, a series of fluorinated alkyl methacrylate polymers containing the shorter and non-biopersistant perfluorobutyl group as the fluorinated component of the side chains are synthesized starting from perfuorobutyl iodide. Thermal properties of the polymers were characterized by thermogravimetric analysis (TGA) and differential scanning calorimetry (DSC). Static and dynamic contact angle measurements

were used to quantify the surface properties of the thin films for these new non-biopersistant materials (C4 materials). The surface construction, especial the orientation of the fluorinated side chains, were recorded by near edge X-ray fine absorption structure (NEXAFS) experiments. In all, C4 materials displayed the hydrophobic and oleophobic properties with low surfaces tensions and their wetting properties were tuned by varying the "spacer" structures between the backbones and the perfluorinated groups of the side chains.

DEDICATION

To my parents, Tianlu Guo and Sanziang Tu, for love and support

ACKNOWLEDGEMENTS

I would love to express my gratitude to all the people who support and love me during my whole graduate study. I sincerely thank my research advisor, Prof. Joseph M. DeSimone for invaluable guidance and constant encouragement. I especially grateful to him who provided me such an amazing free and open atmosphere and great opportunities to work on exciting projects. I have learned immensely from him in the past four years and enjoyed being a part of DeSimone Group.

I thank my Prof. Rubinstein for his time and guidance, especially fro his extra patience. I thank Dr. Paul Resnick who gave me a significant amount of valuable advice and guidance. I also thank my graduate committee for their guidance and time.

I would like to extend my appreciation to all the members of DeSimone groups. It is a precious experience for me to wok work with such intelligent and great people. Especially I would thank Dr. Pascal Andre, Dr. Zhilian Zhou and Jennifer Kelly for all the help and great time we shared. I thank Prof. Genzer and his groups for his kind help in work of NEXAFS experiments. I thank Sherryl Yu for her help in AFM measurements. I would also like to thank Dr. Colin Wood, Dr. Libin Du, Dr. Jason Rolland, Dr. Panyukov, Zhangkang Hu and rest of all my friends at Chapel Hill for help and friendship.

I would like to thank my family for their endless love and support: my mom and dad and my little sister and her husband, especially to a lovely angle of our hearts, baby Hanzhang Lu.

TABLE OF CONTENTS

Page

LIST OF TABLES

LIST OF FIGURES

LIST OF ABBREVIATIONS AND SYMBOLS

AFM	atomic force microscopy
AIBN	2,2'-azobis(isobutyronitrile)
DCP	disease control and prevention
DLS	dynamic light scattering
DSC	differential scanning calorimetry
EGB	entrance grid bias
EPA	environmental protective agency
FOMA	1,1,2,2-tetrahydroperfluorooctyl methacrylate
FY	fluorescence yield
IR	infrared spectroscopy
NEXAFS	near edgy X-ray absorption fine structure
NMR	nuclear magnetic resonance
PFOA(C8)	perfluorooctanoic acid
PCMA	poly(cyano methyl acrylate)
PDMS	polysiloxane
PEEK	poly(ether ether ketone)
PEM	polymer electrolyte membrane or proton exchange membrane
PEY	partial-electron-yield
PFOA	poly(1,1-dihydroperfluorooctyl acrylate)
PFOMA	poly(1,1,2,2-tetrahydroperfluorooctyl methacrylate)
PFOS	perfluorooctyl sulfonates
PFPE	perfluoropolyether
PMMA	poly(methayl methacrylate)
PS	polystyrene

PTFE	poly(tetrafluoroethylene)
SAXS	small angle x-ray scattering
SANS	small angle neutron scattering
$scCO_2$	ssupercritical carbon dioxide
SLS	static light scattering
SPI	sulfonated copolyimide
sPFPE	styrenically functionalized perfluoropolyether
SS	sulfonated styrenic monomer
SSA	styrene sulfonic acid
SSE	styrene sulfonate ester
TFE	tetrafluoroethylene
Tg	glass transition temperature
TFT	trifluorotoluene
TGA	thermogravimetric analyzer
UCST	upper critical solution temperature
UV	ultraviolet chromatography

PART I

POLYMER SOLUTIONS IN SUPERCRITICAL CARBON DIOXIDE

I-1 Introduction

I-1.1 Carbon dioxide

Supercritical carbon dioxide ($scCO_2$) has been touted as an environmental friendly medium for polymerizations and processing. It possesses an easily accessible critical point[1] (critical temperature, T_c = 31.1°C and critical pressure, p_c = 73.8 bar). Advantages of $scCO_2$ include gas-like diffusivity, liquid-like density and low viscosity.[2] In addition, small variations in temperature (T) or density (ρ) result in dramatic changes in solvent quality of supercritical CO_2, which makes it an unusually tunable, versatile, and selective solvent.[3] Polymer synthesis and processing in this "green" solvent have created new opportunities in manufacturing[1,4-8] such as spin-coating, spray coating, separations and complexation of organic acids and heavy metals in CO_2.[9-17] DuPont has commercialized the manufacturing of polytetrafluoroethylene (PTFE) in CO_2 to replace 1,1,2-trichloro-1,2,2-trifluoroethane or an aqueous emulsion system, which was comprised of a biopersistent fluorinated surfactants.[1] Although studies for $scCO_2$ systems have emerged over last past four decades, significant challenges still remain which require a better understanding of the underlying physical and chemical prosperities of polymer solutions in $scCO_2$.

I-1.2 Characterization of solvent quality

Solubility plays a very important role for polymer synthesis and processing in different solvent systems. Most nonpolar and some polar small molecules are soluble in CO_2, however, it is still a poor solvent for most high molecular weight polymers under mild conditions, the exception being amphous fluoropolymers and silicone-based materials.[1-3,18,19] To date, many studies have addressed the mechanism of solubility of polymers in $scCO_2$. Some factors have

been identified to be important such as the specific solute-solvent interactions, solute-solute interactions, van der Waals interactions, Lewis acid-base interactions, the free volume and cohesive energy density of the polymer, and so forth. [20-24] Other studies have attributed the nature of the interactions between polymers and solvents to a large quadrupole moment of CO_2.[25] Infrared Spectroscopy (IR) data of CO_2 polymer solutions suggested that the specific interactions between CO_2 and the polar fluorine containing groups, as CO_2 behaves as a weak electron acceptor.[20]

Various experimental techniques have been used to characterize solvent quality for CO_2 such as scattering, UV and IR spectroscopy, viscometry, NMR and etc.[26-31] The most commonly used method to characterize polymer solubility in a supercritical fluid is to perform phase equilibrium measurements to determine cloud point data as a function of temperature or density at a given polymer concentration.[32] The typical phase diagram for a polymer solution (UCST, upper critical solution temperature) in an organic system is shown in Figure 1.1A.[33] The solvent quality varies with temperature, which is also displayed in terms of the interaction parameter (χ) or the excluded volume (v). However, the phase diagram for liquid or supercritical CO_2 is more complicated and solubility is related to not only temperature but also density (or pressure). Therefore, the cloud point curve represents the temperature or pressure when the system first appears cloudy due to phase separation or aggregation. Examples of cloud point were shown in Figure 1.1B, which the solubility of the fluorinated polymers increased with increasing temperature and CO_2 denstiy.[24] O'Neil and coworkers managed to survey the solubility of many homopolymers and copolymers in CO_2 by cloud point measurements.[24] The solubility of amorphous polymers was found to increase with a decrease in surface tension and was found to be governed by polymer-polymer

interactions. For copolymers, the cloud-point temperatures were functions of the length of both hydrophobic and hydrophilic blocks.[34,35] Cloud point data was also collected on 130 commercial surfactants in CO_2.[36] The critical emulsion concentrations of water emulsions in $scCO_2$ can be observed for the system that was optically transparent and thermodynamically stable.[37,38] In general, cloud point measurements give the information about the kinetic solubility of a polymer over a specified range of temperature, pressure and concentration. However, the accuracy given by cloud point experiments is limited and the results can not supply information such as interaction strength, size and solvent quality variations. In addition, for polydisperse polymers, the cloud point is only an approximate measure of solubility.

Scattering is one of the most powerful methods for the study of polymer solutions. It is a non-invasive and is an absolute method for characterizing macromolecules in solution. The different wave length of radiation source used includes light, X-rays or Neutrons, which dictates the different ranges of the length scale on can observe. The scattering of a solution arises from the contrast between the scattering from solute and solvent background. And for light scattering, the contrast strength is determined by the difference in refractive indices between solute and solvent.[39-41] Important parameters such as radius of gyration (R_g) and second virial coefficient (A_2) can be obtained by static light scattering. According to the lattice fluid theory, three primary factors affect the solubility of amorphous polymers in CO_2: solute-solute interactions, solute-solvent interactions, and solvent-solvent interactions. A_2 reflects the net interaction between two polymer chains which includes the relative strength of all three interactions. Hence, the phase diagrams of polymer solution are classified as good ($A_2 > 0$), theta (θ) ($A_2 = 0$) and poor ($A_2 < 0$) solvent region. Dynamic light scattering can

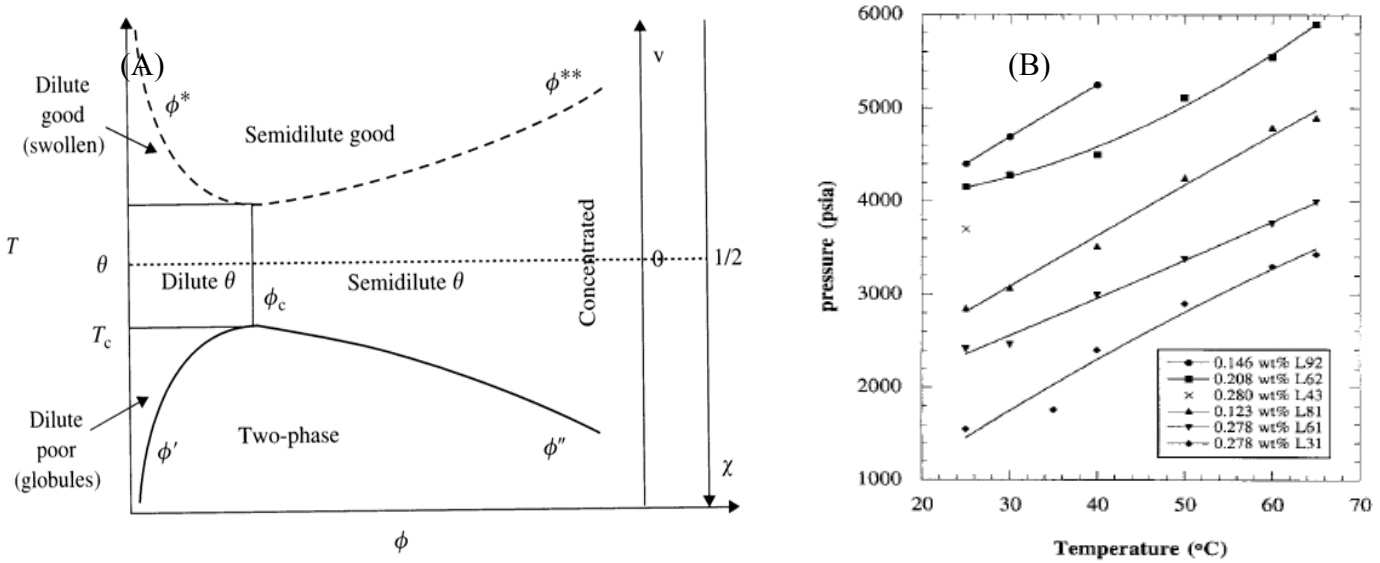

Figure 1.1 Phase diagram for polymer solutions with an upper critical solution temperature (USTC) in (A) organic solvent[33] and (B) in CO_2.[24]

provide information on the diffusion coefficient [42] (including thermodynamic and hydrodynamic contributions), the hydrodynamic radius (R_h) and particle size distribution in terms of R_h.

Numerous studies have been reported on phase behavior, aggregation phenomena and assessment of solvent quality in CO_2 by means of small angle neutron (SANS) and X-ray scattering (SAXS).[28,43] From SANS experiments, the solvent quality of CO_2 was found to increase with temperature and density.[44] The observation of aggregation and micro-emulsion of water in CO_2 formed by phosphorus fluorosurfactants displayed rapid exchange of water between the bulk CO_2 and the microemulsion droplets.[45,46] Compared to SANS and SAXS, light scattering is more available in academic and industrial labs, yet only a few of studies on solvent quality have been carried out for $scCO_2$ systems.[47,48] The low contrast between solute and solvent background make it difficult for utilizing light scattering in supercritical solvents system, along with the need for a more intricate experimental setup involving in high pressure. Only recently has high pressure light scattering been applied in quantitative measurements of polymer solution behavior in carbon dioxide, especially for micelles and copolymer systems,[41,44,47,49-61] One example is the observation of micellization transition introduced by CO_2-density through light scattering.[40,47]

I-1.3 Theory background

The investigation for physical and chemical properties of polymers has been mainly accomplished in solution.[62-64] In fact, thermodynamic and conformational properties related to polymer solutions have been the major emphasis for a long time.[64-66] In 1966, Berry[67] experimentally confirmed with polystyrene that the positive second virial coefficient A_2 is

simply related to three parameters: the unperturbed state in which the conformation of a chain molecule is described by random walk statistics, the number of Kuhn segments, and the excluded volume for any pair of segments. The second virial coefficient, A_2, is expressed as a universal function of the interaction parameter z, assuming that: (1) z is a simple function of temperature; (2) the Kuhn length b is independent of solvent and molecular weight; and (3) there is no end-group effect. This concept is also confirmed with Monte Carlo methods.[68-70] The simulation data was found to collapse onto the experimental data without the use of additional adjustable parameters with various chain lengths and segment-segment interactions.

Yamakawa et al. reported a quasi-two-parameter (QTP) scheme wherein the radius of gyration expansion factor α_g[71-74] and viscosity-radius expansion factor α_s,[75-78] can be expressed as functions only of the scaled interaction parameter z (related to exclude-volume) defined by Yamakawa-Stockmayer-Shimada (YSS) theory.[79-81] The hydrodynamic radius expansion factor α_H was approximated by a linear function of the interaction parameter z in near θ region.[82,83] As a consequence, this model is expected to apply to all uncharged linear polymers in theta and good solvents.

The interaction parameter z described above was found to be only dependent on temperature in organic solvent systems. Though important thermodynamic variables of polymer solution systems include composition, temperature[68,69,84-87] and pressure[88-91], the solvent density is usually kept constant and the effects of pressure are typically deemed to be trivial. Schulz and Lechner[89] pioneered the scattering studies of the effects of pressure on polymer solutions using a high pressure optical cell. Most of the studies of interactions in polymer solutions were accomplished using either static light scattering (SLS)[39,85,92,93] or

small angle neutron scattering (SANS)[94] in traditional organic solvents with external pressure. The correlation between radius of gyration (R_g) and second virial coefficient (A_2) showed that pressure influenced these quantities through its effects on the polymer-solvent interaction. At a high temperature, A_2 and R_g should increase with temperature, while they should decrease with pressure.[93] This can be easily understood since the free volume contribution was dominant at higher temperature, considering the minor density changes of organic solvent. However, in the case of $scCO_2$, small temperature or pressure variations can result in dramatic changes of solvent quality, since the solvent density is tunable during the process.

A few of studies have focused on the interaction parameter in compressed CO_2 systems. Scattering has been used to investigate the solubility of polysiloxanes (PDMS),[47-48] and fluoropolymers such as poly(hexafluoropropylene oxide)[95] and poly(1,1-dihydroperfluorooctyl acrylate) (PFOA) in CO_2.[44,47,50,96] PDMS was found to be soluble on the molecular level only in the limit of dilute solution and seems to form aggregates as the concentration increases.[50] In the PDMS- CO_2 solution, the strength of the interactions was found to be weak and no universal behavior was observed in the poor solvent region with negative A_2 values.[48] However, PFOA exhibited a good solubility in CO_2 and possessed a positive second virial coefficient under the experiment conditions.[47] Hence, an analog linear fluorinated polymer to PFOA was chosen herein as the solute to investigate the solvent quality of CO_2.

I-1.3.1 Length scale of investigation

The length scale of light scattering is determined by the inverse of the scattering wave factor q, which is given by

$$q = \frac{4\pi n_s}{\lambda}\sin(\Theta/2) \tag{1.1}$$

where n_s is the refractive index of the solvent, λ is the wavelength of the light in a vacuum and Θ is the scattering angle.[97] The length scale is a function of scattering angles. The scattering angle Θ in our work is not equal to the external detection angle for the non-cylindrical samples holders. The scattered light does not exit the sample holder at 90^o to the window, and internal scattering angles need to be calculated considering the refractions of light at interfaces between CO_2 and the sapphire window and between the sapphire window and air (Figure 1.2).

$$\pi = (\alpha_1 + \psi) + \frac{\pi}{2} + \theta_1 \tag{1.2}$$

$$\theta_1 = \left(\frac{\pi}{2} - \psi\right) - \mathrm{a}\sin\left[\frac{\mathrm{n}_3}{\mathrm{n}_1}\sin\left(\frac{\pi}{2} - \psi - \theta_3\right)\right] \tag{1.3}$$

where ψ is the angle of the sapphire window relative to perpendicular (to the sapphire window) with respective to the laser beam and equal to $\pm\ 45^o$ and 0^o. n_1, n_2 and n_3 are refractive index of CO_2 solutions, sapphire window and air, respectively. θ_1 and θ_3 are internal and external scattering angles, respectively. α_1 and α_3 are the angles of refraction of the light on the surfaces of the sapphire windows.

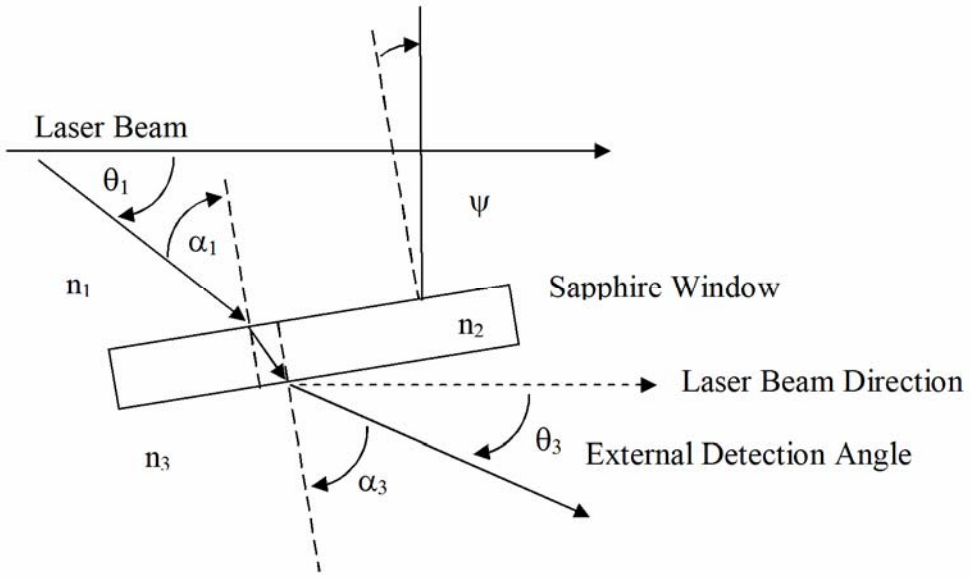

Figure 1.2 Scheme of internal detection angle and external detection angle

I-1.3.2 Static light scattering

Static light scattering experiments measure the relative excess of scattering intensity with respect to the solvent $I(q,c)$ at a scattering wavevector q and a given polymer concentration c for various polymer concentrations. The intensity of the scattered light is measured as a function of angle. For the case of macromolecules, this is often called Rayleigh scattering and can yield the molar mass (M_w), radius of gyration (R_h), and second virial coefficient (A_2). For certain classes of particles, static light scattering can yield the size, shape, and structure. For a polymer solution in CO_2, scattering $I(q,c)$ can expressed as

$$I(q,c) = (I_s - I_{CO_2}) / I_{CO_2} \tag{1.4}$$

where the I_s and I_{CO_2} are the scattering from the polymer solution and from CO_2, respectively. The scattering data were converted into the excess Rayleigh's ratio, Rc, using the following equation[98]

$$R(q,c) = I(q,c)R_\theta^{CO_2} = I(q,c)R_\theta^{toluene} I_{CO_2} / I_{toluene} \tag{1.5}$$

By measuring the scattering intensity of pure CO_2 at different densities, the Rayleigh ratio of CO_2 could be calculated using toluene as the standard. The Rayleigh ratio of toluene is $R_\theta^{toluene} = 3.21\times10^{-5}$ cm^{-1} at 25°C for λ = 514 nm. Rayleigh ratios of CO_2 ($R_\theta^{CO_2}$) at 25°C with different CO_2 density are listed in Table 1.1.

In a dilute polymer solution, this dependence is expressed as[98]

$$\frac{Kc}{R(q,c=0)} = \frac{1}{M_w}(1 + \frac{1}{3}R_g^2 q^2 ...) \tag{1.6}$$

$$\frac{Kc}{R(q=0,c)} = \frac{1}{M_w}(1 + 2M_w A_2 c...) \tag{1.7}$$

Here A_2 is the second virial coefficient, R_g is the z-average radius of gyration and M_w is the

weight average molecular weight. The optical constant K is defined by[98]

$$K = \frac{4\pi^2 n_s^2}{\lambda^4 N_{av}} \left(\frac{dn}{dc} \right)^2 \tag{1.8}$$

where N_{av} is the Avogadro's number.

Table 1.1 The Rayleigh ratios $R_\theta^{CO_2}$ of CO_2 at scattering angle 90° for different CO_2 densities at 25 °C.

CO_2 Density (g/mL)	0.86	0.89	0.93	0.97	1.01
$R_\theta^{CO_2} \times 10^5$ (cm^{-1})	3.87	3.37	2.75	2.26	1.97

I-1.1.3 Dynamic light scattering

In a dynamic light scattering measurement, the time-dependent fluctuations in the scattered light are measured by a fast photon counter. The fluctuations are directly related to the rate of diffusion of the molecule through the solvent. Therefore, the fluctuations can be analyzed to determine a hydrodynamic radius for the sample. Dynamic light scattering (DLS) measures the autocorrelation function $g^{(2)}(q,t)$ of the scattering intensity[98], and $g^{(2)}(q,t)$ was fitted to a single exponential decay with decay time inversely proportional to q^2.

$$g^{(2)}(q,t) = 1 + \left| A\, exp(-t/\tau) \right|^2 \quad \textbf{(1.9)}$$

where A is an instrument constant. The autocorrelation function depends on how molecules move and rearrange on the length scale $1/q$ during time t. τ is the correlation time and also depends on q.

$$\tau = \frac{1}{Dq^2} \quad (1.10)$$

where D is the diffusion coefficient. For dilute solutions, the concentration dependence of the diffusion coefficient $D(c)$ can be approximated as[84]

$$D(c) = D_0\,(1 + k_D c) \quad (1.11)$$

where k_D is the diffusional second virial coefficient and D_0 is the diffusion coefficient at infinite dilution. The diffusion coefficient can be related to the hydrodynamic radius R_h of a diffusing sphere via the Stokes-Einstein equation

$$D_0 = \frac{k_B T}{6\pi \eta_s R_h} \quad (1.12)$$

where η_s is the solvent viscosity, k_B is the Boltzmann constant, T is the absolute temperature and R_h is the hydrodynamic radius. Equation 1.12 was used to calculate hydrodynamic radius

R_h from the diffusion coefficient D_0 obtained by extrapolation of $D(c)$ (Equation 1.11) to infinite dilution ($c \rightarrow 0$).

I-1.3.4 Interaction parameter

The second virial coefficient of polymers dissolved in organic solvents can be collapsed onto a single curve without any adjustable parameters as was first demonstrated by Berry for polystyrene solutions.[67] In a good solvent and in a θ-region,[33] $A_2 M_w^{1/2}$ is only a function of chain interaction parameter, z.

$$A_2 M_w^{1/2} \frac{M_0^{3/2}}{N_{av} b^3} = f(z) \approx C^{A_2} \begin{cases} z & \text{for} \quad |z| < 1 \quad (\theta \quad \text{region}) \\ z^{0.528} & \text{for} \quad z > 1 \quad (\text{good} \quad \text{solvent}) \end{cases} \tag{1.13}$$

where C^{A_2} is a numerical coefficient. Kuhn segment mass, M_s, and length, b, are defined through the equivalent freely jointed chain model.[33]

$$b = \frac{6 R_{g\theta}^2}{\ell} \frac{m_s}{M_w} \tag{1.14}$$

$$M_s = 6 \left(\frac{R_{g\theta} m_s}{\ell} \right)^2 \frac{1}{M_w} \tag{1.15}$$

where m_s is the molar mass of the monomer, $R_{g\theta}$ is the radius of gyration at θ condition and the contour length of the monomer is $\ell = 2 \times 1.54 \text{ Å} \times \sin(68^\circ) = 2.6 \text{ Å}$. The length b and the mass M_s of the Kuhn segment for PFOMA, polystyrene (PS)[67] and poly(methyl methacrylate) (PMMA)[62] are listed in Table 1.2.

The interaction parameter z at constant solvent density can be expressed in terms of the reduced temperature (see direction (1) in Figure 1.3),

Table 1.2 The mass of Kuhn segment M_s and Kuhn length b of PFOMA, PMMA[62] and PS.[67]

Polymer	M_s (Dalton)	b (nm)
PFOMA	6300	3.0
PMMA	666	1.7
PS	728	1.8

$$z = C_T N^{1/2} \frac{T - \theta(\rho)}{T} \qquad (\rho = \text{const}) \tag{1.16}$$

where C_T is a numerical coefficient related to the temperature dependence of interaction parameter *z*, and *N* is the number of Kuhn segments $N = M_w / M_0$.

Similarly, the interaction parameter z at constant temperature can be expressed in terms of the reduced density (see direction (2) in Figure 1.3).

$$z = C_\rho N^{1/2} \frac{\rho - \rho_\theta(T)}{\rho} \qquad (T = \text{const}) \tag{1.17}$$

where C_ρ is a numerical coefficient related to the density dependence of the interaction parameter *z*. In the Discussion section, we present a theoretical analysis of the temperature and density dependencies of the second virial coefficient in supercritical solvents and derive the temperature dependence of the theta density $\rho_\theta(T)$. Numerical coefficients C^{A_2}, C_T and C_ρ can depend on chemical structure of polymer. For a particular polymer-solvent pair, these coefficients should be independent of molecular weight and we will demonstrate in later discussions that C_T and C_ρ are equal to each other for PFOMA in CO_2.

In the near θ region, the second virial coefficient is linearly proportional to the interaction parameter *z* (see Equation 1.13 with Equation 1.16 for temperature variations and Equations 1.17 for density variations).

$$A_2 M_w^{1/2} \frac{M_\theta^{3/2}}{N_{av} b^3} = C^{A_2} z = \begin{cases} C_T^{A_2} N^{1/2} \left[1 - \dfrac{\theta(\rho)}{T} \right] & \text{for temperature variations} \quad (C_T^{A_2} = C^{A_2} C_T) \\ C_\rho^{A_2} N^{1/2} \left[1 - \dfrac{\rho_\theta(T)}{\rho} \right] & \text{for density variations} \quad (C_\rho^{A_2} = C^{A_2} C_\rho) \end{cases} \tag{1.18}$$

The hydrodynamic radius expansion factor α_h is defined as the ratio of hydrodynamic radius R_h at a given condition to the hydrodynamic radius at the θ condition, $R_h(\theta)$. This

expansion ratio α_h, describing the swelling of the chain, is also a function of a single interaction parameter z,[84, 99] (related to the excluded volume interactions). The hydrodynamic radius expansion factor α_h can be approximated in θ region by a linear function of the interaction parameter z.[83]

$$\alpha_h = 1 + C^R z = \begin{cases} 1 + C_T^R N^{1/2}\left[1 - \dfrac{\theta(\rho)}{T}\right] & \text{for temperature variations} \quad (C_T^R = C^R C_T) \\ 1 + C_\rho^R N^{1/2}\left[1 - \dfrac{\rho_\theta(T)}{\rho}\right] & \text{for density variations} \quad (C_\rho^R = C^R C_\rho) \end{cases} \tag{1.19}$$

where C^R is a numerical coefficient. Furthermore, the existence of a single interaction parameter for both temperature and density variations implies that these coefficients are not independent, but are related to each other by

$$\frac{C_T^R}{C_T^{A_2}} = \frac{C^R}{C^{A_2}} = \frac{C_\rho^R}{C_\rho^{A_2}} \tag{1.20}$$

as can be deduced from Equations 2.18 and 2.19.

I-2 Objective and overview

In this chapter we present the measurements of the molecular weights and sizes of fractionated polymer samples, using high pressure static and dynamic light scattering. The focus of this work was to construct functions of a single interaction parameter which enable one to quantitatively predict the strength of interactions and sizes of a fluorinated poly(alkyl methacrylate) (PFOMA) in CO_2 with the change of temperature or solvent density for different molecular weights. We will also discuss in the influence of solvent density and temperature on the solution properties of PFOMA in CO_2. The solvent quality is tuned using two different approaches as shown in Figure 1.3: (1) by varying the temperature at a constant CO_2 density; (2) by changing CO_2 density at a constant temperature. We demonstrate that

both the second virial coefficient and the hydrodynamic radius expansion coefficient can be expressed as functions of a single interaction parameter z that varies with temperature (T) at constant CO_2 density (ρ) as $N^{1/2}[1-\theta(\rho)/T]$ and with CO_2 density at constant temperature as $N^{1/2}[1-\rho_\theta(T)/\rho]$, where $\theta(\rho)$ is the theta temperature for given density ρ, ρ_0 is the theta density (the CO_2 density at the theta condition) and N is the number of Kuhn segments of the polymer chains. The relationship between the second virial coefficient (A_2) and the hydrodynamic radius expansion factor (α_h) was found to follow the same behavior (independent of directions in Figure 1.3). Therefore, we verified that two different ways of varying the interaction parameter z (directions (1) and (2) in Figure 1.3) are directly related and found that θ-temperature varies reciprocally proportional to CO_2 density $\theta(\rho) = (260/\rho)(KmL/g)$, while θ-density varies reciprocally proportional to the absolute temperature $\rho_\theta(T) = (260/T)(gK/mL)$. Thus we have confirmed the existence of a single interaction parameter that combines the temperature, the solvent density, and the degree of polymerization into a single variable.

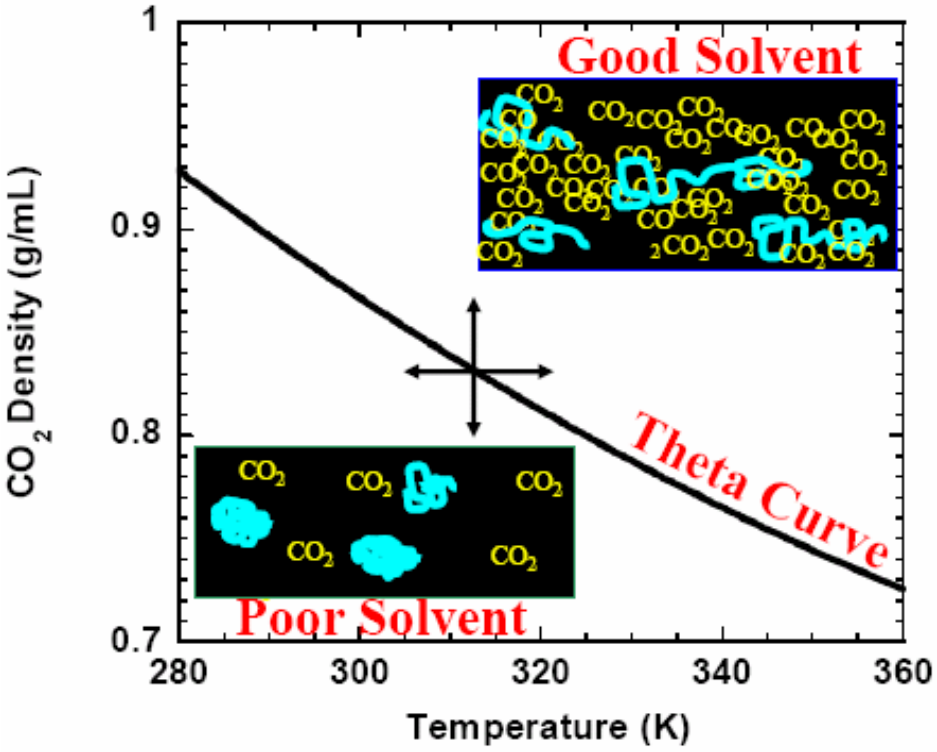

Figure 1.3 Phase diagram of PFOMA in CO_2.

I-3 Experimental

I-3.1 Polymer preparation

The monomer 1,1,2,2-tetrahydroperfluorooctyl methacrylate (FOMA) (provided by DuPont) was purified and deinhibited by passing it through an alumina column. The initiator 2,2'-azobis(isobutyronitrile) (AIBN, Kodak, 99%) was recrystallized twice in methanol (Aldrich). All purification solvents were purchased from Aldrich and used as received. FOMA monomers were purged with Argon for approximately 15 minutes prior to transferring into a 25 mL high pressure view cell containing AIBN (0.5-1 wt %) and a magnetic stirring bar. The contents of the high pressure cell were purged with Argon for additional 15 minutes and then the reaction cell was heated to 60 ^{o}C while CO_2 was added via syringe pump (Isco) over ca. 15 minutes of time to a pressure of 345 bar. The polymerization was continued for 24 h at 60 ^{o}C and 345 bar. The resulting polymer and any unreacted monomer were removed from the reaction cell by dissolving all of the contents in 1,1,2-trifluorothrichoroethane. The polymer was precipitated into a large excess of methanol, isolated by suction filtration, washed several times with methanol and dried in a vacuum oven overnight under reduced pressure.

I-3.2 Fractionation

The isolated poly(1,1,2,2-tetrahydro perfluorooctyl methacrylate) (PFOMA) was fractionated to reduce the polydispersity of samples for the later light scattering analysis. The scheme of the fractionation setup was shown displayed in Figure 1.5. Under isothermal conditions, the polymer was fractionated by applying an increasing CO_2 pressure profile.[3]

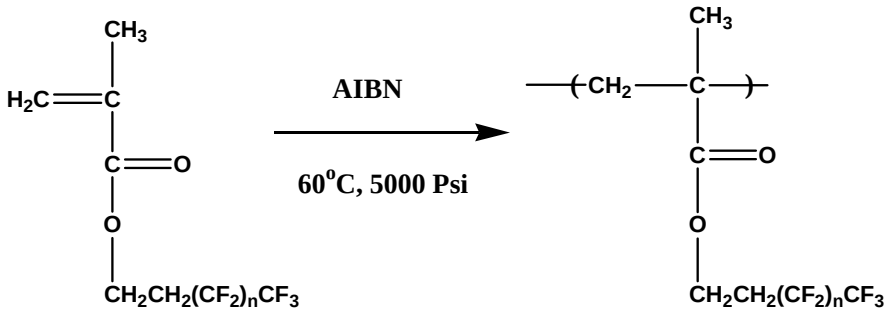

Figure 1.4 The synthesis process of PFOMA with n = 6 (35%), 8 (30%), 10 (17%).

The fractionation temperature was 60 ^{o}C and the pressure was increased from 106 bar to 414 bar with a step interval of 14 bar. A total of 13 fractions were isolated at different CO_2 densities. Each fraction was 1.5 to 2 grams in mass and was numbered consecutively from 1 to 13. Fractions 2 and 8 were used to measure the refractive index and fractions 3 and 6 were used to do all other measurements.

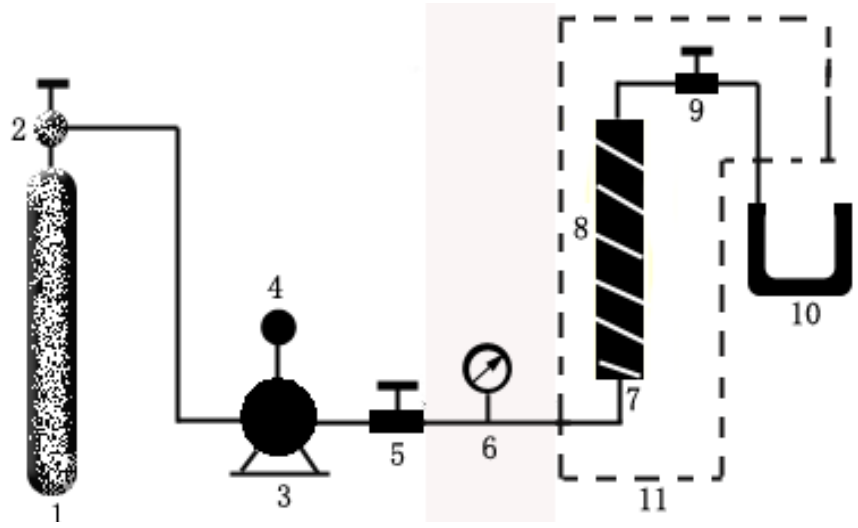

Figure 1.5 Supercritical CO_2 Fractionation system: (1) CO_2 cylinder; (2) Cylinder valve; (3) High pressure compressor (Dual isco pump); (4) Pressure controller; (5&9) High pressure on/off valve; (6) Pressure gauge; (7) Separation column; (8) Heating tape; (10) Glass U-tube; (11) Thermal control area.

I-3.3 Cloud point and phase curve

The specific solubility of polymers in compressed CO_2 is usually determined by cloud point measurements. Cloud point curves are typically represented by a plot of pressure versus temperature for a certain polymer concentration and are measured in a variable volume high pressure optical cell (Figure 1.6). In order to determine the working range of light scattering experiments, cloud point curve and phase curve for PFOMA have been measured with variations of both temperature and density.

The optical cell was sealed with certain amount of polymer, a stir bar and then filled with CO_2 (as low pressure as 12 to 14 bars). After heating to the desired temperature 60 ^{o}C, the optical cell was pressurized until the transparent polymer solution was observed. The initial temperature and pressure was used to calculate the CO_2 density inside the cell. When the temperature decreased, the volume of the cell was reduced or increased to observe the polymer solutions passing through the cloud point. The pressure at which the polymer began to precipitate was recorded as the cloud point pressure. The cloud point curve of PFOMA (fraction 8) is displayed in Figure 1.7, and the lowest density at 25 ^{o}C for one-phase region is 120 bar (1700 psi).

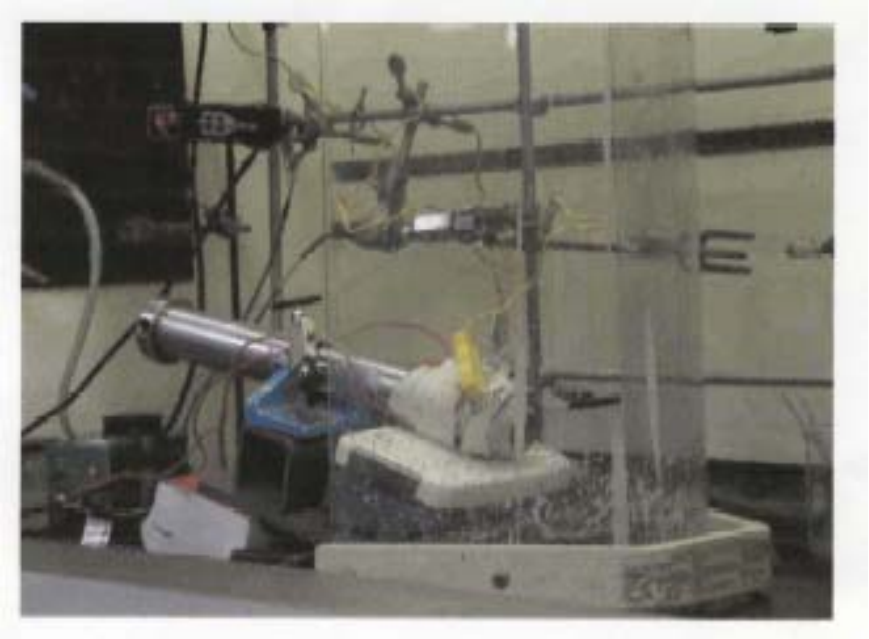

Figure 1.6 High pressure apparatus for cloud point measurement in CO_2

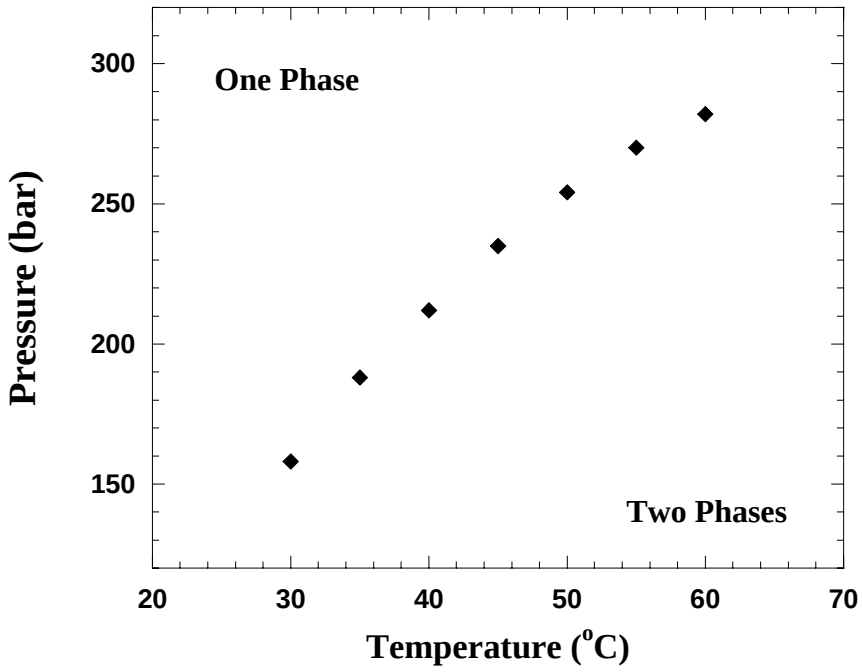

Figure 1.7 Cloud point curve of PFOMA in CO_2

I-3.4 Refractive index increment

The refractive index increment (d*n*/d*c*) quantifies how the refractive index of the polymer solution changes with polymer concentration. For traditional solvents, d*n*/d*c* is measured with a differential refractometer and the values for many systems are available in the literature.[100] The values of d*n*/d*c* for most polymers in CO_2, however, are unknown and needed to be measured directly in order to determine the molecular weights of the various PFOMA fractions.

The apparatus shown in Figure 1.8 was used to determine the refractive index of CO_2 and dn/dc for PFOMA in CO_2. A 2.5 mL cylindrical stainless steel cell with 1.0 cm thick sapphire windows on both ends was used as the sample holder and reaction vessel. The total volume (3.4 mL) of the apparatus included the volume of the pressure transducer and the high pressure tubing, without the volume of the prism and the stirring bar. The prism was made of BK7 glass (Sinocera Photonics) and had a refractive index of 1.52. The known distance, d (from the face of the sapphire window of the cell to the wall) was measured to be 3.8 m. The temperature of the cell was monitored by a thermocouple and adjusted with the use of a heating tape. The experiments were performed at 25°C with pressure varying from 131 to 414 bar. The deviation of an incident HeNe laser beam (λ = 633 nm) with the refractive index of the solution surrounding an equilateral prism in the high pressure cell determined the values of dn/dc for PFOMA in carbon dioxide.

The refractive index of the solution can be expressed as a function of n_{prism}, n_{air}, and θ_{out}.

$$n_{\text{solution}} \times \sin\left(\left\{\frac{n_{\text{prism}}}{n_{\text{solution}}}\sin\left[60^\circ - \sin^{-1}\left(\frac{n_{\text{solution}}}{n_{\text{prism}}}\sin 30^\circ\right)\right]\right\} - 30^\circ\right) = n_{\text{air}} \times \sin\theta_{out} \qquad (1.21)$$

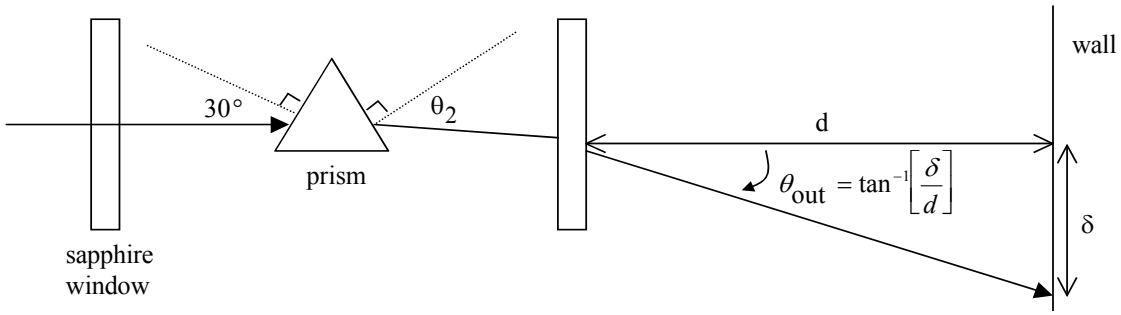

Figure 1.8 Overall schematic of the d*n*/d*c* setup

where the optical index of the prism (n_{prism}) = 1.52 and n_{air} = 1. Measuring the distance d from the cell to the wall and the distance δ between the spots on the wall due to the non-refracted and refracted beams allowed us to calculate the angle θ_{out} (Figure 1.8). The refractive index of the solution $n_{solution}$ was then calculated using the experimentally measured angle θ_{out} using an iterative procedure.

The efficiency and accuracy of the dn/dc apparatus (Figure 1.8) were testified first by measuring the refractive index of pure CO_2. The values of refractive index of carbon dioxide were reported in the literature[97] as following.

$$(n-1)d^{-1} = A_n + dB_n \tag{1.22}$$

where d is the molar density of compressed solvent at a given temperature and pressure.

$$A_n = \frac{3}{2} A_r \tag{1.23}$$

where A_r is the first refractive index virial coefficient and $A_r = 6.701 \times 10^6 \, m^3 / mol$.

$$B_n = \frac{3}{2}(B_r + \frac{1}{9} A_n) \tag{1.24}$$

where B_r is second refractive index virial coefficient and $B_r = 0.729 \times 10^{12} \, m^6 / mol^2$. The values calculated from literature have been confirmed in our experiments, as shown in Figure 1.9. The refractive index values of carbon dioxide were found to increase linearly with CO_2 density.

Linear approximation for the refractive index of the solution is valid at low concentrations.

$$n_{\text{solution}} = n_{\text{co}_2} + \frac{\mathrm{d}n}{\mathrm{d}c} c \tag{1.25}$$

where the intercept of the linear regression is equal to the refractive index of pure carbon

dioxide and the slope is equal to the refractive index increment, dn/dc, at the specified pressure and temperature. Two fractions (fractions 2 and 8) were used for the refractive index increment experiments.

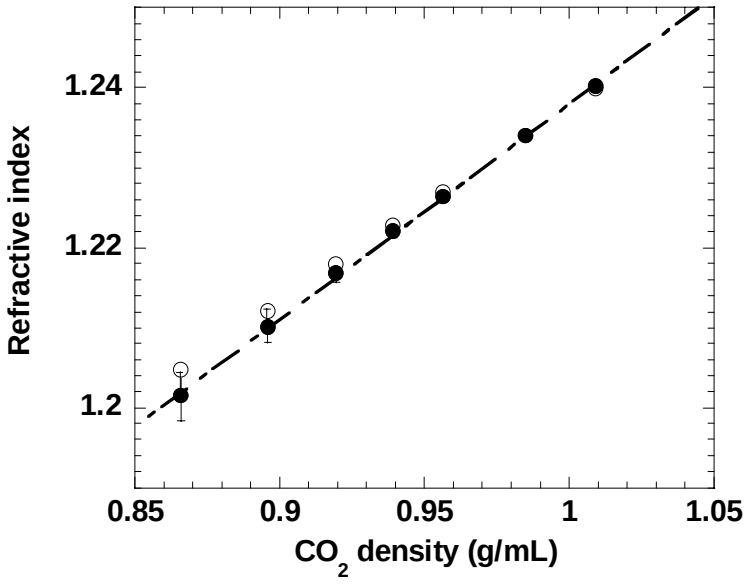

Figure 1.9 Refractive index of carbon dioxide as a function of CO_2 density at 25°C: values calculated from reference 25 (O); our measurements (●).

I-3.5 Preparation of polymer solutions for light scattering

The schemes of the light scattering experiments have been displayed in Figure 1.10 and 1.11. The solution properties were tuned by changing the temperatures at fixed CO_2 density or changing CO_2 density at fixed temperature.

The concentration of the polymer solutions used in the light scattering experiments ranged from 0.01 to 0.04 g/mL. The polymer samples were weighed and sealed into the high pressure optical cell. The cell volume was adjusted using a piston at the top of the optical cell. Carbon dioxide was filtered and injected slowly into the cell at room temperature, until the initial pressure reached 131 bar. The polymer solution was then heated to 60^{o}C with constant stirring until it became completely transparent. Subsequently, the solution was stabilized without stirring for 1.5 hours while the transmission intensity of the polymer solution was detected using a LaserPAD power meter (Coherent Inc.). All experimental conditions were reached by decreasing the temperature and/or by increasing the CO_2 density. The scattering intensity was monitored by a photometer with each temperature and density change until the intensity became stable.

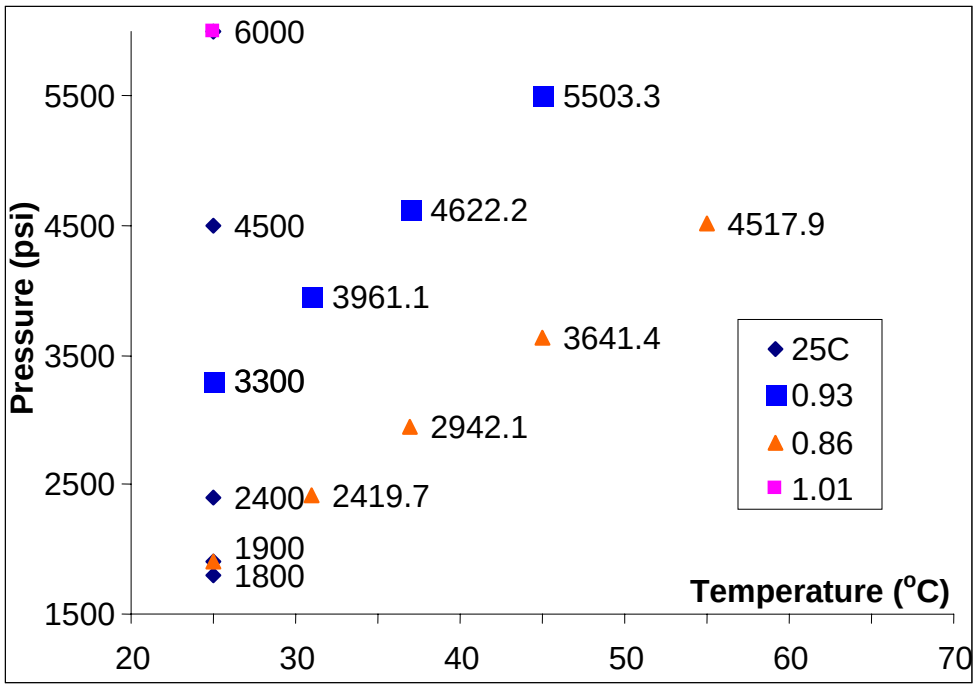

Figure 1.10 The operations of varying CO_2 density at fixed temperature

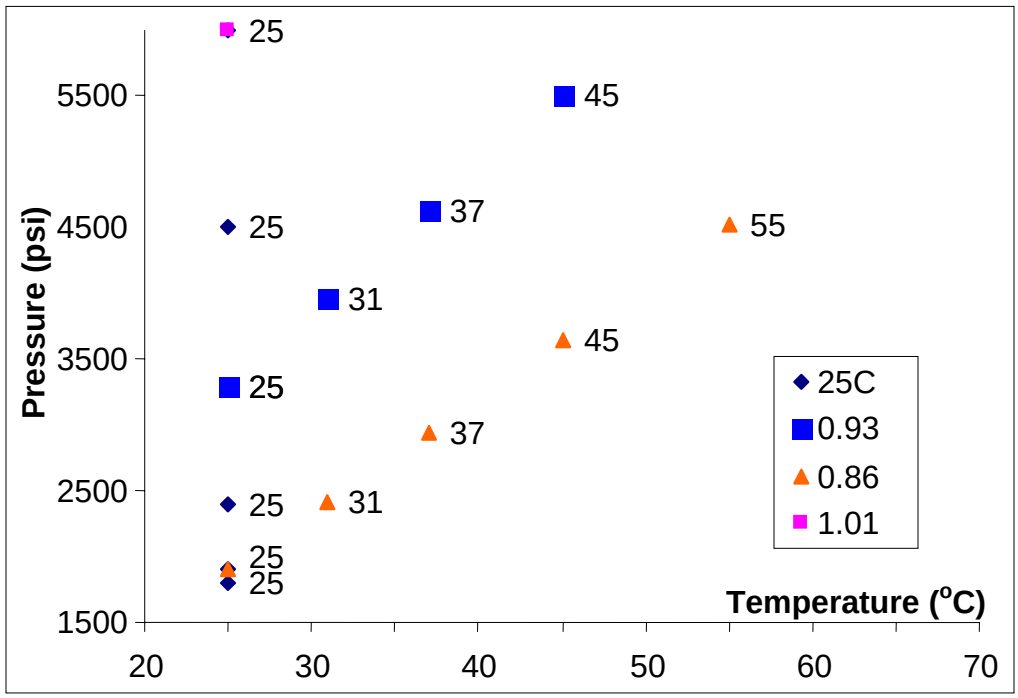

Figure 1.11 The operations of varying temperature at fixed CO_2 density

I-4 Results

I-4.1 Refractive index increments and molecular weight

The refractive index as functions of polymer concentrations under different CO_2 density at 25 ^oC is presented in Figure 1.12 and 1.13. The values of the refractive index increments (dn/dc) at 25^oC with different CO_2 densities for two PFOMA fractions (fractions 2 and 8) were displayed in Figure 1.14. The data for fractions 2 and 8 at the same CO_2 density agreed with each other within experimental accuracy. The dn/dc values were found to be independent of PFOMA molecular weight, as expected for long polymeric chains where the end groups have negligible effects on the polymer solution properties. As the carbon dioxide density was increased, the dn/dc values for both fractions of PFOMA in CO_2 decreased from 0.12 to 0.10 mL/g. The effect of CO_2 density on the dn/dc of the polymer solutions could be mostly attributed to the change of CO_2 refractive index with CO_2 density. The refractive index increments of PFOMA solution in CO_2 can be expressed as,

$$\frac{\mathrm{d}n}{\mathrm{d}c} = \frac{n_{\text{solution}} - n_{\text{CO}_2}}{c} \approx \frac{n_{\text{PFOMA}} - n_{\text{CO}_2}}{\rho_{\text{PFOMA}}} \tag{1.26}$$

where n_{CO_2} and n_{solution} are the refractive of CO_2 and polymer solution, n_{PFOMA} and ρ_{PFOMA} are the refractive index and density of PFOMA. Assuming that the refractive index of polymer is approximately independent of the CO_2 density variations in our experiment range, the variations of refractive index of CO_2 (n_{CO_2}) and refractive index increment (dn/dc) of polymer solution with CO_2 density (ρ_{CO_2}) are related to each other by the polymer density (ρ_{PFOMA}) via following expression.

$$\mathrm{d}\left(\frac{\mathrm{d}n}{\mathrm{d}c}\right) / \mathrm{d}\rho_{\text{CO}_2} = -\frac{1}{\rho_{\text{PFOMA}}}\left(\frac{\mathrm{d}n}{\mathrm{d}\rho_{\text{CO}_2}}\right) \tag{1.27}$$

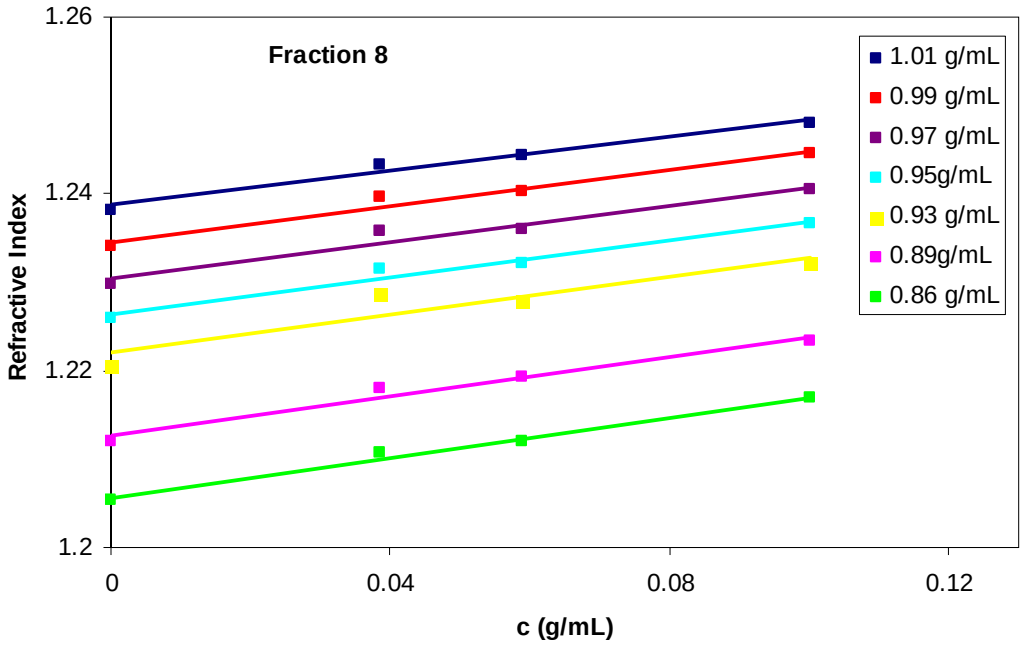

Figure 1.12 Refractive index as a function of the concentration at temperature 25°C with different CO_2 density for PFOMA fraction 8.

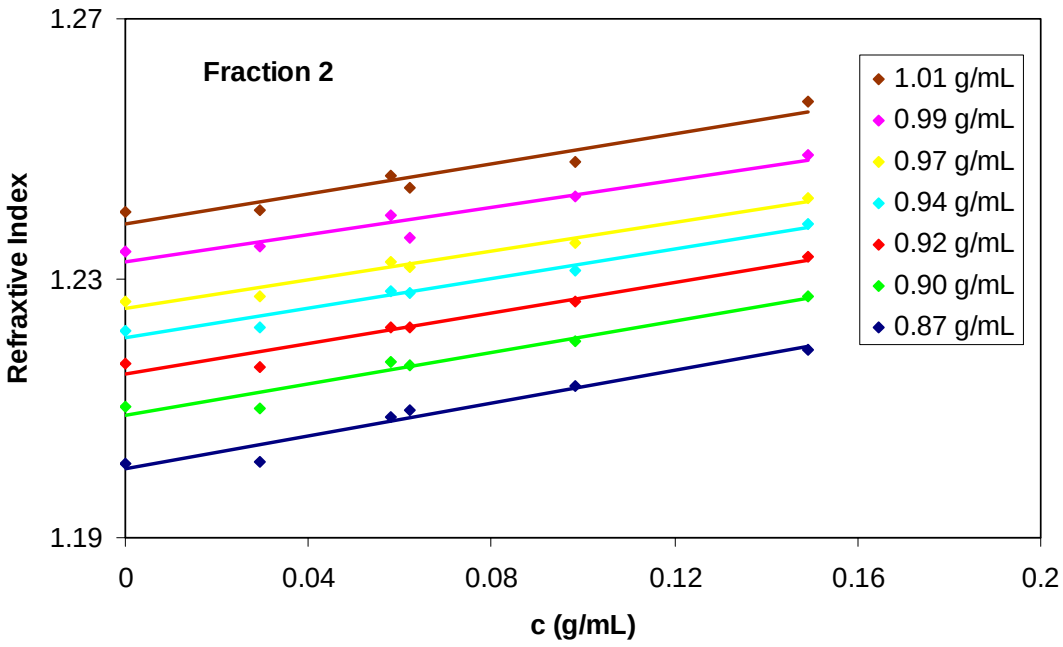

Figure 1.13 Refractive index as a function of the concentration at temperature 25°C with different CO_2 density for PFOMA fraction 2.

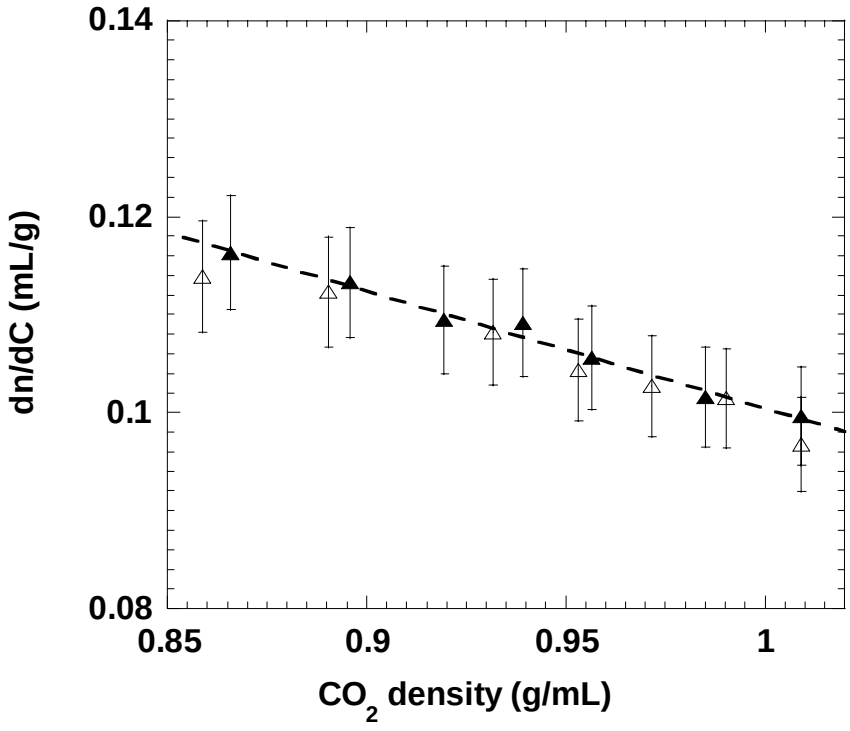

Figure 1.14 d*n*/d*c* as a function of CO_2 density at 25°C for two PFOMA fractions: fraction 2 (Δ) and fraction 8 (▲).

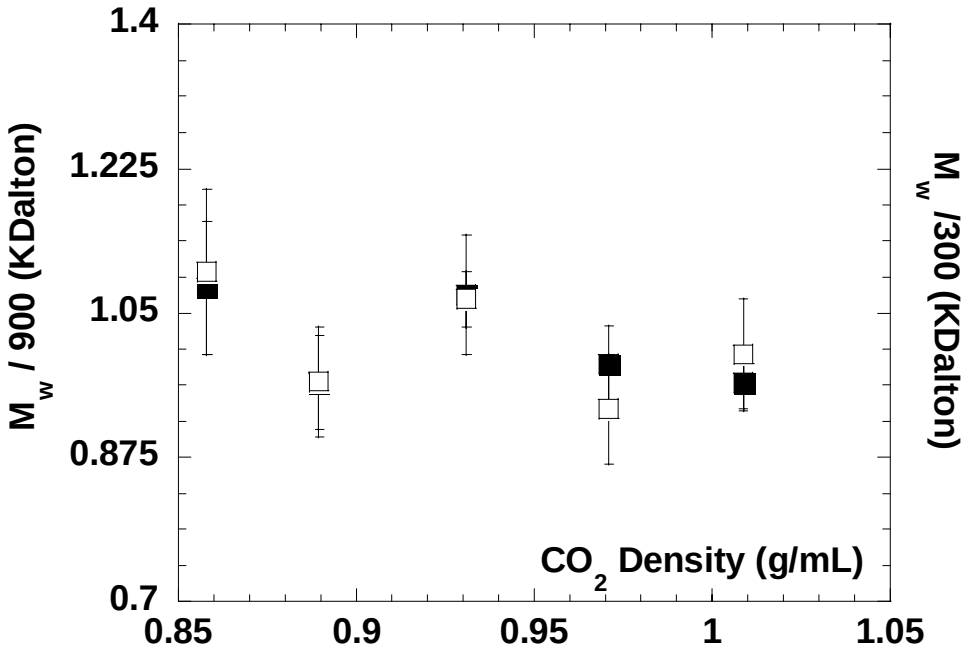

Figure 1.15 Molecular weight determined by static light scattering in CO_2, plotted as a function of CO_2 density at a constant temperature 25 ^{o}C; for two fractions: (■) Fraction with $\overline{M_w}$ = 900 ± 70 kDalton and (□) Fraction with $\overline{M_w}$ = 300 ± 30 kDalton.

This equation was verified by our measurements since the slopes of lines in Figure 1.9 and Figure 1.14 are 0.25 mL/g and -0.12 mL^2/g^2, respectively, and the density of PFOMA was between 1.8 and 2.0 g/mL. The molecular weights of fractions 3 and 6 were measured by light scattering using dn/dc values determined from fractions 2 and 8 (Figure 1.15). The molecular weights of fractions 3 and 6 were found to be 300 ± 30 kDalton and 900 ± 70 kDalton, respectively.

I-4.2 Static light scattering

In the static experiments, the scattering intensity was measured at various polymer concentrations, c, and the relative excess of scattering intensity with respect to the solvent, $I(q,c)$, was calculated. Figure 1.16 and 1.17 displayed the dependence of the $c/I(q.c)$ on polymer concentration c and on the square of wavevector q^2. These results allowed determinations of the weight-average molecular weight, M_w, and the second virial coefficient, A_2 (see Equation 1.7 and Figure 1.16). Results of one example of the relative excess light scattering intensity measurement at different dilute concentrations at the zero were shown in Figure 1.16. The solvent quality change can be monitored through measurements of A_2 at different temperatures and solvent densities of CO_2. The extrapolation of the ratio $c/I(q,c)$ to zero concentration as a function of q^2 (see Equation 1) allowed the determination of the radius of gyration, R_g. Figure 1.17 exhibited the dependence of $c/I(q,c)$ on the square of the scattering vector, q^2, at concentration c = 0.033 g/mL.

The temperatures and densities corresponding to θ conditions with the second virial coefficient equal to zero can be determined at constant density by varying the temperature or

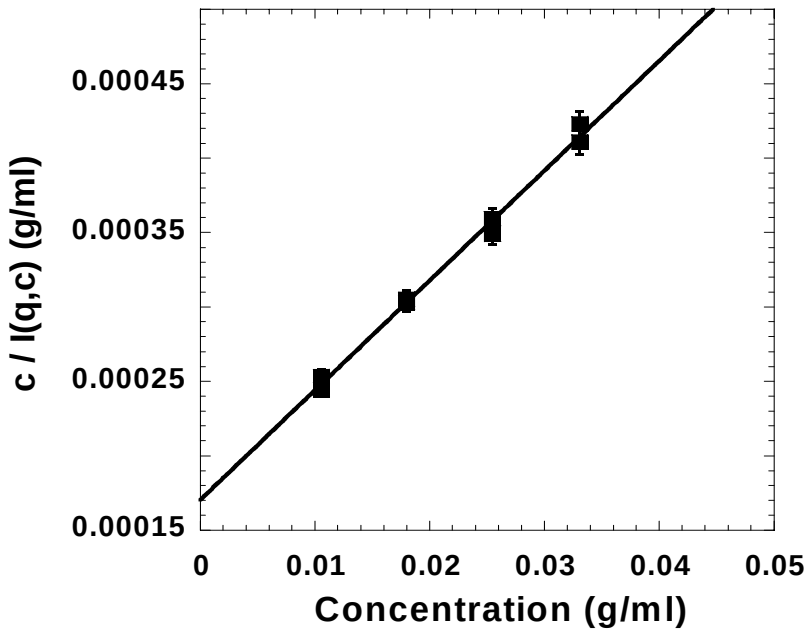

Figure 1.16 The dependence of $c/I(q,c)$ for PFOMA with M_w = 900 kDalton at temperature 25^oC and CO_2 density 1.01 g/mL on polymer concentrations (with wavevector q extrapolated to zero)

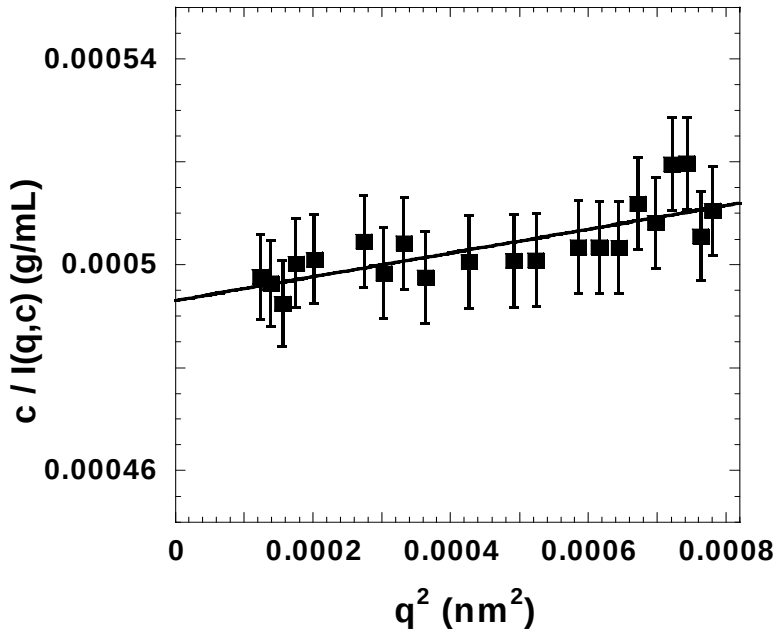

Figure 1.17 The dependence of $c/I(q,c)$ for PFOMA with M_w = 900 kDalton at temperature 25°C and CO_2 density 1.01 g/mL on the square of the scattering wave factor q (at concentration c = 0.033 g/mL).

at constant temperature by varying the density. Previous small-angle neutron scattering experiments have demonstrated that not only a θ-temperature but also a θ-density exist for a CO_2-polymer solution.[101] When the CO_2 density was kept constant (0.86 g/mL), A_2 was found to increase with increasing temperature (Figure 1.18A), changing from negative to positive values. In the range of experimental conditions investigated, the PFOMA samples with both molecular weights (300 kDalton and 900 kDalton) had the same θ point [$\theta = 27 \pm 1$ ^oC, $\rho_\theta = 0.86$ g/mL]. The variation of A_2 with carbon dioxide density at constant temperature (25^{o}C) was displayed in Figure 1.18B. A_2 was found to increase with increasing density, ranging from negative to positive values. The increase of the second virial coefficient with density was stronger for the lower molecular weight fraction. The θ condition was determined to be [$\theta = 25^oC$, $\rho_\theta = 0.88 \pm 0.02$ g/mL].

Figure 1.19 presents the variations of the radius of gyration as a function of temperature (Figure 1.19A) and CO_2 density (Figure 1.19B). The radius of gyration of the fraction with M_w = 900 kDalton was $R_g = 15 \pm 4$ nm, at θ conditions [$\theta = 27 \pm 1$ ^oC, $\rho(\theta) = 0.86$ g/mL] and [$\theta = 25$ ^oC, $\rho(\theta) = 0.88 \pm 0.02$ g/ml]. There was no measurable change of R_g within the experimental error with variations of either CO_2 density or temperature (see Figure 1.21). For the fraction with M_w = 300 kDalton, the radius of gyration could not be measured by static light scattering. The values of R_g for PFOMA with M_w = 900 kDalton were close to the detection limit of our instrument. The difficulty of the measurements of R_g for the high molecular weight sample was clearly displayed in the plot of $c/I(q,c) \sim q^2$ (see Figure 1.17). This could be attributed to the lower contrast between the polymer and supercritical CO_2 relative to conventional organic systems.

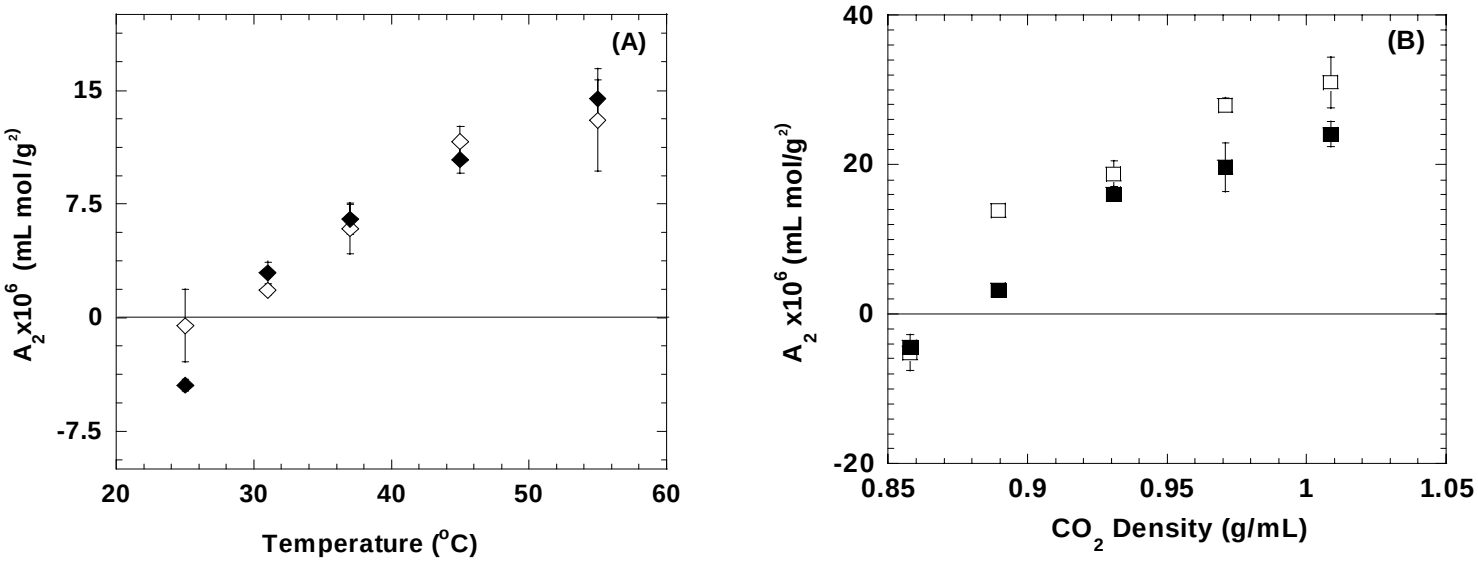

Figure 1.18 Variation of the second virial coefficient A_2 with (A) temperature at constant CO_2 density $\rho = 0.86$ g/mL, PFOMA with M_w = 300 kDalton (◊) and M_w = 900 kDalton (♦); (B) CO_2 density at constant temperature $T = 25^oC$, PFOMA with M_w = 300 kDalton (□) and M_w = 900 kDalton (■).

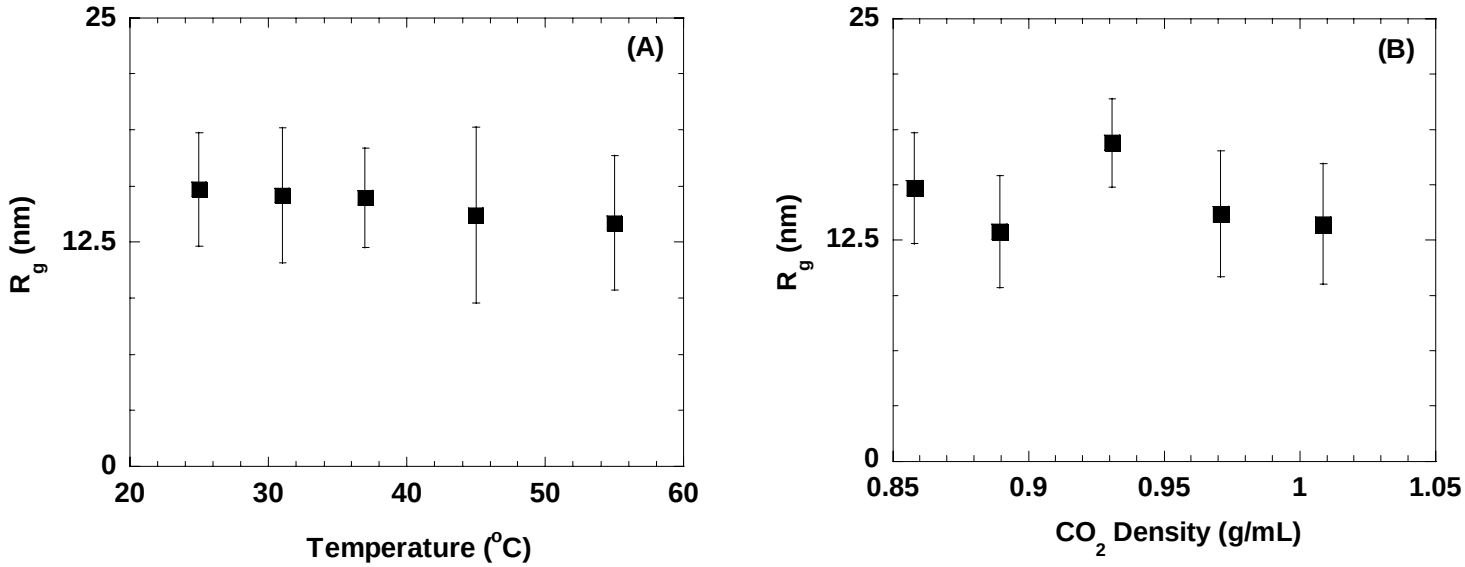

Figure 1.19 Radius of gyration, $R_{g,}$ of PFOMA with M_w = 900 kDalton: (A) as a function of temperature at constant CO_2 density of $\rho = 0.86$ g/mL; (B) as a function of CO_2 density at constant temperature $T = 25^oC$.

II-4.3 Dynamic light scattering

Dynamic light scattering (DLS) measures the autocorrelation function of the scattering intensity. The experimental time autocorrelation function, $g^{(2)}(q,t)$, was fitted to a single exponential decay with decay time inversely proportional to q^2, $g^{(2)}(q,t) = 1 + \left| A\,exp\left(-Dq^2/t\right)\right|^2$ (see Equation 1.9). Figure 1.20 presents the correlation functions of the scattering intensity at 25°C and CO_2 density 0.86 g/mL observed at the three scattering angles of 40°, 90° and 140° for PFOMA with M_w = 900 kDalton. The linear fittings in Figure 20 suggested the narrow polydispersity which was expected from the CO_2 fractionation.

The diffusion coefficient, D, was calculated according to Equation 1.10 and was found to be independent of q and was averaged over three scattering angles 40°, 90° and 140°. The linear relationship between D and polymer solution concentrations was presented in Figure 1.21 and D_0 was obtained by extrapolating to zero concentration.

The coefficient k_D is a critical parameter determined from dynamic light scattering relevant to the interactions in polymer solutions. The coefficient k_D contains both hydrodynamic and thermodynamic contributions and is qualitatively consistent with the changes in the thermodynamic interactions (A_2) gained from SLS. Akcasu reported the temperature and concentration dependence of the diffusion coefficient in dilute solutions (organic solvent) which illustrated the continuous transition of k_D from negative values under θ conditions to positive values in the good solvent regime.[102] In dynamic scattering experiments, the diffusion coefficient *D* was found to vary linearly with concentration in all cases yielding hydrodynamic interaction coefficient k_D. The diffusion second virial coefficient k_D increased with temperature and CO_2 density as shown in Figure 1.22.

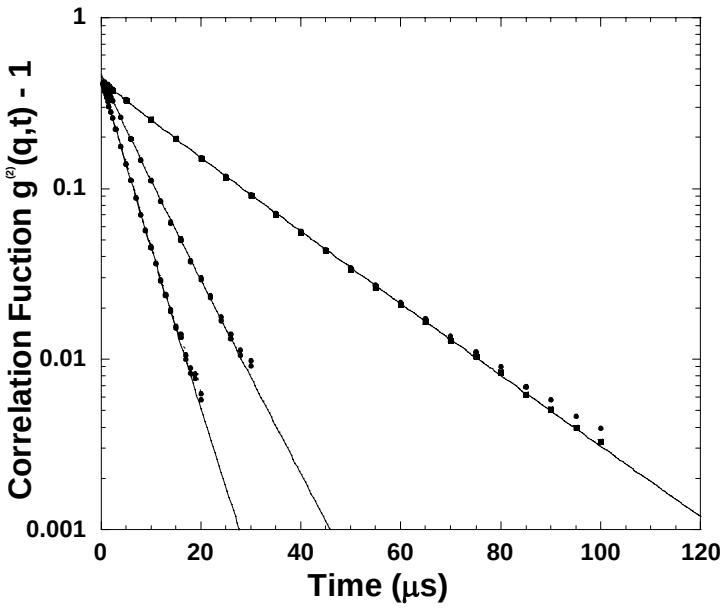

Figure 1.20 The autocorrelation function $[g^{(2)}(q,t)-1]$ of the scattering intensity at 25°C and CO_2 density 0.86 g/mL measured at angles 40°, 90° and 140°, PFOMA with M_w = 900 kDalton at concentration c = 0.033 g/mL.

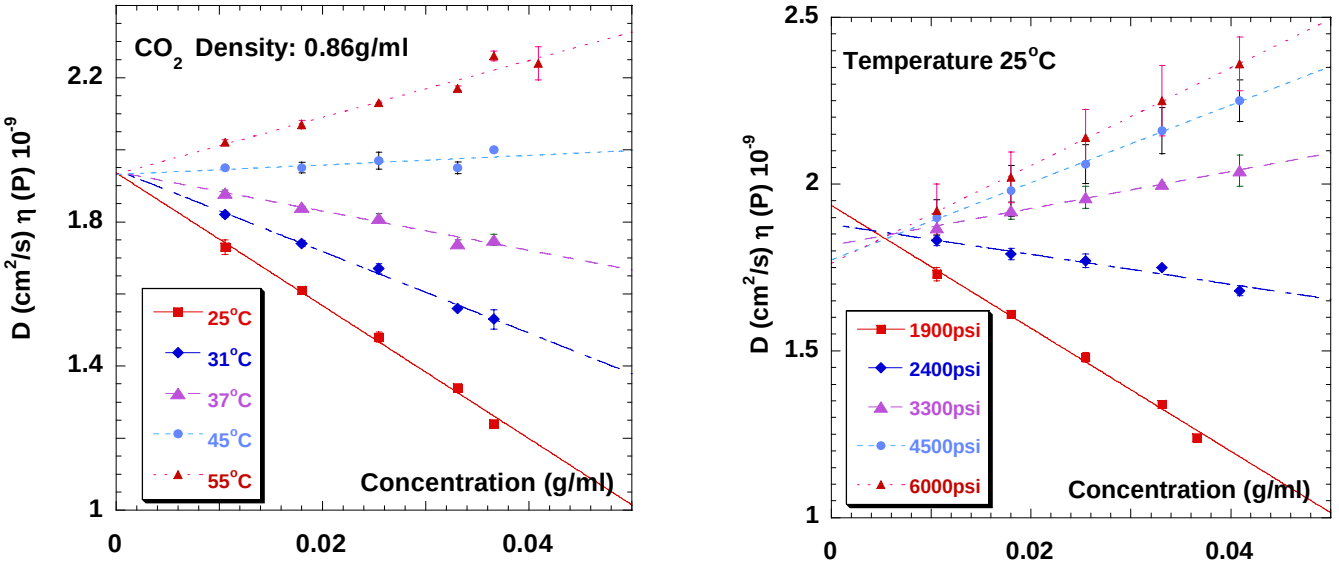

Figure 1.21 Variation of the diffusional coefficient *D* with concentration (A) at constant CO_2 density of 0.86 g/mL; (B) at constant temperature of 25°C. PFOMA with M_w = 900 kDalton.

The coefficient k_D for the high molecular weight fraction changed sign from negative to positive with increasing temperature or CO_2 density, while k_D for the low molecular weight fraction was negative over the whole temperature variation range. At θ conditions [$\theta = 27^oC$, $\rho(\theta) = 0.86$ g/mL] and [$\theta = 25^oC$, $\rho(\theta) = 0.88$ g/mL], the values of k_D were found to be negative for both fractions. The coefficient has three principal contributions[84], $k_D = 2M_w A_2 - k_s - \bar{\upsilon}$, where k_s is the friction coefficient, and the $\bar{\upsilon}$ is the partial specific volume of the polymer. The coefficient k_D was negative at the θ points, since A_2 vanishes and $\bar{\upsilon}$ can be neglected in comparison with k_s which is positive. The change of k_D as a function of temperature or CO_2 density was consistent with the variations of A_2, which showed an improvement in solvent quality with temperature.

The hydrodynamic radius R_h was calculated using the Stokes-Einstein equation and plotted in Figure 1.23. The values of R_h increased with increasing temperature and CO_2 density. This observation verified that the polymer size increases with the improvement of solvent quality both along the temperature and density directions. The increase of hydrodynamic radius with temperature or density was stronger for the higher molecular weight fraction. The hydrodynamic radii R_h at θ conditions [$\theta = 27 \pm 1\ ^oC$, $\rho_\theta = 0.86$ g/mL] and [$\theta = 25\ ^oC$, $\rho_\theta = 0.88 \pm 0.02$ g/mL] were measured to be 6.4 ± 0.1 nm and 11.4 ± 0.2 nm for the low (300 kDalton) and the high (900 kDalton) molecular weight fractions (fractions 3 and 6), respectively. The ratio of R_g / R_h for the sample with molecular weight 900 kDalton was found to be 1.3 ± 0.4 at θ conditions, which is very close to the value reported for monodisperse linear polymers.[33]

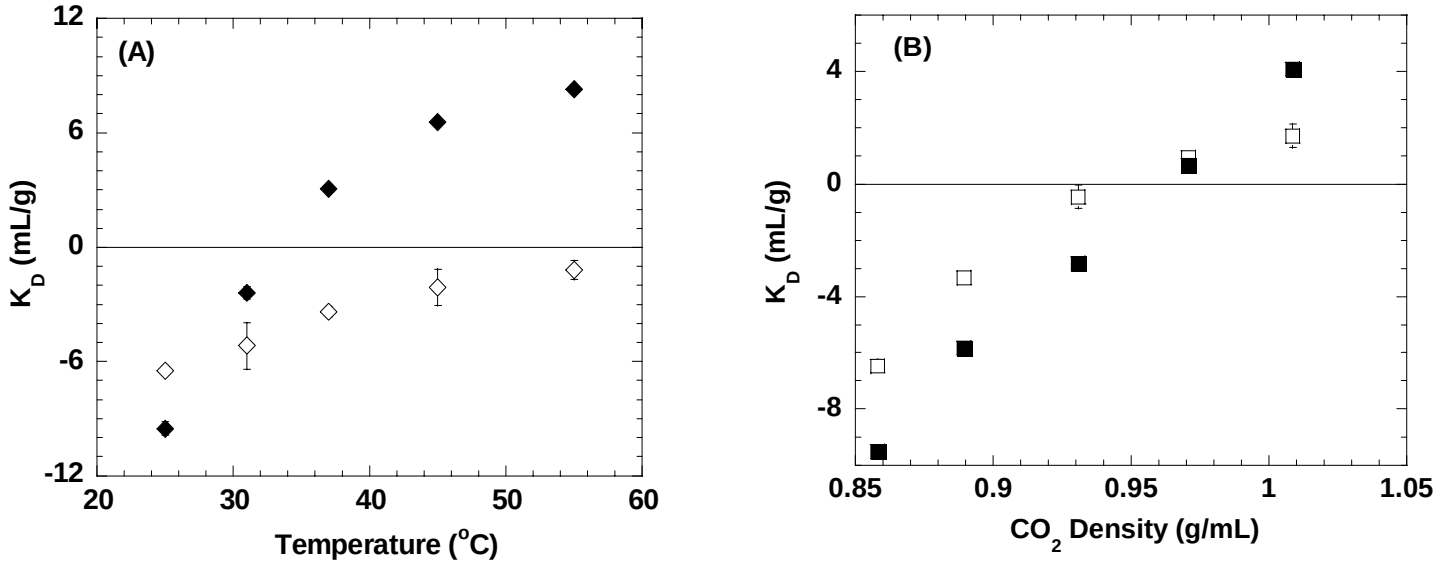

Figure 1.22 Variation of the diffusional second virial coefficient k_D (A) with temperature at constant CO_2 density of 0.86 g/mL, PFOMA with M_w = 300 kDalton (◊) and M_w = 900 kDalton (♦), (B) with CO_2 density at constant temperature of 25°C. PFOMA with M_w = 300 kDalton (□) and M_w = 900 kDalton (■).

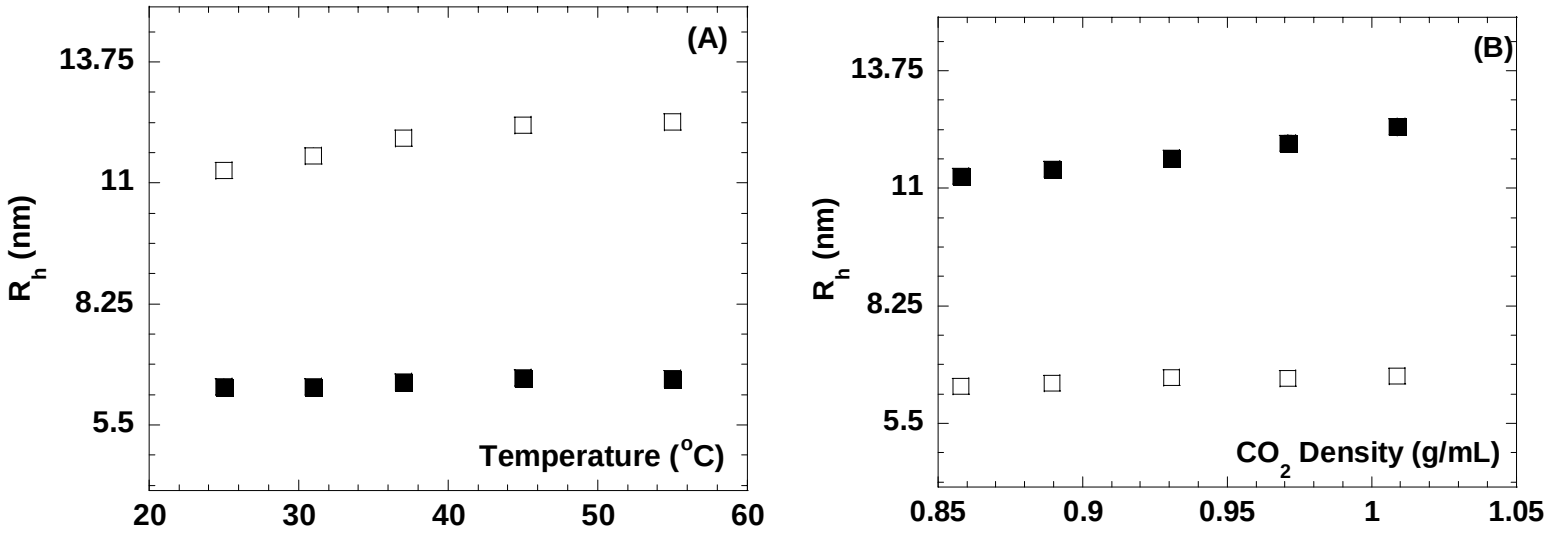

Figure 1.23 Hydrodynamic radius (R_h): (A) as a function of temperature at constant CO_2 Density of 0.86g/mL; (B) as a function of CO_2 density at constant temperature of 25°C; (■)M_w of 870 kDalton and (□) 300 kDalton in CO_2 .

II-5 Discussions

II-5.1 Hydrodynamic radius

The hydrodynamic radii R_h at θ conditions [θ = 27 ±1 ^{o}C , ρ_θ = 0.86 g/mL] and [θ = 25 ^{o}C , ρ_θ = 0.88 ± 0.02 g/mL] were measured to be 6.4 ± 0.1 nm and 11.4 ± 0.2 nm for the low (300 kDalton) and the high (900 kDalton) molecular weight fractions (fractions 3 and 6), respectively. Figure 1.24 illustrated the dependence of hydrodynamic radius expansion ratio α_h on temperature (A) and CO_2 density (B). The values of α_h increased with increasing temperature and CO_2 density. This observation verifies that the polymer size increases with the improvement of solvent quality both along the temperature and density directions (see Figure 1.2). The increase of hydrodynamic radius expansion factor with temperature or density was stronger for the higher molecular weight fraction.

It is demonstrated in Figure 1.25A that the hydrodynamic radius expansion factor for different polymer solutions can be expressed as the universal function of the reduced temperature $N^{1/2}[1-\theta(\rho)/T]$ (Equation 1.19) including the data for PFOMA in CO_2 and the data from earlier experiments on polystyrene (PS) in two different solvents.[83,103] In the θ region, α_h was found to be approximately a linear function of reduced temperature $N^{1/2}[1-\theta(\rho)/T]$, and the numerical coefficient C_T^R is 0.06 ± 0.01 for both PFOMA in CO_2 and polystyrene in organic solvents.[83,103,104] The radius of gyration expansion factor α_g (defined as the ratio of R_g at a given condition to the radius of gyration $R_{g\theta}$ at the θ point) was also a universal function of reduced temperature $N^{1/2}[1-\theta(\rho)/T]$.[67,105] The earlier experimental results for PS[83,103] and PMMA[106] in different organic solvents also exhibited the linear relationship between α_g and reduced temperature in the θ region that can be written as

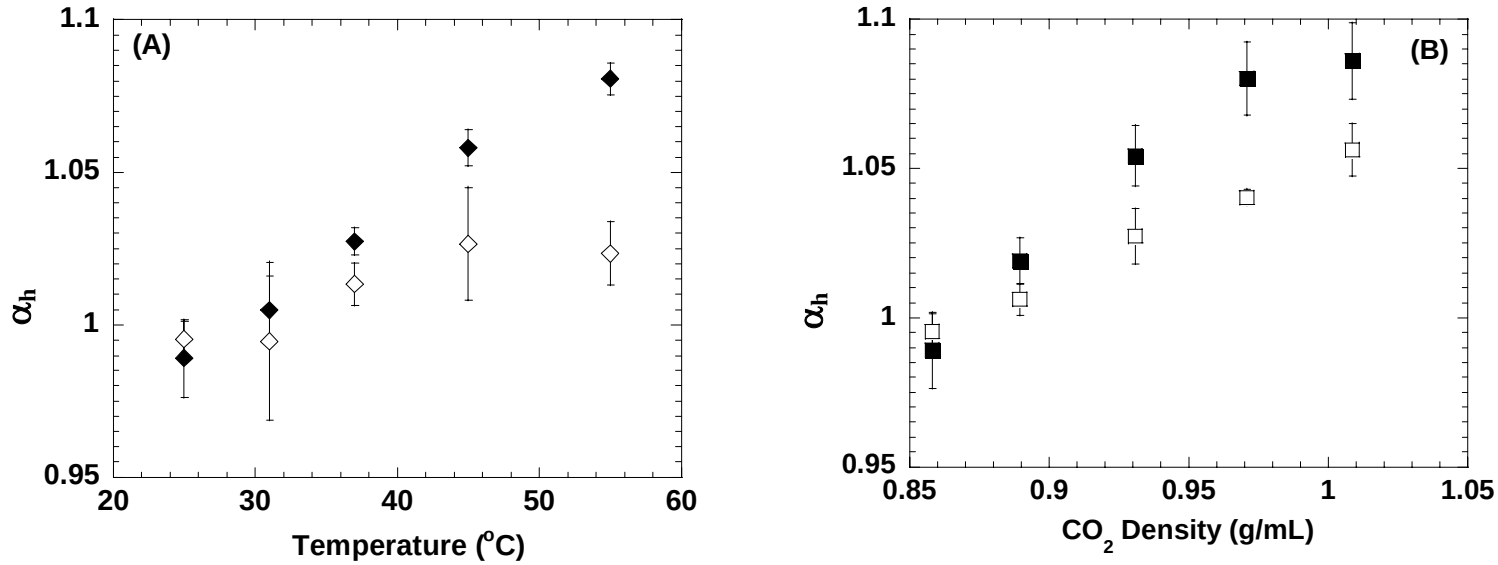

Figure 1.26 Hydrodynamic expansion factor α_h: (A) as a function of temperature at constant CO_2 density of $\rho = 0.86$ g/mL, PFOMA with M_w = 300 kDalton (◊) and M_w = 900 kDalton (♦); (B) as a function of CO_2 density at constant temperature $T = 25^oC$. PFOMA with M_w = 300 kDalton (□) and M_w = 900 kDalton (■).

$\alpha_g = 1 + (0.08 \pm 0.02) N^{1/2} (1 - \theta / T)$. The coefficients C_T^R for hydrodynamic radius expansion factor α_h and for the radius of gyration expansion factor α_g of PS in trans-decalin were equal to each other within experimental error, as expected from the fact that the ratio of R_g / R_h should not have a significant temperature dependence in the θ region. It is interesting to note that numerical coefficients C_T^R for different polymers (PFOMA, PS and PMMA) are close to each other.

We observed for the first time that polymer size is a function of the reduced solvent density $N^{1/2}\left[1 - \rho_\theta(T)/\rho\right]$ (direction (2) in Figure 1.3). There was a linear relationship between the hydrodynamic radius expansion factor α_h and the reduced density in the θ region (see Figure 1.25B and Equation 1.19) and the numerical coefficient $C_\rho^R = 0.06 \pm 0.01$ turned out to be equal to C_T^R within the experimental accuracy.

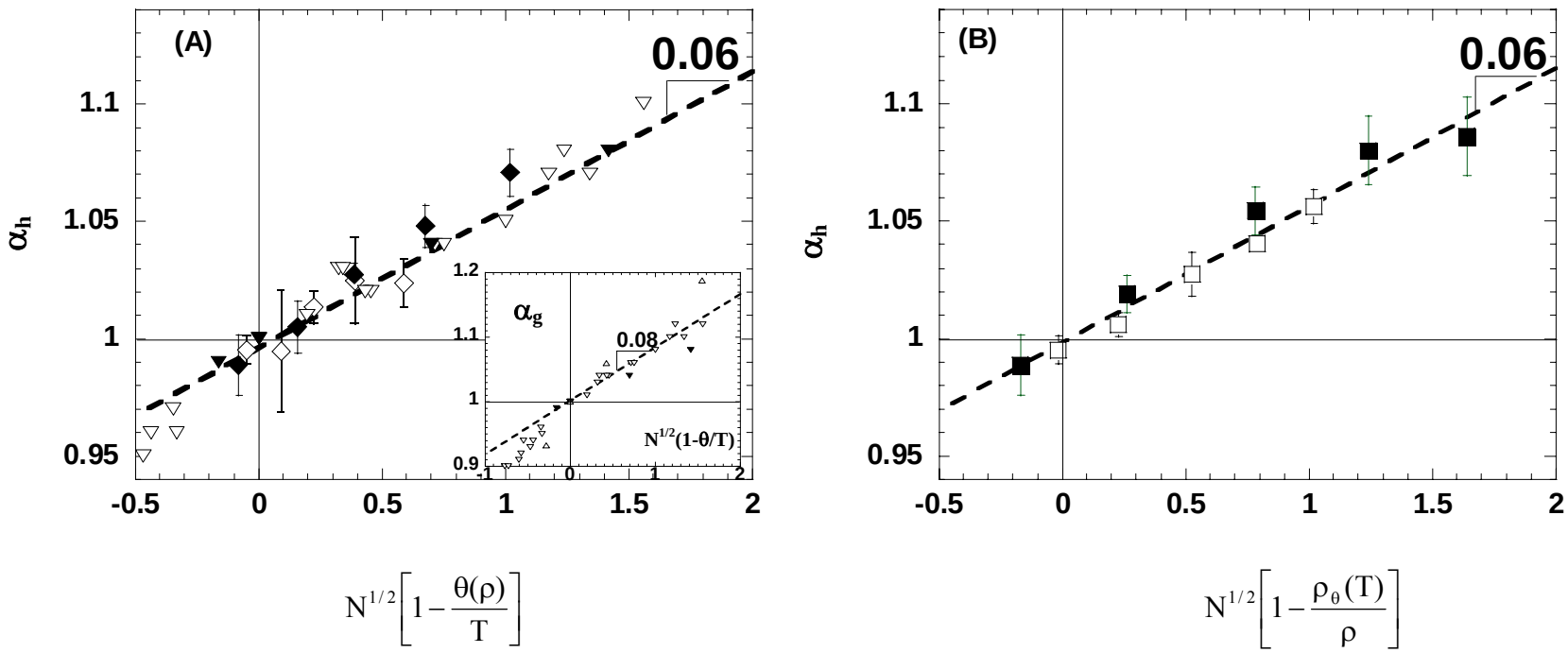

Figure 1.25 (A) Hydrodynamic radius expansion factor α_h as a function of the reduced temperature $N^{1/2}[1-\theta(\rho)/T]$ at constant CO_2 density $\rho = 0.86$g/mL with $\theta(\rho) = 27\ ^oC$, for PFOMA with $M_w = 300$ kDalton (◊) and $M_w = 900$ kDalton (♦), PS in cyclohexane[83] (∇), PS in trans-decalin[103] (▼). Insert: radius of gyration expansion factor $\alpha_g = R_g / R_g(\theta)$ as a function of the chain interaction parameter $N^{1/2}(1-\theta/T)$, for PS in cyclohexane[83] (∇), PS in trans-decalin[103], PMMA in water and tert-butyl alcohol[106] (△); (B) The hydrodynamic radius expansion ratio α_h as a function of the reduced density $N^{1/2}[1-\rho_\theta(T)/\rho]$ at constant temperature $T = 25^oC$ with $\rho_\theta = 0.88$ g/mL, for PFOMA with $M_w = 300$ kDalton (□) and $M_w = 900$ kDalton (■).

II-5.2 Second virial coefficient

It was reported that experimental data, as well as computer simulation data for the second virial coefficient of different polymers (e.g. polystyrene[67] and poly(methyl methacrylate)[62]) in various organic solvents can be expressed as functions of the interaction parameter $z \sim N^{1/2}(1-\theta/T)$ (see Equation 1.13). The dependence of the normalized second virial coefficient on the reduced temperature $N^{1/2}[1-\theta(\rho)/T]$ of PFOMA solutions in CO_2 was presented in Figure 1.26A. The data of PFOMA samples for both molecular weights collapse onto a single curve. Most of the PFOMA points were in θ region, where the interaction parameter was small and the dependence of normalized second virial coefficient on reduced temperature $N^{1/2}[1-\theta(\rho)/T]$ was linear. The numerical coefficient for the θ region of the PFOMA solution in CO_2 was measured to be $C_{\mathrm{T}}^{\mathrm{A}2} = 0.50 \pm 0.05$ (Equation 1.18), which was larger than the coefficients 0.39 ± 0.04 for PS and PMMA in organic solvents (shown in the insert in Figure 1.26A). This difference in coefficients is probably due to different chemical structures of the polymers, since the PFOMA has a larger Kuhn segment than PS and PMMA (see Table 1.2).

In a compressible solvent like CO_2, the interaction parameter can be easily varied by changing the solvent density. The behavior of the second virial coefficients as a function of reduced density $N^{1/2}\left[1-\rho_\theta(T)/\rho\right]$ was presented in Figure 1.28B. The data for two different molecular weight fractions of PFOMA collapsed onto a single curve similar to the curve in Figure 1.26A. This is the first demonstration that the second virial coefficient A_2 of polymers in compressible solvents is a function of the single interaction parameter $z \sim N^{1/2}\left[1-\rho_\theta(T)/\rho\right]$. The numerical coefficient of the linear dependence of the normalized

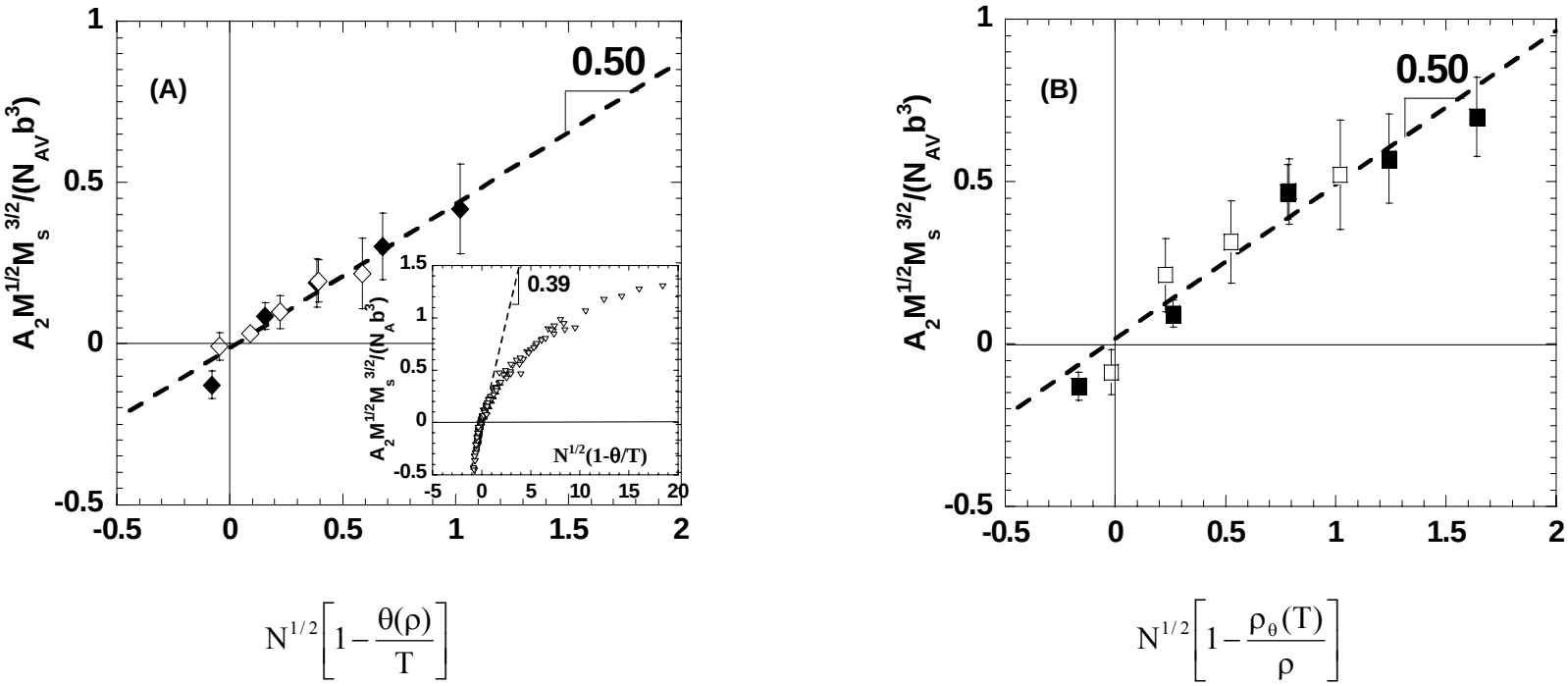

Figure 1.26 (A) The plot of $A_2M^{1/2}M_s^{3/2}N_{AV}^{-1}b^{-3}$ as a function of reduced temperature $N^{1/2}[1-\theta(\rho)/T]$ at constant CO_2 density ρ_{CO_2} = 0.86 g/mL with $\theta(\rho)$ = 27°C, of PFOMA with M_w = 300 kDalton (◊) and M_w = 900 kDalton (♦). Insert: the plot of $A_2M^{1/2}M_s^{3/2}N_{AV}^{-1}b^{-3}$ as a function of reduced temperature $N^{1/2}(1-\theta/T)$ for PMMA in 46.8% butanol / 53.2% isopropanol [62] (▽) and PS in decalin [67] (▼) ; (B) the plot of $A_2M^{1/2}M_s^{3/2}N_{AV}^{-1}b^{-3}$ as a function of reduced density $N^{1/2}[1-\rho_\theta(T)/\rho]$ at constant temperature T = 25°C with ρ_0 = 0.88 g/mL, PFOMA with M_w = 300 kDalton (□) and M_w = 900 kDalton (■).

second virial coefficient on the reduced density $N^{1/2}\left[1-\rho_\theta(T)/\rho\right]$ for the θ region is C_ρ^{A2} = 0.50 ± 0.05 (Equation 1.18), which was equal to the value of coefficient C_T^{A2} within experimental error. The ratios of numerical coefficients for the temperature variation ($C_T^R / C_T^{A2} = C^R / C^{A2} \cong 0.12$) and for the density variation ($C_\rho^R / C_\rho^{A2} = C^R / C^{A2} \cong 0.12$) were equal to each other as expected from Equation 1.20.

The plots in Figure 1.25 and 1.26 are based on assumptions that the interaction parameter is a linear function of either reduced temperature or reduced density. In order to combine solvent quality changes with both temperature and density variations (both directions in Figure 1.3), the dependence of hydrodynamic radius expansion factor α_h on the second virial coefficient $A_2M^{1/2}M_s^{3/2}N_{av}^{-1}b^{-3}$ has been plotted in Figure 1.27 for the PFOMA solutions at different CO_2 densities and temperatures. In the experimental range, the PFOMA data collapsed onto a single curve with the slope $C^R / C^{A_2} = 0.12 \pm 0.02$. The hydrodynamic radius expansion factor of PFOMA in CO_2 can be approximated in the θ region by a linear function of the second virial coefficient.

$$\alpha_h = 1 + \frac{C^R}{C^{A_2}} A_2 M_w^{1/2} \frac{M_0^{3/2}}{N_{av} b^3} = 1 + (0.12 \pm 0.02) A_2 M_w^{1/2} \frac{M_0^{3/2}}{N_{av} b^3} \tag{1.28}$$

The data of PS and PMMA also collapsed onto a single curve but with a higher slope of 0.2 ± 0.03. These curves provide a more direct way of predicting the interactions and polymer size in solutions, either getting size information from interactions or obtaining interactions information from polymer size, since both A_2 and α_h can be measured directly and independently by the light scattering experiments.

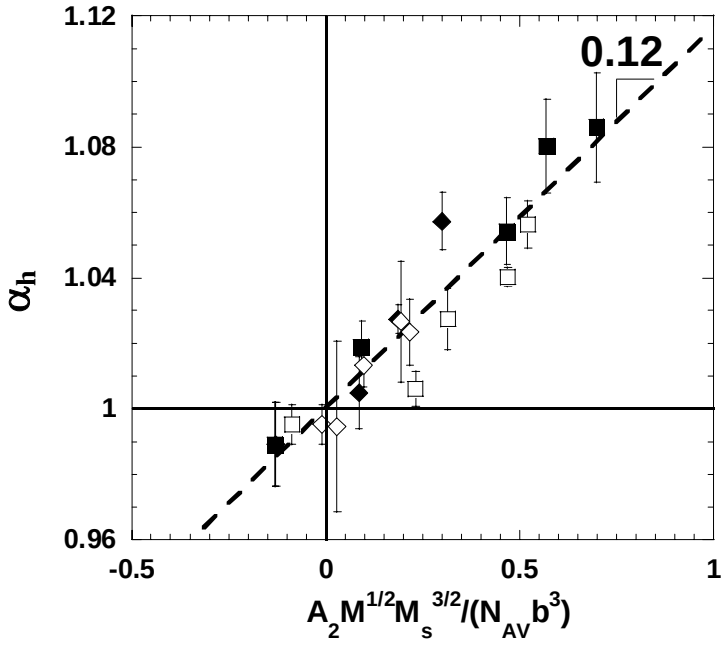

Figure 1.27 The plot of the hydrodynamic radius expansion factor α_h as a function of $A_2M^{1/2}M_s^{3/2}N_{av}^{-1}b^{-3}$: PFOMA at constant temperature T = 25°C with ρ_0 = 0.88 g/mL, of PFOMA with M_w = 300 kDalton (□) and M_w = 900 kDalton (■); PFOMA at constant CO_2 density ρ_{CO2} = 0.86 g/mL with $\theta(\rho)$ = 27°C, of PFOMA with M_w = 300 kDalton (◊) and M_w = 900 kDalton (♦).

II-5.3 Theta curve

We independently verified that numerical coefficients C_T^R and C_ρ^R were equal to each other (see Figure 1.25) and that the numerical coefficients C_T^{A2} and C_ρ^{A2} were equal to each other (see Figure 1.26). Thus we have two independent verifications that coefficients C_T and C_ρ in Equation 1.18 and 1.19 were the same, since these two equations were two different representations of the same interaction parameter z. We conclude that $\theta\rho_\theta$ = constant and the density dependence of θ-temperature is

$$\theta(\rho) = \frac{260}{\rho}\left(\frac{gK}{mL}\right) \tag{1.29}$$

while the temperature dependence of θ-density is

$$\rho_\theta(T) = \frac{260}{T}\left(\frac{KmL}{g}\right) \tag{1.30}$$

Below we presented a theoretical justification of the hyperbolic CO_2 density dependence of θ-temperature (Figure 1.28).

In highly compressible solvents (such as CO_2 near its critical point), the second virial coefficient of interaction between solvent molecules is small and the free energy density of the solvent is dominated by the third virial term

$$F_{CO_2} \approx \frac{B_3\rho^3}{3} \tag{1.31}$$

where B_3 is solvent interaction parameter. There are additional interaction terms in the free energy density of a polymer solution with Kuhn segment number density c_k in this compressible solvent: a term proportional to $\rho_{CO_2} c_k$ due to polymer-solvent interaction and a term proportional to c_k^2 due to direct polymer-polymer interaction

$$F \approx \frac{B_3 \rho^3}{3} + B_2 \rho c_k + k_B T \nu \frac{c_k^{\,2}}{2} \tag{1.32}$$

where B_2 is the polymer-solvent interaction parameter, k_B is the Boltzman constant and ν is the excluded volume of monomers. Because of small interval of temperature variations, we neglect temperature dependences of the interaction parameters B_2 and B_3. In order to take into account the density fluctuation of a compressible solvent, we can write the local density ρ as a sum of an average density $\bar{\rho}$ and a density fluctuation $\delta\rho$.

$$\rho = \bar{\rho} + \delta\rho \tag{1.33}$$

Substituting this expression into the free energy density (Equation 1.32) and expanding it to quadratic terms in density fluctuation, we find

$$F \approx \frac{B_3 \bar{\rho}^3}{3} + B_3 \bar{\rho}^2 \delta\rho + B_3 \bar{\rho} (\delta\rho)^2 + B_2 \bar{\rho} c_k + B_2 c_k \delta\rho + k_B T \nu \frac{c_k^{\,2}}{2} \tag{1.34}$$

The sum of density fluctuations over the solution volume is zero $\int_V \delta\rho \, \mathrm{d}V = 0$ and therefore the second term in Equation 1.34 vanishes. Note that linear term in solvent density fluctuation $B_2 c_k \delta\rho$ does not vanish because the polymer concentration c_k fluctuates in a correlated way with solvent density. Minimizing the free energy density

$$F \approx \frac{B_3 \bar{\rho}^3}{3} + B_3 \bar{\rho} \ (\delta\rho)^2 + B_2 \bar{\rho} c_k + B_2 c_k \delta\rho + k_B T \nu \frac{c_k^{\,2}}{2} \tag{1.35}$$

with respect to the solvent density fluctuation δρ

$$\frac{\partial F}{\partial(\delta\rho)} = 2 B_3 \bar{\rho} \delta\rho + B_2 c_k = 0 \tag{1.36}$$

We find the optimal solvent density fluctuation

$$\delta\rho = -\frac{B_2 c_k}{2 B_3 \bar{\rho}} \tag{1.37}$$

Substituting it back into Equation 12, we obtain the free energy density

$$F \approx \frac{B_3 \overline{\rho}^3}{3} + B_2 \overline{\rho} c_k + \frac{c_k^2}{2}\left(k_B T \nu - \frac{B_2^2}{2B_3 \overline{\rho}}\right) \approx \frac{B_3 \overline{\rho}^3}{3} + B_2 \overline{\rho} c_k + RT \frac{A_2}{2} c^2 \tag{1.38}$$

where $R = k_B N_{av}$ is the gas constant.

The solution concentration c can be expressed in terms of the number density of Kuhn segment c_k as

$$c = \frac{M_0}{N_{av}} c_k \tag{1.39}$$

Thus polymer-solvent interactions lead to an effective second virial coefficient in the θ-region

$$A_2 \approx \frac{\nu N_{av}}{M_0^2}\left(1 - \frac{B_2^2}{2k_B T \nu B_3 \overline{\rho}}\right) = \frac{\nu N_{av}}{M_0^2}\left(1 - \frac{\theta}{T}\right) \tag{1.40}$$

that vanishes at the theta temperature

$$\theta = \frac{B_2^2}{2k_B \nu B_3 \overline{\rho}} \tag{1.41}$$

Thus we derived that θ-temperature is inversely proportional to the average solvent density

$$\theta = \frac{const}{\overline{\rho}} \tag{1.42}$$

We have verified this dependence and found the value of the constant 260 gK/mL (Equation 1.29) in our experiments.

Substituting the second virial coefficient A_2 (Equation 1.40) into Equation 1.18, and using an estimation $\nu \approx db^2$ for the excluded volume of the rod of the length b and the effective diameter d, we find that $C_T^{A_2} \approx \nu / b^3 \approx d / b$. Therefore, we conclude that the coefficient $C_T^{A_2}$ is not universal and it depends on chemical structure of the polymer in

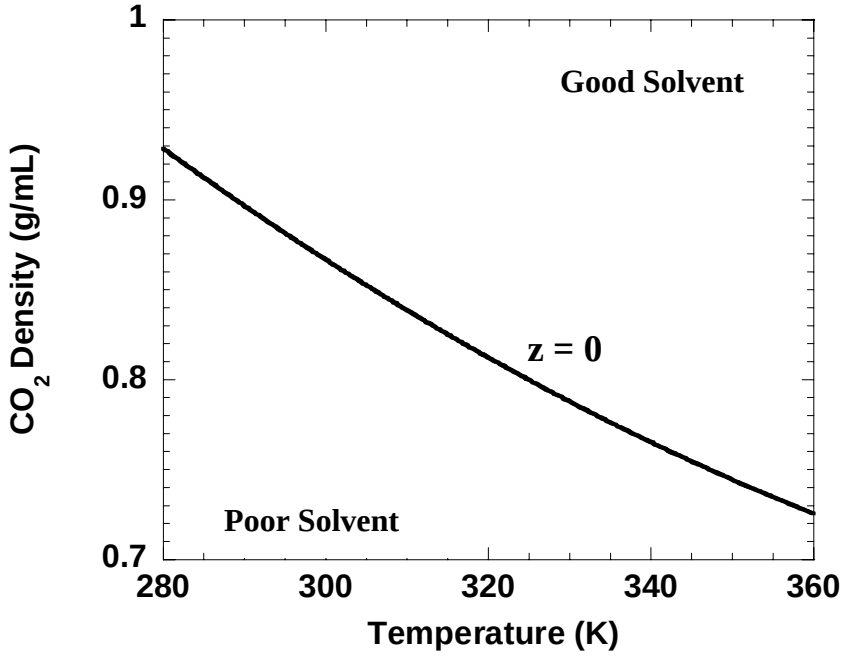

Figure 1.28 The theta-curve (dependence of θ-density on θ-temperature) for PFOMA solution in CO_2.

solution. The effective diameter d and the Kuhn length b for PS are 8 Å and 18 Å, respectively. The effective diameter of the PFOMA is calculated to be 10 Å using the mass of Kuhn segment M_s, Kuhn length b (Table 1.2) and polymer density 2 g/cm^3. The ratio of d/b for PS and PFOMA are 0.44 and 0.33, and we find that

$$(d/b)_{PFOMA}/(d/b)_{PS} = 0.75 \quad (1.43)$$

This simple theoretical estimate is in good agreement with experimentally observed ratio.

$$(C_T^{A_2})_{PFOMA}/(C_T^{A_2})_{PS} = 0.78 \pm 0.07 \quad (1.44)$$

II-6 Conclusions and future directions

PFOMA homopolymers have been synthesized and fractionated in CO_2, and were analyzied as solutions in supercritical CO_2. The refractive index increments of the PFOMA solution in CO_2 decrease from 0.12 mL/g to 0.10 mL/g with increasing CO_2 density at 25°C and the molecular weights of the two fractions studied were found to be 900 ± 70 and 300 ± 30 kDalton, respectively. The solvent quality of CO_2 was shown to improve with increasing temperature or CO_2 density. This trend was confirmed by the evaluation of the second virial coefficient A_2 and diffusional second virial coefficient k_D measured through static and dynamic light scattering, respectively. The θ conditions were determined to be [θ = 27 ±1 °C, ρ_θ = 0.86 g/mL] and [θ = 25°C, ρ_θ = 0.88 ± 0.02 g/ml]. The polymer size was found to swell with increasing temperature and CO_2 density as confirmed by variations of the hydrodynamic radius R_h.

Both the hydrodynamic radius expansion factor and the normalized second virial coefficient of PFOMA dissolved in CO_2 were verified to be functions of the interaction parameter z,

which is proportional to $N^{1/2}[1-\theta(\rho)/T]$. This is in excellent agreement with data for other polymers dissolved in traditional organic solvents. We have for the first time demonstrated that the hydrodynamic radius expansion factor α_h and the normalized second virial coefficient are also functions of the same interaction parameter *z* and are proportional to the reduced solvent density $N^{1/2}\left[1-\rho_\theta(T)/\rho\right]$ at constant temperature. We have determined and theoretically justified reciprocal dependence of the theta temperature on CO_2 density for PFOMA as $\theta(\rho)=(260/\rho)(\text{gK/mL})$. These results provide an important explanation of the observation that the solvent quality can be tuned by not only the solvent temperature but also the solvent density in a universal way.

We have also established that the hydrodynamic radius expansion factor can be expressed as a single function of the normalized second virial coefficient, independently of the methods used to vary the solvent quality.

$$\alpha_h = 1 + \frac{C^R}{C^{A_2}} A_2 M_w^{1/2} \frac{M_0^{3/2}}{N_{av} b^3}$$

Note that coefficients are $C^R/C^{A_2} = 0.12 \pm 0.02$ for PFOMA in CO_2 and 0.2 ± 0.03 for PS and PMMA solutions. The non-universality of the ratio of coefficients C^R/C^{A_2} indicated the existence of additional physical interactions that were not considered in existing polymer models.

The investigations of polymer solutions prepared in CO_2 in this chapter have laid the ground work for many future directions:

1) The radius of gyration of low molecular weight PFOMA fractions in CO_2 could not be measured by static light scattering because it was beyond the detector limit. Small angle neutron scattering (SANS) is a better tool to

observe smaller size particles. Another important parameter, the radius of gyration expansion factor, could be obtained to testify the validity of interaction parameter functions.

2) Only two PFOMA fractions (two molecular weights) have been investigated by light scattering. It is hard to address the influence of molecular weight on polymer solution behavior with just two different molecular weight fractions. The light scattering studies could be extended to other PFOMA fractions with higher molecular weights, or even other fluorinated oligomers and polymers.

3) The temperature and density range in this work was only narrowed to near θ-region. The experiment conditions could be broadened to the bad or good solvent region to complete the phase diagram of $scCO_2$. These operations might rely on improvements of current experiment setup, especially modifications of the optical light scattering cell are essential.

Appendix A. High Pressure Light Scattering Apparatus

Static and dynamic light scattering (SLS and DLS) experiments in CO_2 were performed by the means of a spectrometer equipped with an argon ion laser (Coherent Innova 70-3) operating at λ=514 nm, a BI9000 correlator from Brookhaven Instrument, and a computer-controlled and stepping-motor-driven variable angle detection system. Scattering experiments were performed using the rectangular high pressure cell shown in Figure A-1 and A-2. The rectangular cell was designed to operate at pressures up to 420 bar and was constructed to fit on the top of a BI-200SM goniometer without modification. The high pressure rectangular cell was made of alloy tool steel and was heat-treated for strength. Two circular sapphire windows are positioned on both sides of the cell for the laser light to go through. The polymer concentration in the cell can be lowered by increasing the inner volume from 10.6 to 48.8 mL using a stainless steel cylindrical piston. The scattering was measured through a band-pass filter (514.5 nm) and a pinhole (400 μm for the static and 200 μm for the dynamic experiment) with a photomultiplier tube (BI-PMT9836).

The carbon dioxide light scattering cell offers a good opportunity not only to explore much wider angle range, but also to tune the concentration by varying the volume of the cell. The carbon dioxide was filtered using a 0.5 μm porous metal filter (Swagelok Co.) and the pressure was measured by a pressure transducer (Sensotoc TJF/743-11). The external detection angle was from 25^o to 155^o which gives the wavefactor q range from 0.010 to $0.027 nm^{-1}$. All the DLS experiments were performed with angles 40^o, 90^o and 140^o.

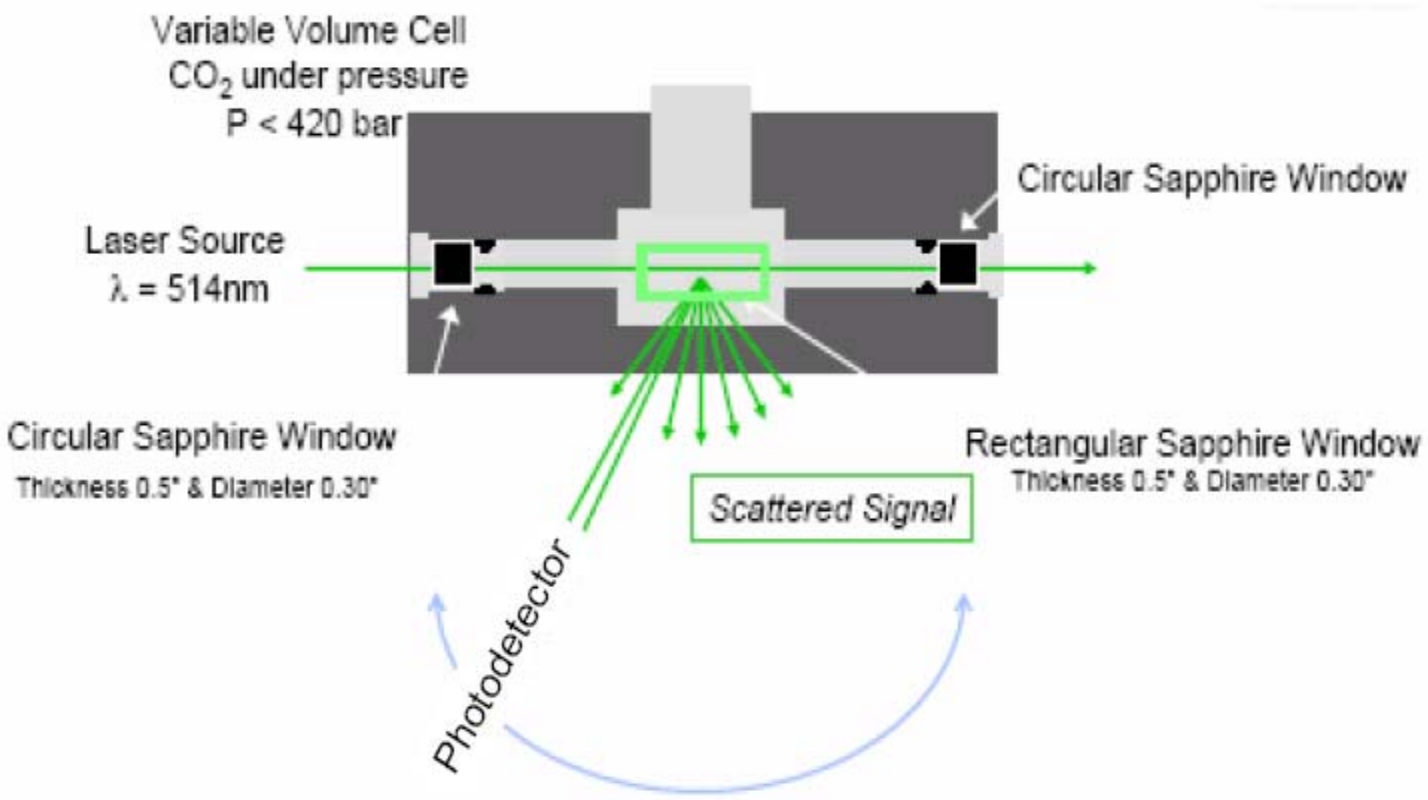

Figure A-1 Scheme of the high pressure light scattering optical cell.

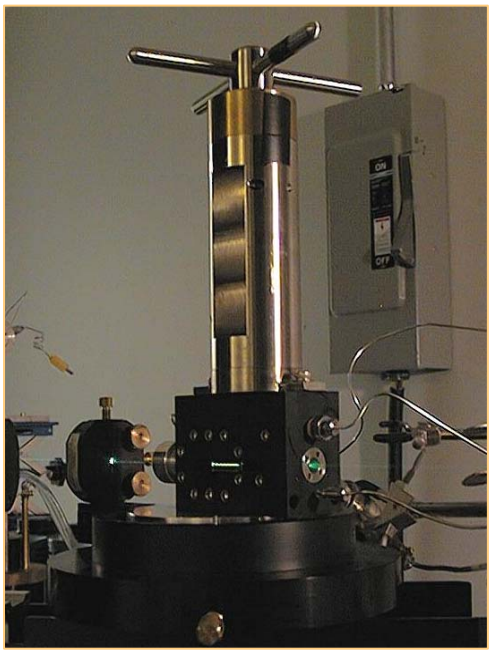

Figure A-2 Photo of the high pressure light scattering apparatus

II-7 References

(1) DeSimone, J. M.; Guan, Z.; Elsbernd, C. S. *Science* **1992**, *257*, 945-947.

(2) Quinn, E. L.; Jones, C. L. *Carbon dioxide*; Reinhold Publishing Corporation: New York, 1936.

(3) McHugh, M. A.; Krukonis, V. J. *Supercritical Fluid Extraction: Principles and Practice*, 2nd ed. ed.; Butterworth-Heineman: stoneham, 1993.

(4) Johnston, K. P.; Barry, S. E.; Read, N. K.; Holcomb, T. R. *Ind Eng Chem Res* **1987**, *26*, 2372-2377.

(5) Johnston, K. P. *Acs Sym Ser* **1989**, *406*, 1-12.

(6) Jacobson, G. B.; Lee, C. T.; Johnston, K. P. *J Org Chem* **1999**, *64*, 1201-1206.

(7) DeSimone, J. M. *Science* **1995**, *269*, 1060-1061.

(8) DeSimone, J. M. *Science* **2002**, *297*, 799-803.

(9) Garg, A.; Gulari, E.; Manke, C. W. *Marcromolecules* **1994**, *27*, 5643-5653.

(10) Tomasko, D. L.; LI, H.; Liu, D.; Han, X.; Wingert, M. J.; J., L. L.; Koelling, K. W. *Ind. Eng. Chem. Res.* **2003**, *42*, 6431-6456.

(11) DeSimone, J. M.; Maury, E. E.; Menceloglu, Y. Z.; Mcclain, J. B.; Romack, T. J.; Combes, J. R. *Science* **1994**, *265*, 356-359.

(12) Adamsky, F. A.; Beckman, E. J. *Macromolecules* **1994**, *27*, 312-314.

(13) Dillow, A. K.; Yun, S. L.; Suleiman, D. S.; Boatright, D. L.; Liotta, C. L.; Eckert, C. A. *Ind. Eng. Chem. Res.* **1996**, *35*, 1801-1806.

(14) Johnston, K. P.; Harrison, K. L.; Clarke, M. J.; Howdle, S. M.; Heitz, M. P.; Bright, F. V.; Carlier, C.; Randolph, T. W. *Science* **1996**, *271*, 624-626.

(15) Randolph, T. W. *Trends Biotechnol.* **1990**, *8*, 78.

(16) McAllister, K.; Sazani, P.; Adam, M.; Cho, M. J.; Rubinstein, M.; Samulski, R. J.; DeSimone, J. M. *J Am Chem Soc* **2002**, *124*, 15198-15207.

(17) Lemert, R. M.; Johnston, K. P. *Ind. Eng. Chem. Res.* **1991**, *30*, 1222.

(18) Kirby, C. F.; McHugh, M. A. *Chem Rev* **1999**, *99*, 565-602.

(19) McHugh, M. A.; Garach-Domech, A.; Park, I.; Li, D.; Barbu, E.; Graham, P.; Tsibouklis, J. *Macromolecules* **2002**, *35*, 6479-6482.

(20) Oshea, K. E.; Kirmse, K. M.; Fox, M. A.; Johnston, K. P. *J Phys Chem-Us* **1991**, *95*, 7863-7867.

(21) Shim, J. J.; Johnston, K. P. *Aiche J* **1991**, *37*, 607-616.

(22) Mertdogan, C. A.; S., B. H.; McHugh, M. A.; Tuminello, W. H. *Macromolecules* **1996**, *29*, 6548-6555.

(23) Mertdogan, C. A.; DiNoia, T. P.; McHugh, M. A. *Macromolecules* **1997**, *30*, 7511-7515.

(24) O'Neill, M. L.; Cao, Q.; Fang, R.; Johnston, K. P.; Wilkinson, S. P.; Smith, C. D.; Kerschner, J. L.; Jureller, S. H. *Ind Eng Chem Res* **1998**, *37*, 3067-3079.

(25) Rindfleisch, F.; DiNoia, T. P.; McHugh, M. A. *J. Phys. Chem.* **1996**, *100*, 15581-15587.

(26) Mertsch, R.; Wolf, B. A. *Macromolecules* **1994**, *27*, 3289.

(27) Cotts, P. M. *Macromolecules* **1994**, *27*, 6487.

(28) Fulton, J. L.; Pfund, D. M.; McClain, J. B.; Romack, T. J.; Maury, E. E.; Combes, J. R.; Samulski, E. T.; DeSimone, J. M.; Capel, M. *Langmuir* **1995**, *11*, 4241 - 4249.

(29) Guan, Z. In *Department of Chemistry*; University of North Carolina: Chapel Hill, 1994.

(30) Chu, B.; Lin, J. S. *J. Chem. Phys.* **1970**, *53*, 4454.

(31) Nagashima, K.; Lee, C. T.; Xu, B.; Johnston, K. P.; DeSimone, J. M.; Johnson, C. S. *J Phys Chem B* **2003**, *107*, 1962-1968.

(32) Folk, S. L. In *Department of Chemistry*; University of North Carolina: Chapel Hill, 2003.

(33) Rubinstein, M.; Colby, R. H. *Polymer physics*; Oxford University Press: New York, 2003.

(34) Liu, T. B.; Nace, V. M.; Chu, B. *J Phys Chem B* **1997**, *101*, 8074-8078.

(35) Liu, T. B.; Nace, V. M.; Chu, B. *J Phys Chem B* **1998**, *102*, 1065-1065.

(36) Consani, K. A.; Smith, E. D. *Journal of Supercritical Fluids* **1990**, *3*, 51-65.

(37) Clarke, M. J.; Harrison, K. L.; Johnston, K. P.; Howdle, S. M. *J Am Chem Soc* **1997**, *119*, 6399-6406.

(38) Heitz, M. P.; Carlier, C.; deGrazia, J.; Harrison, K. L.; Johnston, K. P.; Randolph, T. W.; Bright, F. V. *J Phys Chem B* **1997**, *101*, 6707-6714.

(39) McDonald, C. J.; Claesson, S. *Chemica Scripta* **1976**, *9*, 36-46.

(40) Zhou, S. Q.; Chu, B. *Macromolecules* **1998**, *31*, 5300-5308.

(41) Berger, T.; Steffen, W. *Rev Sci Instrum* **2000**, *71*, 2467-2470.

(42) Sherman, M. A.; Kennedy, J. P.; L;, E. D.; D, S. *Journal of Biomaterials Science. Polymer edition* **1999**, *10*, 259-269.

(43) McClain, J. B.; Londono, J. D.; Betts, D. E.; Canelas, D. A.; Samulski, E. T.; Wignall, G. D.; DeSimone, J. M. *Abstr Pap Am Chem S* **1996**, *211*, 145.

(44) McClain, J. B.; Londono, D.; Combes, J. R.; Romack, T. J.; Canelas, D. A.; Betts, D. E.; Wignall, G. D.; Samulski, E. T.; DeSimone, J. M. *J Am Chem Soc* **1996**, *118*, 917-918.

(45) Johnston, K. P.; Cho, D. M.; DaRocha, S. R. P.; Psathas, P. A.; Ryoo, W.; Webber, S. E.; Eastoe, J.; Dupont, A.; Steytler, D. C. *Langmuir* **2001**, *17*, 7191-7193.

(46) Xu, B.; Lynn, G. W.; Guo, J.; Melnichenko, Y. B.; Wignall, G. D.; McClain, J. B.; DeSimone, J. M.; Johnson, J., C. S. *Journal of Physical Chemistry B* **2005**, *109*, 10261-10269.

(47) Buhler, E.; Dobrynin, A. V.; DeSimone, J. M.; Rubinstein, M. *Macromolecules* **1998**, *31*, 7347-7355.

(48) Andr? P.; Folk, S. L.; Adam, M.; Rubinstein, M.; DeSimone, J. M. J *Phys Chem A* 2**004,** 1*08,* 9901-9907.

(49) Wignall, G. D.; Melnichenko, Y. B.; Triolo, R.; McClain, J. B.; DeSimone, J. M. A*bstr Pap Am Chem S* 2**001,** 2*21,* U374-U375.

(50) ChilluraMartino, D.; Triolo, R.; McClain, J. B.; Combes, J. R.; Betts, D. E.; Canelas, D. A.; DeSimone, J. M.; Samulski, E. T.; Cochran, H. D.; Londono, J. D. J*ournal of Molecular Structure* 1**996,** 3*83,* 3-10.

(51) Otake, K.; Webber, S. E.; Munk, P.; Johnston, K. P. L*angmuir* 1**997,** 1*3,* 3047-3051.

(52) Yates, M. Z.; ONeill, M. L.; Johnston, K. P.; Webber, S.; Canelas, D. A.; Betts, D. E.; DeSimone, J. M. M*acromolecules* 1**997,** 3*0,* 5060-5067.

(53) Harrison, K. L.; da Rocha, S. R. P.; Yates, M. Z.; Johnston, K. P.; Canelas, D.; DeSimone, J. M. L*angmuir* 1**998,** 1*4,* 6855-6863.

(54) Zhou, S. Q.; Chu, B. M*acromolecules* 1**998,** 3*1,* 7746-7755.

(55) Liu, L. Z.; Cheng, Z. G.; Inomata, K.; Zhou, S. Q.; Chu, B. M*acromolecules* 1**999,** 3*2,* 5836-5845.

(56) Wells, S. L.; Buhler, E.; Dobrynin, A.; DeSimone, J. M.; Rubinstein, M. A*bstr Pap Am Chem S* 1**999,** 2*17,* U604-U604.

(57) Johnston, K. P. C*urr Opin Colloid In* 2**000,** 5*,* 351-356.

(58) Li, G.; Yates, M. Z.; Johnston, K. P.; Kim, K. T.; Webber, S. E. M*acromolecules* 2**000,** 3*3,* 1606-1612.

(59) Triolo, F.; Triolo, A.; Triolo, R.; Londono, J. D.; Wignall, G. D.; McClain, J. B.; Betts, D. E.; Wells, S.; Samulski, E. T.; DeSimone, J. M. L*angmuir* 2**000,** 1*6,* 416-421.

(60) Psathas, P. A.; Sander, E. A.; Ryoo, W.; Mitchell, D.; Lagow, R. J.; Lim, K. T.; Johnston, K. P. J *Disper Sci Technol* 2**002,** 2*3,* 81-92.

(61) Lee, C. T.; Ryoo, W.; Smith, P. G.; Arellano, J.; Mitchell, D. R.; Lagow, R. J.; Webber, S. E.; Johnston, K. P. J *Am Chem Soc* 2**003,** 1*25,* 3181-3189.

(62) Schulz, G. V.; Inagaki, H.; Kirste, R. *Zeitschrift fuer Physikalische Chemie (Muenchen, Germany)* 1**960,** 2*4,* 290-404.

(63) Huglin, M. B. L*ight Scattering From Polymer Solutions;* academic press: London and New York, 1972.

(64) Cotton, J. P.; Nierlich, M.; Boue, F.; Farnoux, B.; Daoud, M.; Jannink, G.; R.Duplessix; Picot, C. J *Chem Phys* 1**976,** 6*5,* 1101.

(65) de Gennes, P.-G. S*caling concepts in polymer physics;* Cornell University Press: Ithaca, N.Y., 1979.

(66) Flory, P. J. P*rinciples of Polymer Chemistry;* Cornell University Press: Ithaca, NY, 1953.

(67) Berry, G. C. J *Chem Phys* 1**966,** 4*4,* 4550-4564.

(68) Withers, I. M.; Dobrynin, A. V.; Berkowitz, M. L.; Rubinstein, M. J *Chem Phys* 2**003,** 1*18,* 4721-4732.

(69) Yamakawa, H.; Yoshizaki, T. J *Chem Phys* 2**003,** 1*19,* 1257-1270.

(70) Yamakawa, H.; Yoshizaki, T. J *Chem Phys* 2**003,** 1*18,* 2911-2918.

(71) Abe, F.; Einaga, Y.; Yoshizaki, T.; Yamakawa, H. M*acromolecules* 1**993,** 2*6,* 1884-1890.

(72) Abe, F.; Horita, K.; Einaga, Y.; Yamakawa, H. M*acromolecules* 1**994,** 2*7,* 725-732.

(73) Kamijo, M.; Abe, F.; Einaga, Y.; Yamakawa, H. M*acromolecules* 1**995,** 2*8,* 1095-1102.

(74) Yamada, M.; Osa, M.; Yoshizaki, T.; Yamakawa, H. M*acromolecules* 1**997,** 3*0,* 7166-7170.

(75) Abe, F.; Einaga, Y.; Yamakawa, H. M*acromolecules* 1**993,** 2*6,* 1891-1897.

(76) Horita, K.; Abe, F.; Einaga, Y.; Yamakawa, H. M*acromolecules* 1**993,** 2*6,* 5067-5072.

(77) Yoshizaki, T.; Yamakawa, H. J *Chem Phys* 1**996,** 1*05,* 5618-5625.

(78) Tominaga, Y.; Suda, I.; Osa, M.; Yoshizaki, T.; Yamakawa, H. M*acromolecules* 2**002,** 3*5,* 1381-1388.

(79) Yamakawa, H.; Stockmayer, W. H. J *Chem Phys* 1**972,** 5*7,* 2843.

(80) Yamakawa, H.; Shimada, J. J *Chem Phys* 1**985,** 8*3,* 2607-2611.

(81) Yamakawa, H. A*nnu Rev Phys Chem* 1**984,** 3*5,* 23-47.

(82) Shimada, J.; Yamakawa, H. J*ournal of poymer Science Polymer Physics Edition* 1**978,** 1*6,* 1927.

(83) Arai, T.; Abe, F.; Yoshizaki, T.; Einaga, Y.; Yamakawa, H. M*acromolecules* 1**995,** 2*8,* 5458-5464.

(84) Yamakawa, H. M*odern Theory of Polymer Solutions;* Harper and Row: New York, 1970.

(85) Schulz, G. V.; Lechner, A. In L*ight scattering from polymer solutions;* Huglin, M. B., Ed.; Academic Press: New York, 1972.

(86) Chu, B. A*ppl Optics* 1**997,** 3*6,* 7650-7656.

(87) Withers, I. M.; Dobrynin, A. V.; Rubinstein, M. i*n preparation.*

(88) Andersson, G. R. A*rkiv Kemi* 1**963,** 2*0,* 513.

(89) Schulz, G. V.; Lechner, A. L*ight scattering from polymer solutions: Influence of pressure and temperature (chap 12);* Huglin, M. B.; Academic Press: New York, 1972.

(90) Saeki, S.; Kuwahara, N.; Nakata, N.; Kaneto, M. P*olymer* 1**975,** 1*6,* 445-449.

(91) Fytas, G.; Dorfmuller, T.; Chu, B. J *Polym Sci Pol Phys* 1**984,** 2*2,* 1471-1481.

(92) Kubota, K.; Kubo, K.; Ogino, K. B*ulletin of the Chemical Society of Japan* 1**976,** 4*9,* 2410-2418.

(93) Gaeckle, D.; Patterson, D. M*acromolecules* 1**972,** 5*,* 136-141.

(94) DiNoia, T. P.; Kirby, C. F.; van Zanten, J. H.; McHugh, M. A. M*acromolecules* 2**000,** 3*3,* 6321-6329.

(95) Londono, J. D.; Dharmapurikar, R.; Cochran, H. D.; Wignall, G. D.; McClain, J. B.; Betts, D. E.; Canelas, D. A.; DeSimone, J. M.; Samulski, E. T.; Chillura-Martino, D.; Triolo, R. J*ournal of Applied Crystallography* 1**997,** 3*0,* 690-695.

(96) McClain, J. B.; Betts, D. E.; Canelas, D. A.; Samulski, E. T.; DeSimone, J. M.; Londono, J. D.; Cochran, H. D.; Wignall, G. D.; ChilluraMartino, D.; Triolo, R. S*cience* 1**996,** 2*74,* 2049-2052.

(97) Burns, R. C.; Graham, C.; Weller, A. R. M. M*ol Phys* 1**986,** 5*9,* 41-64.

(98) Chu, B. L*aser light scattering: basic principles and practice,* 2nd ed. ed.; Boston : Academic Press, 1991.

(99) Arai, T.; Abe, F.; Yoshizaki, T.; Einaga, Y.; Yamakawa, H. M*acromolecules* 1**995,** 2*8,* 3609-3616.

(100) Huglin, M. B. J *Appl Polym Sci* 1**965,** 9*,* 3963-4001 & 4003-4024.

(101) Melnichenko, Y. B.; Kiran, E.; Heath, K. D.; Salaniwal, S.; Cochran, H. D.; Stamm, M.; Van Hook, W. A.; Wignall, G. D. J *Appl Crystallogr* 2**000,** 3*3,* 682-685.

(102) Akcasu, A. Z. P*olymer* 1**981,** 2*2,* 1169-1180.

(103) Nose, T.; Chu, B. M*acromolecules* 1**979,** 1*2,* 1122.

(104) Chu, B.; Nose, T. M*acromolecules* 1**980,** 1*3,* 122-132.

(105) Konishi, T.; Yoshizaki, T.; Saito, T.; Einaga, Y.; Yamakawa, H. M*acromolecules* 1**990,** 2*3,* 290-297.

(106) Mitsuo, N. P*hys Rev E* 1**995,** 5*1,* 5770.

PART II

ALTERNATIVE FLUOROPOLYMERS TO THE AVOID CHALLENGES ASSOCIATED WITH PERFLUOROOCTANOIC ACID

II-1 Introduction

II-1.1 Repellency

Dew drops naturally bead up on the surface of plant leaves. This special property, called repellency, was then introduced to man-made fabrics by textile treating. Repellency is a condition of limited wetting, normally regarded as resistance to water and oil under static conditions. The resistance of a fabric to penetration and wetting of a liquid depends on the chemical compositions, geometry and roughness of fiber surfaces, as well as the mesh spaces between the fibers.[1]

Two methods are commonly used to predict the chemical nature and surface tensions of the resistant materials. One measurement is the critical surface tension, first proposed by Zisman and defined to be the surface tension of a liquid that just spreads on the solid surface.[2] It is a very useful tool in mapping out water and oil-repellency finishes. The critical surface tensions of some common polymeric materials are summarized in Table 2.1. Liquids with a lower surface tension will bead up to form a finite contact angle on the surface. However, there are several limitations to this technique. For instance, several contact angle measurements involving a series of homolog liquids are needed to determine the critical surface tension of an unknown solid (Zisman plot). In addition, Zisman plots may not be completely linear, i.e. it has some curvature even for a homolog series, which can cause considerable error when extensive extrapolation is necessary. Therefore, another approach has been made to evaluate the surface free energy of solids, known as the Owen-Wendt-Fowkes method.[3-5] In this method, only two or three liquids, such as water and diiodidemethane are needed for the measurements. The surface free energy of a solid is the sum of the contributions from intermolecular forces on the surface, dispersion forces and

Table 2.1 Critical surface tensions (γ_c)[6,7] and surface free energies (γ_s)[3,8] of common polymers.

Polymer	γ_c (mN / m)	γ_s (mN / m)
Perfluoroalkyl polyacrylates	10-11	8-10
Poly(tetrafluoroethylene)	18	19
Poly(trifluororthylene)	22	24
Poly(vinylidene fluoride)	25	30
Polyethylene	31	33
Polystyrene	33	42
Poly(vinyl alcohol)	37	-
Poly(methyl methacrylate)	39	40
Polysiloxane	24	-

hydrogen bonding forcers. Table 2.1 summarizes surface tensions of common polymers measured by both Zisman analysis and Owen-Wendt-Fowkes method. In general, the two measurements reasonably agree with each other. It is known that water has a high surface tension of 72.8 mN / m at 25 ^{o}C and hydrocarbon oils have values that range from 20 to 30 mN / m. Hence, mmaterials containing hydrocarbon or polysiloxane are sufficient enough for water repellency. In order to repel oil, fluorinated materials with surface tension of 15 mN / m or lower are needed in order to be effective repellent materials.

Repellency tests for treated textiles in industry include two parts, the water-repellency test and oil-repellency by measuring the contact angle of two liquids against a solid surface. The water repellency test can be further divided into three main classes: spray test, hydrostatic pressure test, and water sorption. The spray test is the most frequently used one and it is the simulation of exposure to the rain. Figure 2.1 is the AATCC spay tester developed by the DuPont Co. Oil repellency is tested by placing a drop of oil on the fabric and observing the resistance of the oil by the fabric. As shown in Figure 2.2, a series of homolog hydrocarbons are used to rate oil repellency.

Spill resistance and durability of the textile are also very important criterion in addition to repellency. Spill resistance is the ease of removing a liquid from a solid surface, which is the repellency performance under dynamic conditions. It is quantified by contact angle measurements. Durability indicates the maxim time of the textile performance, and it is influenced by the deposition method of the textile treating agents on the fabric.

AATCC Spray Tester.

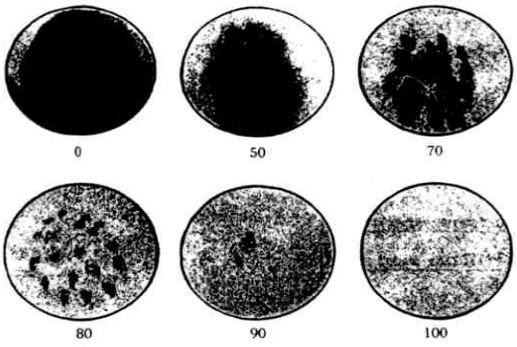

0: Indicates wetting on the entire surface and back.

50: Indicates wetting on the entire surface.

70: Indicates wetting on half of the surface with some wetting penetrating through the cloth.

80: Indicates small drops of wetting on the surface.

90: Indicates no wetting, but small water drops on the surface.

100: Indicates no wetting, nor water drops on the surface.

Figure 2.1 Water repellency test: AATCC spray tester.[9]

Oil Repellency Test

AATCC test method 118-1992

Standard Test Liquids

AATCC Oil Repellency Grade Number	Composition
0	None(Fails;liquid paraffin)
1	Liquid paraffin
2	65:35 Liquid paraffin:n-hexadecane by volume
3	n-hexadecane
4	n-tetradecane
5	n-dodecane
6	n-decane
7	n-octane
8	n-heptane

Grading Example

A = Passes; clear well-round drop
B = Borderline pass; rounding drop with partial darkening
C = Fails; wicking apparent and/or complete wetting
D = Fails; complete wetting

Figure 2.2 Oil repellency test.[9]

II-1.2 Conventional fluorinated repellents

A very important process in the textile industry involves imparting stain resistance properties to fabric by treating with different finishing materials called repellents. Fabrics treated with repellent materials have the ability to repel water and oil, and to withstand wetting and penetration by liquid soil. According to different chemical compositions, repellents can be classified as hydrocarbon, polysiloxane and fluorocarbon hydrophobes. Of the three, only the fluorinated repellents are both hydrophobic and oleophobic and thus, can be used as stain resistant materials.

In general, the repellency of fluorinated materials is determined by the ratio of fluorinated and non-fluorinated segments, the orientation of the fluorinated tails, the distribution of the fluorocarbon moiety on fibers, and the composition and geometry of the fibers.[1] Approximately ten fully fluorinated carbon atoms must be present in an alkane chain in order to achieve maximum repellency, and linear perfluoroalkane chains are more effective than branched chains with an equal number of fluorocarbon atoms.[10] The highest repellency is obtained from surfaces comprised of closely-packed $–CF_3$ groups. Therefore, most commercially available polymeric fluorinated repellents are acrylates or methacrylates. These polymers are comprised of long perfluoroalkyl groups (over eight fluorocarbons long) as the pedants of the side chains. Usually the fluorinated pendant is a mixture of different perfluorocarbon lengths. The polymer backbone and perfluoro groups are separated by non-fluorinated linkages, known as “spacers”. The performance of fluorinated materials are reported to depend on the identity of the spacers. Table 2.2 lists some patents of fluorinated textile treating materials. Other fluorinated repellants include vinyl ethers, vinyl esters, allyl esters and thiomethacrylates.

Table 2.2 Some patents of fluorinated repellents.[9]

Patent	Date issued	Inventor	Assignee	Structure of monomers
Ger. Offen. 1,918,079	1969	E. Kleiner, M. Knell	Geigy	Fluorinated esters of fumaric acid.
U.S. 3,462,296	1969	S. Raynolds, T. K. Tandy	Du Pont	~75% (I) $CH_2{=}C(CH_3){-}COOCH_2CH_2C_nF_{2n+1}$ (n = 6, 8, 10) ~25% (II) 2-ethylhexyl methacrylate 0.25% (III) 2-hydroxyethyl methacrylate 0.25% (IV) *N*-methylolacrylamide Polymer mixed with terpolymer of II, IV, and ethylene dimethacrylate
U.S. 3,424,785	1969	A. G. Pittman, W. L. Wasley	U. S. Dept. of Agric.	$FC(CF_3)_2O(CH_2)_5OCOCH{=}CH_2$
U.S. 3,529,995	1970	S. Smith	3M	Fluorinated acrylate of methacrylate 1 hydroxyalkyl acrylate or methacrylate, e.g., $(C_8F_{17})_2CC(CH_3){=}CH_2$ $HOC_3H_6O_2CC(CH_3){=}CH_2$ $C_8F_{17}SO_2N(CH_3){-}C_{11}H_{22}{-}O_2C{-}C(CH_3){=}CH_2$ $CH_2(O)CH{-}CH_2O_2C{=}CH_2$ (CH_3)
Br. 1,123,829	1968	P. O Sherman		
U.S. 3,491,169	1970	S. Raynolds, R. E. Read	Du Pont	$CH_2{=}C(CH_3)CO_2(CH_2)C_nF_{2n+1}$ (n = 6, 8, 10, copolymerized with lauryl methacrylate, *N*-methylol acrylamide, 2-hydroxethyl methacrylate)
U.S. 3,497,575	1970	E. K. Kleiner, P. L. Pacini	Geigy	$F_{2n+1}C_nCONH(CH_2)_2SCOC(CH_3){=}CH_2$ or copolymer with octyl methacrylate
Ger. Offen. 2, 115,612	1971	H. Jaeger	Ciba-Geigy	$CF_3(CF_2)_6CH_2CH_2{-}CH(CH_2OH){-}CH_2CH_2O_2C(CH_3){=}CH_2$
Jap. 7,526,783	1975	H. Ukihashi, T. Hayashi	ASAHI	$CH_2{=}CRCO_2CH_2CH_2N$ (R = H, CH_3, copolymers e.g., with methyl methacrylate and $C_nF_{2n+1}(CH_2CF_2)_mCH_2CH_2O_2CH{=}CH_2$; ($n$ = 4, 6, 8, 10, 12; m = 1, 2, 3)
Ger. Offen. 2,609,462	1977	K. Waldmann	Hoechst	$C_nF_{2n+1}CH_2CH_2O_2CCH{=}CH_2$ (n = 6–12 + C_{10}–C_{16} alkyl acrylates + vinylidene chloride + butyl *N*-acrylolylurethane

The manufacture of fluorinated repellents are based on either electrochemical fluorination or telomerization of the tetrafluoroethylene. A typical telomerization involves the reaction of tetrafluoroethylene with iodofluoroalkane to produce telomers with different lengths of carbon chains. The synthesized telomers are used to react with ethylene to obtain different alkyl iodides. The alkyl iodides are readily converted into the corresponding fluorinated alcohols or amines for synthesis of fluorinated acrylates or methacrylates.[11,12] Fluorinated repellents based on different telomers have been widely used in coating and textile area to supply resistance to the fabrics.

$$C_2F_5I + nC_2F_4 \longrightarrow C_2F_5I(C_2F_4)_nI \longrightarrow C_2F_5(C_2F_4)_nOH$$

In order to lower the cost and improve the performance, a large majority of repellents are copolymers comprising of fluorinated and non-fluorinated monomers or mixture of fluoropolymers and a non-fluorinated extender (acrylic or methacrylic type). The structure of the non-fluorinated parts and their incorporation ratio of the copolymers play an important role of the performance of such materials. Varied hydrocarbon monomers are introduced as co-monomers, including vinyl acetate (stearyl methacrylates), vinyl chloride, vinylidene chloride, maleic anhydride, 2-ethylhexy; methacrylate, hydroxyethyl methyacrylate, glycidyl methacrylate, terbutyl methacrylate etc. Co-monomers with cross-linking functions such as hydroxyl, epoxyl or vinyl groups are used to increase the durability of the repellent materials.

II-1.2 Environmental challenges

In the late 1990's, perfluorooctyl sulfonates (PFOS) were found to be widespread in the blood of the general population, and presented concerns for persistence, bioaccumulation, and toxicity.[13,14 13,14] As a result, 3M Company terminated production of these chemicals in 2000. This finding prompted the US Environmental Protective Agency (EPA) to investigate similar chemicals, including perfluorooctanoic acid (PFOA), to determine whether they might present similar concerns to those associated with PFOS. The EPA found that PFOA was very persistent and has a long half life in the environment.[14] Moreover, according to the Centers for Disease Control and Prevention (DCP), an estimated 95 percent of the population in the United States has the chemical in their blood albeit at very low levels. In addition, both toxicity and exposure studies indicated that PFOA can cause developmental issues and other adverse effects in laboratory animals and is a "likely" carcinogen.

PFOA, also called as C8, is a synthetic chemical that has been used for almost 40 years in a wide range of commercial applications under a variety of brand names. These compounds are directly used as the surfactants in the manufacture of polytetrafluoroethylene (PTFE). However, most of the PFOA found in the environment is believed to be from the gradual degradation of products derived from fluorinated telomers, short-chain fluorinated alcohols used as stain- and grease-resistant coatings on carpets, textiles, and paper.[15-18] Fluorotelomers can form a protective layer on fabrics and slowly degraded to PFOA by oxidization in the environment. Ellis et al. reported the degradation path of different fluorotelomer alcohols in the atmosphere as shown in Figure 2.3.[15,17] PFOA tends to accumulate in cells possibly due to its amphiphilicity, having both hydrophobic (water-repelling) and hydrophilic (water-loving) parts, which is similar to the cell membrane

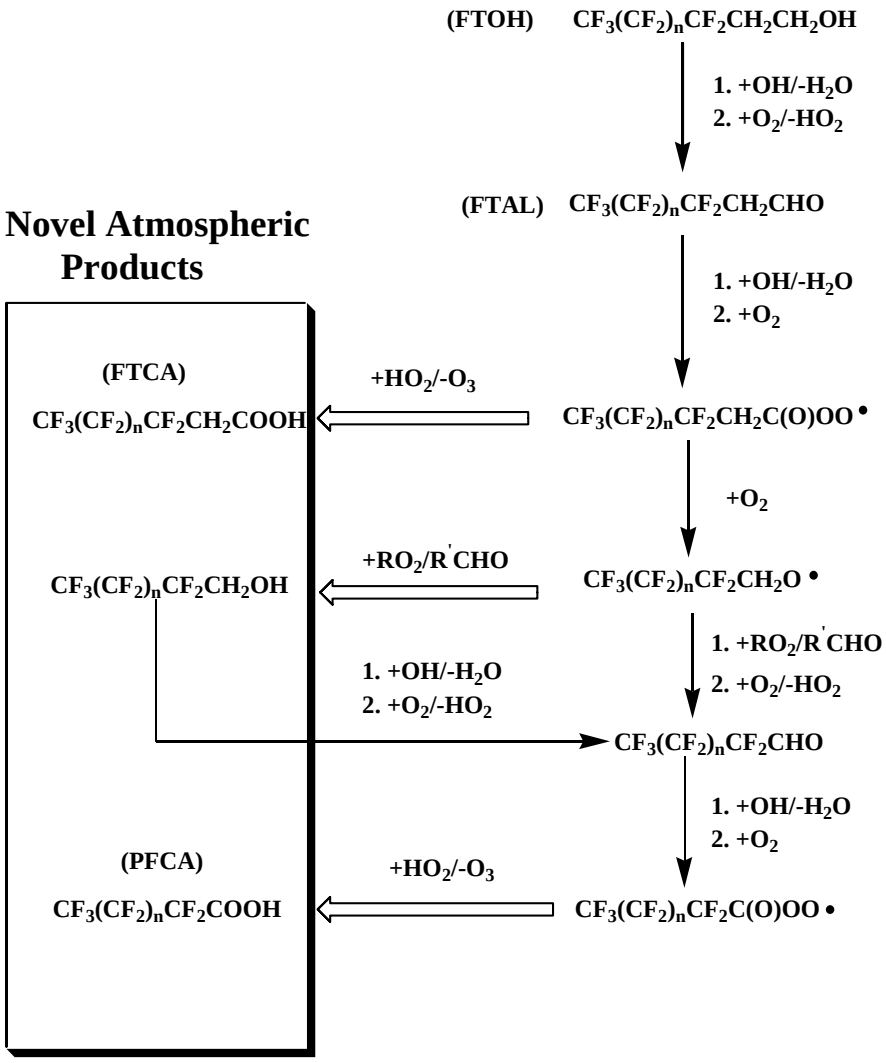

Figure 2.3 Degradation of the fluorinated alcohols in the atmosphere to produce PFOA.[15]

structure. The high durability, strong bond strength, and low solubility in water of these chemicals make it difficult to remove them from the human body. But it is still unclear how the chemicals are getting into the body and limited information is available about its long-term health effects.

The widespread occurrence, biopersistance and unexpected toxicity of PFOA have raised world wide environmental concerned. The U. S. EPA has released a preliminary risk assessment for the chemical PFOA recently, and it also encouraged the public and other interested parties to participate in its risk assessment actions.[16] Canada is temporarily banning three volatile fluorinated polymers used in stain repellents because they are suspected to be a source of long-chain perfluorocarboxylates.[23] Many countries have joined the force to start the survey of the level of PFOA and control of its release to human body and the environment.[19-22] It is envisioned that long chain perfluorocarboxylic acids such as PFOA and materials that may degrade to them will be severely restricted by the EPA and comparable agencies world wide in the near future. In 2006, Washington Post estimated that PFOA related chemicals will be eliminated by 2015. Thus, it is imperative that alternative materials be found in order to replace these conventional fluorinated repellents.

II-1.4 Current approaches

The potential substitute materials for the fluorinated repellent include silicones and perfluoropolyethers. Silicones (polysiloxane) are known for their hydrophobicity and so are traditionally used as water repellents materials. The outstanding feature of polysiloxane repellents is that they can soften the fabric in addition to the good water repellency.[23] The water repellence of fabrics finished with silicones is attributed to the unique orientation of the

polysiloxane chains: oxygen atoms oriented towards the fiber surface while methyl groups are exposed to outside. However, polysiloxanes do not provide oil repellency and stain resistance compared to fluorinated repellents. In fact, introduction of silicones may reduce the oil repellency.[24] The oil repellency is only obtained by combining polysiloxanes with fluorinated materials.[25-32] Although polysiloxanes have a low cost advantage over fluorinated polymers, they are not ideal competitive materials as substitute repellents for the C8 based materials.

Perfluoropolyethers (PFPE) are a low molecular weight perfluorinated liquids with a low glass transition temperature, $T_g << 0$ °C.[33-35] PFPE elastomers can be obtained by thermal or photo-chemical cross-linking.[33-35] PFPE materials exhibited very a low surface energy (~ 12 mN / m) and high chemical stability because of the fluorine rich moieties. Due to their hydrophobic and lipophobic properties,[36,37] PFPE materials have been widely used as coatings and components for microfluidic device [38], medical applications[39] and soft lithography. For example, the hydrophobic-oleophobic coatings were prepared by using the sol-gel process based on PFPE-polycapralactone copolymers.[40] However, PFPE-based polymers have limited solubility in water and common organic solvent, preventing the wide applicability of these materials in textile industry. Moreover, the cost of these materials is comparably expensive.

Instead of varying the compositions of materials, surface roughness and topography were also found to have substantial impact on the surface properties of polymer materials.[41-43] Many biological surfaces, such as the lotus leaf, have a hierarchically structured surface roughness which is optimized for superhydrophobicity through natural selection.[44] Two criteria define superhydrophobicity[45-48]: a very high water contact angle (over 150^o) and a

very low roll-off angle. Superhydrophobicity have important practical applications ranging from self-cleaning window glasses, paints, and fabrics to low-friction surfaces.[45-50] Superhydrsphobic polysiloxane finished microfibers displayed higher water contact angles and lower hysteresis, even better than the lotus leaf.[51] Perfluoropolyether materials with a lotus-leaf-like topography also exhibited superhydrophobic behaviors.[52] However, in most practical cases, it is not possible to modify the surface roughness without simultaneously affecting the chemical nature of the surface. The surface roughening will increase the heterogeneity of the surfaces and result in the exposure of bulk parts with different surface energies.

II-2 Objective and overview

R. Dams from 3M Company reported a systematic study on the biopersistance of perfluorinated chemicals in 14th European Symposium on Fluorine Chemistry.[53] It was found that perfluorinated carboxylic and sulfonic acids containing a short chain of four or less perfluorinated carbon atoms do not bioaccumulate, and therefore are not biopersistent as shown in Table 2.3. In order to find environmentally friendly and nontoxic alternative fluoropolymers to avoid the challenges associated with PFOA, a series of fluorinated comblike polymers containing the shorter and non-biopersistant perfluorobutyl group as the fluorinated component of the side chains, so called C4 materials, has been prepared starting from perfuorobutyl iodide with simple syntheses. [54-61] The advantage of the molecule design is that these new materials are the analog to the conventional textile treating materials with short perfluoro parts and they can be characterized and processed in a similar way as the current treating methods. In addition, the structures and properties of the polymers can be

tuned by changing the “spacers” between the backbones and the perfluorinated groups of the side chains. The “spacer” includes flexible methylene groups and stiff phenyl ring groups. Different characterization techniques will be applied to investigate the surface properties of the new C4 materials, especially the wetting properties and associated side chain packing.

Table 2.3 Biopersistence of different perfluorinated chemicals.[53]

Bioconcentration Factor			
Liver	Blood	Structure	
<1	<1	$C_4F_9SO_3^-$	
54	59	$C_6F_{13}SO_3^-$	
2900	3100	$C_8F_{17}SO_3^-$	
12	25	$C_7F_{15}COO^-$	C-8
1100	1900	$C_9F_{19}COO^-$	C-10
3800	5500	$C_{10}F_{21}COO^-$	C-11
11000	18000	$C_{11}F_{23}COO^-$	C-12
8700	20000	$C_{13}F_{27}COO^-$	C-14

II-3 Experimental

II-3.1 Materials

Chemicals purchased from Aldrich Co. included perfluorobutyl iodide, 5-hexanol, 4-penten-ol, 3-buten-1-ol, methacryloyl chloride, 1H,1H,2H,2H-nonafluoro-1-hexanol, 4-vinylbenzyl bromide, 4-vinylbenzyl chloride, acetonitrile, trifluorotoluene, terbutylammonium hydrogensulfate magnesium, iodine, zinc powder, copper (II) iodide and sodium dithionite. Glacial acetic acid, tetrahydrofuran, methanol, 2-propanol, sodium bicarbonate, magnesium sulfate, potassium hydroxide were purchased from the Fisher Sci. Co. 3-(Perfluorobutyl)propanol was purchased from Oakwood Product Inc. 1,1,1,3,3 – pentafluorobutane was purchased from Microcare Co. 1H,1H,2H,2H-nonafluorohexyl iodide and 3,3,4,4,5,5,6,6,6-Nonafluoro-1-petanol were purchased from Synquest Laboratories Inc. The initiator 2,2'-azobis(isobutyronitrile) (AIBN, Kodak, 99%) was recrystallized twice in methanol (Aldrich). All chemicals and solvents were used as received, except for tertrahydrofuran which was dried over sodium.

II-3.2 Monomer Synthesis

II-3.2.1 Methacrylates

General procedure for the synthesis of adduct 3a-3c (scheme 2.1)[55,56,62-66]

In a typical experiment, vinyl alcohols 2 (10 mmol), sodium dithionate (22 mmole) and sodium bicarbonate (22 mmole) were dissolved in an acetonitrile / water solution (10.0-10.0 mL) while stirring. Perfluorobutyliodide 1 (12 mmole) was added to slowly into the mixture and reacted at ambient temperature for at least 6 hours. Then the mixture was poured in water (ca. 50 ml) and extracted with ether (50 ml × 3). The combined organic layers was washed

with saturated brine and dried by anhydrous magnesium sulfate. Distill under reduced pressure gave the products 3a-3c. The yield is approximately 75% based on the unsaturated alcohol.

3a. Colorless oil. ^{1}HNMR ($CDCl_3$) δ 4.46 (m, 1H), 3.77 (t, 2H, J = 6.6 Hz), 2.86 (m, 2H), 1.98 (m, 2H). ^{19}FNMR ($CDCl_3$) – 81.89 (t, 3F, J = 9.6 Hz), -113.81 (m, 2F), -125.29 (s, 2F), -126.65 (m, 2F).

3b. Colorless oil. ^{1}HNMR ($CDCl_3$) δ 4.30 (m, 1H), 3.59 (t, 2H, J = 6.6 Hz), 2.79 (m, 2H), 1.83 (m, 2H), 1.69 (m, 2H). ^{19}FNMR ($CDCl_3$) – 82.07 (t, 3F, J = 9.6 Hz), -114.20 (m, 2F), -125.40 (s, 2F), -126.78 (m, 2F).

3c Colorless oil. ^{1}HNMR ($CDCl_3$) δ 4.26 (m, 1H), 3.55 (t, 2H, J = 6.6 Hz), 2.72 (m, 2H), 1.78 (m, 2H), 1.58 (m, 4H). ^{19}FNMR ($CDCl_3$) – 81.90 (t, 3F, J = 9.6 Hz), -114.34 (m, 2F), -125.42 (s, 2F), -126.82 (m, 2F).

General procedure for the synthesis of reducts 4a-4c (scheme 2.1)[57]

In a typical experiment, acetic acid (25 mL) was added dropwise into mixture of iodide alkane 3 (10 mmol), zinc dust (40 mmol) and anhydrous ether (20 mL) with stirring. The mixture was then heated to reflux temperature and reacted for 6 hours. The mixture was cooled and decanted, and the zinc slurry was washed with ether (10 mL × 3). The combined organic layer was washed and neutralized with saturated sodium bicarbonate solution (10 mL × 3). The collected water layer was washed with 10 mL ether and combined with ether extracts. After dried over magnesium sulfate, the crude products were distilled under reduced pressure to give 4a-4c. The yield is approximately 70 % based on the iodide alkane.

4a. Colorless oil. ^{1}HNMR ($CDCl_3$) δ 3.60 (t, 2H, J = 6.6 Hz), 2.04 (m, 2H), 1.61 (m, 4H). ^{19}FNMR ($CDCl_3$) – 81.79 (t, 3F, J = 9.6 Hz), -115.35 (m, 2F), -125.21 (s, 2F), -126.77 (t, 2F, J = 12.4 Hz).

4b. Colorless oil. ^{1}HNMR ($CDCl_3$) δ 3.65 (t, 2H, J = 6.6 Hz), 2.06 (m, 2H), 1.61 (m, 4H), 1.46 (m, 2H). ^{19}FNMR ($CDCl_3$) – 81.82 (t, 3F, J = 9.6 Hz), -115.39 (m, 2F), -125.24 (s, 2F), -126.80 (t, 2F, J = 12.4 Hz).

4c Colorless oil. ^{1}HNMR ($CDCl_3$) δ 3.61 (t, 2H, J = 6.6 Hz), 2.01 (m, 2H), 1.57 (m, 4H), 1.38 (m, 4H). ^{19}FNMR ($CDCl_3$) – 81.88 (t, 3F, J = 9.6 Hz), -115.41 (m, 2F), -125.27 (s, 2F), -126.84 (t, 2F, J = 12.4 Hz).

General procedure for the synthesis of methacrylate 5a-5e (scheme 2.1) [59,67,68]

Under an argon atmosphere, a solution of the fluorinated alcohol 4 (10 mmol) and triethylamine (5 mL) in anhydrous ether (100 mL) was cooled to 0 ^{o}C with an ice bath. Methacryloyl chloride (12.5 mmol) was added dropwise with stirring. The mixture was kept at 0 ^{o}C for 1 hour and then reacted at room temperature overnight. The precipitates were filtered off and the ether was evaporated. The crude product was purified by the silica gel column chromatography. The yield range is from 80 to 85%.

5a. Colorless oil. ^{1}HNMR ($CDCl_3$) δ 6.10 (s, 1H), 5.57 (s, 1H), 4.42 (t, 2H, J = 6.6 Hz), 2.48 (m, 2H), 1.91 (s, 3H). ^{19}FNMR ($CDCl_3$) – 81.72 (t, 3F, J = 9.6 Hz), -114.45 (m, 2F), -125.14 (s, 2F), -126. 62 (t, 2F, J = 12.4 Hz).

5b. Colorless oil. ^{1}HNMR ($CDCl_3$) δ 6.08 (s, 1H), 5.56 (s, 1H), 4.20 (t, 2H, J = 6.6 Hz), 2.17 (m, 2H), 1.98 (m, 2H), 1.92 (s, 3H). ^{19}FNMR ($CDCl_3$) – 82.07 (t, 3F, J = 9.6 Hz), -115.45 (m, 2F), -125.26 (s, 2F), -126. 93 (t, 2F, J = 12.4 Hz).

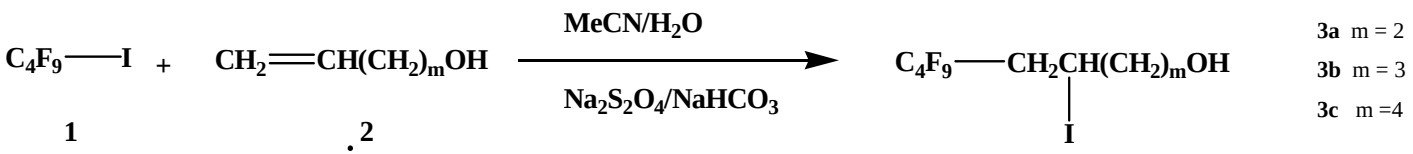

3a m = 2
3b m = 3
3c m =4

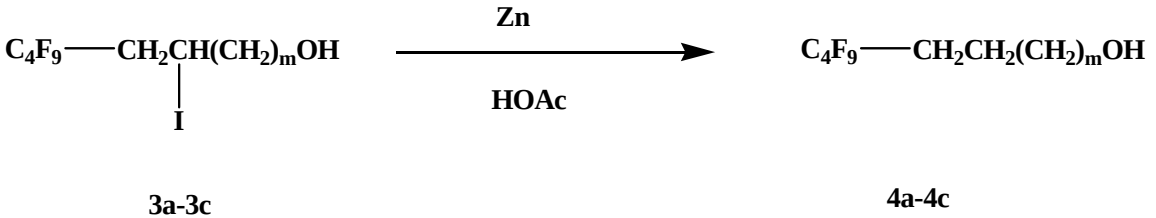

4a n = 2
4b n = 3
4c n =4

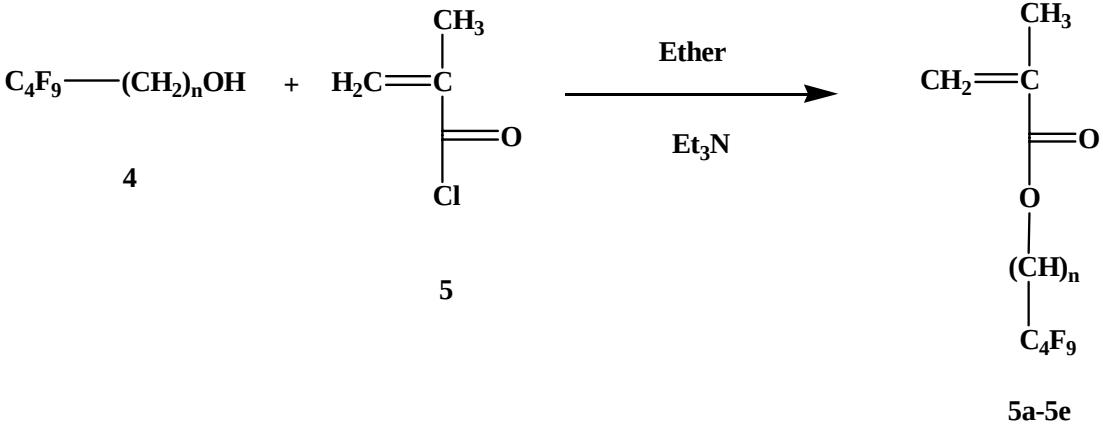

5a n = 2
5b n = 3
5c n =4
5d n = 5
5e n = 6

Scheme 2.1

5c. Colorless oil. ^{1}HNMR ($CDCl_3$) δ 6.07 (s, 1H), 5.54 (s, 1H), 4.16 (t, 2H, J = 6.6 Hz), 2.10 (m, 2H), 1.92 (s, 3H), 1.73 (m, 4H). ^{19}FNMR ($CDCl_3$) – 82.09 (t, 3F, J = 9.6 Hz), -116.05 (m, 2F), -125.30 (s, 2F), -126. 95 (t, 2F, J = 12.4 Hz).

5d. Colorless oil. ^{1}HNMR ($CDCl_3$) δ 6.06 (s, 1H), 5.52 (s, 1H), 4.13 (t, 2H, J = 6.6 Hz), 2.01 (m, 2H), 1.91 (s, 3H), 1.70 (m, 2H), 1.63 (m, 2H), 1.46 (m, 2H). ^{19}FNMR ($CDCl_3$) –82.11 (t, 3F, J = 9.6 Hz), -116.10 (m, 2F), -125.35 (s, 2F), -127.03 (t, 2F, J = 12.4 Hz).

5e. Colorless oil. ^{1}HNMR ($CDCl_3$) δ 6.07 (s, 1H), 5.53 (s, 1H), 4.12 (t, 2H, J = 6.6 Hz), 2.02 (m, 2H), 1.92 (s, 3H), 1.67 (m, 2H), 1.60 (m, 2H), 1.41 (m, 4H). ^{19}FNMR ($CDCl_3$) –82.13 (t, 3F, J = 9.6 Hz), -116.12 (m, 2F), -125.41 (s, 2F), -127.08 (t, 2F, J = 12.4 Hz).

II-3.2.2 Styrene derivatives

General procedure for the synthesis of monomer 8 (scheme 2.2)

Potassium hydroxide (30g) was dissolved in water (30mL). This aqueous solution was added into a mixture of 1,1,1,3,3 – pentafluorobutane (30 mL), terbutylammonium hydrogensulfate and 3,3,4,4,5,5,6,6,6-Nonafluoro-1-hexanol 8 (30 mmol) with vigorous stirring. 4-Vinylbenzyl chloride 7 (30mmol) was added dropwise into the mixture and was allowed to at 42 ^{o}C for 48 hours. Then the organic layer was then collected and extract with brine solution 3 times. After being stirred with carbon black for 1 h, the crude product was filtered and dried with anhydrous magnesium sulfate. Distillation under reduced pressure gave the product at a yield of 80%.

8. Orange liquid. ^{1}HNMR ($CDCl_3$) δ 7.36 (dd, 2H, J = 43.8 Hz, 36.3 Hz), 6.72 (dd, 1H, J = 14.3 Hz, 3.3 Hz), 5.77 (d, 1H, J =17.6 Hz), 5.27 (d, 1H, J = 11.0 Hz), 4.65 (s, 2H), 3.93 (m, 2H). ^{19}FNMR ($CDCl_3$) – 81.62 (t, 3F, J = 9.6 Hz), -120.20 (m, 2F), -124.87 (s, 2F), -

127.0 (t, 2F, J = 13.8 Hz).

General procedure for the synthesis of monomer 11 (scheme 2.3)

A 250 mL three-neck flask with a sealed stirrer unit was equipped with a reflux condenser and an addition funnel. Magnesium (40 mmol), anhydrous tetrahydrofuran (10 mL) and a small crystal of iodide were placed into the flask. The system was evacuated and maintained under an argon atmosphere. The reactor was then heated to 55 ^{o}C. A solution of 4-vinylbenzyl bromide (20 mmol) in anhydrous tetrahydrofuran (50 mL) was introduced dropwise over a period of 35 minutes at a rate to maintain gentle reflux. The reaction mixture was refluxed for 15 minutes and stirred for another 45 minutes without heating.

Cooper (I) iodide (3.1 mmol) and 1H,1H,2H,2H-nonafluorohexyl iodide (10 mmol) mixture was cooled in a dry ice/2-propanol bath under a nitrogen atmosphere. The obtained Grignard reagent was added dropwise to the cooled solution and stirred at -80 ^{o}C for 30 minutes. Then the reactor temperature was slowly raised to reflux over a 2 hour period and the mixture was allowed to react for 6 more hours. Tertrahydrofuran was removed by rotary evaporation and the residue was poured into aqueous ammonium chloride solution (800 mL). The product was extracted with ether (3 × 50 mL) and dried with anhydrous magnesium sulfate. Distill under reduced pressure to yield product about 75%.

11. Orange liquid. ^{1}HNMR ($CDCl_3$) δ 7.24 (dd, 2H, J = 43.8 Hz, 36.3 Hz), 6.67 (dd, 1H, J = 14.3 Hz, 3.3 Hz), 5.70 (d, 1H, J =17.6 Hz), 5.20 (d, 1H, J =11.0 Hz), 2.87 (t, 2H, J = 8.4 Hz), 2.33 (m, 2H). ^{19}FNMR ($CDCl_3$) – 81.74 (t, 3F, J = 9.6 Hz), -115.51 (m, 2F), -125.09 (s, 2F), -126. 68 (t, 2F, J = 13.8 Hz).

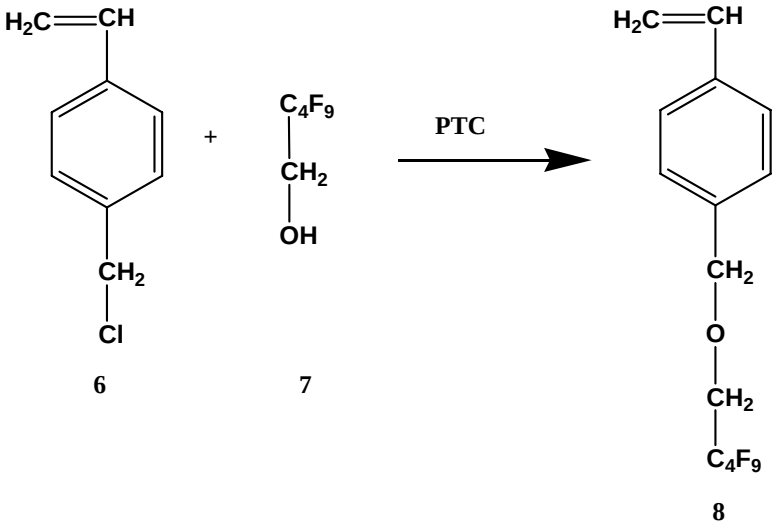

Scheme 2.2

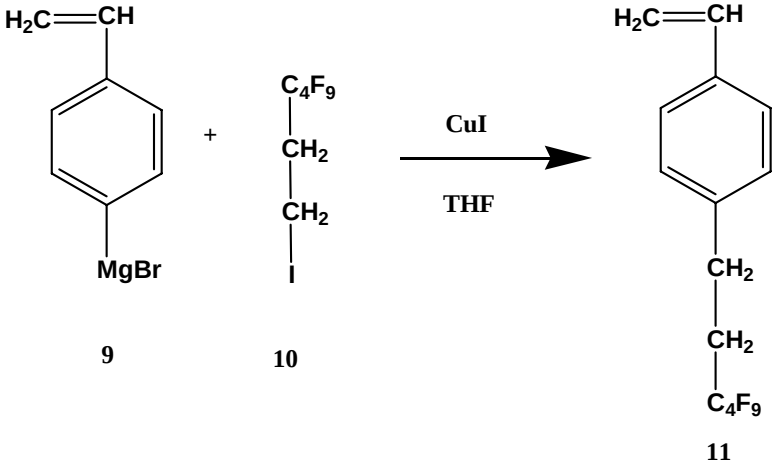

Scheme 2.3

II-3.3 Polymerization

Methacrylate monomers containing AIBN (0.5-1 wt %) were purged with argon for approximately 15 minutes prior to transferring into a 25 mL high pressure view cell. Then contents of the high pressure cell were purged with argon for additional 15 minutes and then the reaction cell was heated to 60 ^{o}C while CO_2 was added via syringe pump (Isco) over ca. 15 minutes of time to a pressure of 345 bar. The homogeneous polymerization proceeded for 24 h at 60 ^{o}C and 345 bar. The polymers and any unreacted monomer were removed from the reaction cell by dissolving in trifluorotoluene and then precipitated into a large excess of methanol. The polymers were isolated by suction filtration, washed several times with methanol and dried in a vacuum oven overnight under reduced pressure. The polymer structures are listed and labeled in Table 2.4.

Styrene-based monomers along with 0.5-1.0 wt% AIBN as the initiator were placed into a 100 mL round flask. The mixture was then purged with argon for 30 minutes. The polymerization proceeded to 24 hours at 70^{o}C inside the sealed flask. The polymers were isolated by precipitate and washed in methanol, and dried in a vacuum oven for overnight.

For the convenience of description, all the polymers with perfluorobutyl groups of the side chains were named as C4 materials. According to different spacers, the C4 materials are classified as C4 methacrylates and C4 styrene, respectively.

Table 2.4 Chemical structures and labels of fluorinated alkyl methacrylate polymers and styrene derivative polymers

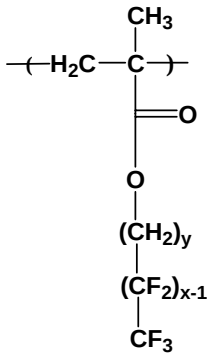

PH_xF_y

x = 4, y = 2, 3, 4, 5, 6

x = 6, y = 4

x = 8, y =2

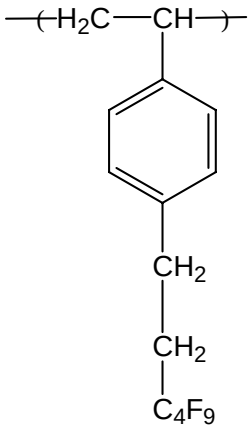

PSI-F4

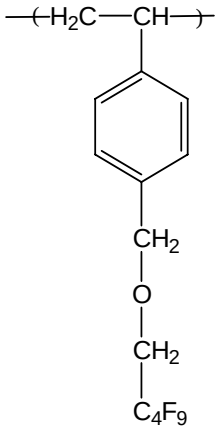

PSII-F4

II-3.4 Analytical techniques

^{1}H and ^{19}F nuclear magnetic resonance (NMR) spectra were recorded with a Bruker 400MHz DRX spectrometer to characterize the chemical structures of monomers and polymers. NMR samples were prepared in Chloroform-D ($CDCl_3$) (Cambridge Isotope Labs) or $CDCl_3$-trifluorotoluene (TFT) solvent systems.

The thermal stability of polymers was measured by a Perkin-Elmer Pyris 1 thermogravimetric analyzer (TGA). The fluorinated polymethacrylate samples were heated from room temperature to 500 ^{o}C with a heating rate of 10 ^{o}C / min under a nitrogen atmosphere. The styrene based materials were heated to 600 ^{o}C with the same heating rate. The temperature for onset of rapid weight loss (5 wt%) was defined as the decomposition temperature.

The thermo physical behavior of polymers was recorded by a Seiko-Haake differential scanning calorimetry (DSC) 220. Samples (~ 5 mg) were placed in aluminum pans which were crimped shut. Thermograms of polymers were collected from a second heat under a nitrogen atmosphere with a heating rate of 10 °C/min, while thermograms of fluorinated alcohols were collected from first heating cycle with a heating rate of 5 °C/min. The temperature sweep typically ranged from -100 to 200 °C for polymer and from -150 to 150 °C for fluorinated alcohols.

Static contact angles on polymer coatings were measured using a KSV Instrument LTD CAM 200 Optical Contact Angle Meter. A screw-top syringe (Fisher) was used to deposit liquid drop onto S_i wafers coated with polymers. S_i wafers were spin-coated with polymer solutions in trifluorotoluene (2 wt %) and dried in vacuum for 2 hours. Water, diiodomethane, hexadecane and n-alcohols (n = 4, 6, 8, 10, 12) were used as testing liquids and their surface

Table 2.5 Surface tension of all the testing liquids for contact angle measurements.[69,70]

Liquid	γ_l (mN/m)	γ_l^d (mN/m)	γ_l^p (mN/m)
Water	72.8	21.8	51.0
Diiodidemethane	50.8	49.5	1.3
n-Hexadecane	27.62	27.62	0
Ethanol	22.20	18.43	3.77
Butanol	25.17	22.21	2.96
Hexanol	26.01	24.70	1.31
Octanol	27.50	25.50	2.00
Decanol	28.29	26.49	1.80

All the surface energy data are measure at 25 ^{o}C. γ_l is the surface tension of the liquid and $\gamma_s = \gamma_l^d + \gamma_l^p$; γ_l^p and γ_l^p are dispersion component and hydrogen bonding component.

tensions were listed in Table 2.5.[70] Each sample was measured at least three identicals and obtained the average.

Dynamic tensiometry measurements were performed on a NIMA Technologies DST 9005 dynamic surface tensiometer, based on the Wilhelmy Plate method.[71,72] Glass coverslips were dip-coated with polymer solutions (5 wt % in trifluorotoluene) and dried in vacuum for 5 hours. Each experiment included multiple immersions and receding to ensure consistent and reproducible data. Each sample was measured at least three identical immersions in succession. The stage speeds for immersion and receding were 50 μm/s.

The surface roughness was measured by a multimode atomic force microscope (AFM) from Veeco Metrology group, equipped with a Nanoscope IIIA control station and silicon cantilevers (from Mikromasch USA). The resonance frequencies were about 160 kHz, with spring constants of 5.0 N/m. The radii less than 10 nm was used for visualization of the prepared films in the tapping mode.

Near edge X-ray absorption fine structure experiments (NEXAFS) is an ideal technique to probe the chemical bonding recognition and their relative population density on the polymer surfaces. The experimental scheme was displayed in Figure 2.4.[73] The sharp core level excitations for C, N, O and F occurred in the soft X-ray spectra region. NEXAFS measurements enable the investigation of molecular bonding chemistry and orientation of specific organic groups that including these elements, especially the semifluorintaed groups. The NEXAFS experiments were carried out on the U7A NIST/Dow materials characterization end-station at the National Synchrotron Light Source at Brookhaven National Laboratory.[74] The U7A beamline is equipped with toroidal mirror spherical grating monochromator. The incident photon energy resolution and intensity were 0.2 eV and 5 ×

10^{10} photon/s, respectively, for an incident photon energy of 300 eV and a typical storage ring current of 500 mA. The materials characterization end station was equipped with a heating/cooling stage positioned on a goniometer, which controls the orientation of the sample with respect to the polarization vector of the X-rays. A differentially pumped ultrahigh vacuum compatible proportional counter is used for collecting the fluorescence yield (FY) signal. The partial-electron-yield (PEY) signal is collected using a channeltron electron multiplier with an adjustable entrance grid bias (EGB). To eliminate the effect of incident beam intensity fluctuations and monochromator absorption features, the FY and PEY signals were normalized by the incident beam intensity obtained from the photo yield of a clean gold grid.

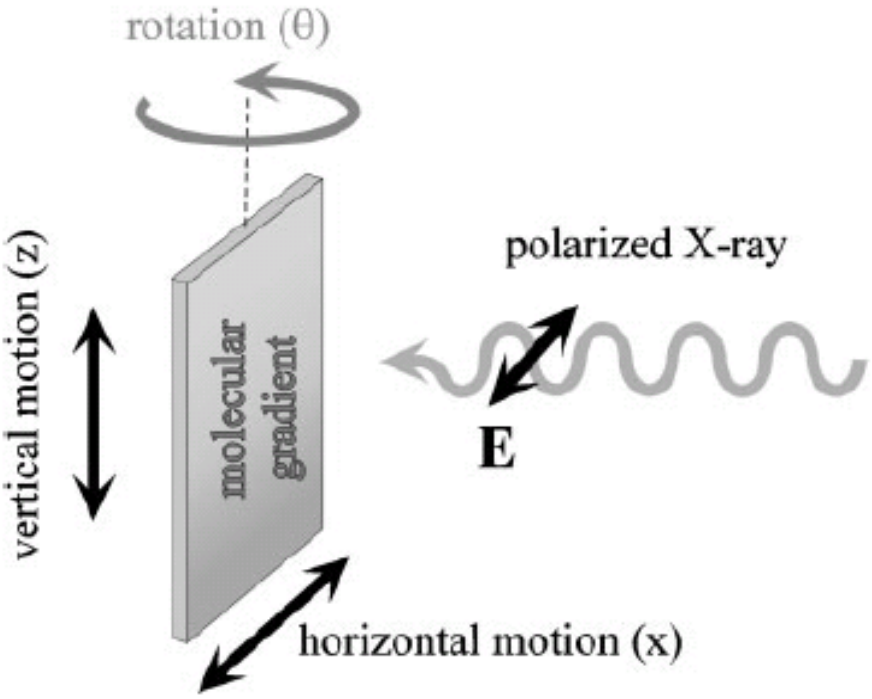

Figure 2.4 Schematic reorientations of NEXAFS experiments.[74]

II-4 Results and Discussions

II-4.1 Thermal properties

The thermal stability of the polymers was investigated by TGA, as shown in Figure 2.5. The TGA thermograms of all the polymers exhibit similar onset decompositions temperature at around 260^{o}C (5 wt% weight loss), indicating good thermal stability. Not only did the "spacer" display no influence on the initial thermal decomposition of the polymers but neither did the perfluoro groups, which disagreed to the literature that decomposition temperature decreases with decreasing fluorinated side chain lengths.[75]. This suggested possible cleavages of hydrocarbon units happened before the fluorine side chain degradations. The maximum decomposition temperatures of styrene based polymers (PSI-F4 and PSII-F4) were higher than that of polymethacrylates, due to the presence stiff phenyl ring groups.

The thermal physical behaviors of the polymers were recorded by DSC. The glass transition temperatures (T_g) of methacrylate polymers were hard to determined by DSC spectra (Figure 2.6), which presented a broad transition ranging from 0 to 20 ^{o}C. Styrene based polymers PSI-F4 and PSII-F4 showed higher T_g due to the existence of the stiffer side chains. No melting transitions were observed by DSC for the polymers with perfluorobutyl side chains. Only the polymer PH2F8 with eight perfluorocarbons in the side chains demonstrated a sharp melting peak at 70 ^{o}C, which was attributed to the side chain crystallization resulting from the inter-side-chain interactions of the fluoroalkyl groups. The hexagonal packing of the long fluorinated side chains has been investigated by XPS and other techniques.[68,76] Another transition peak was expected around 100 ^{o}C, arising from vanishing of the intrinsic microphase-separation between the fluorinated domains and hydrocarbon domains. This special phase transition was reported by Geribaldi et al. for

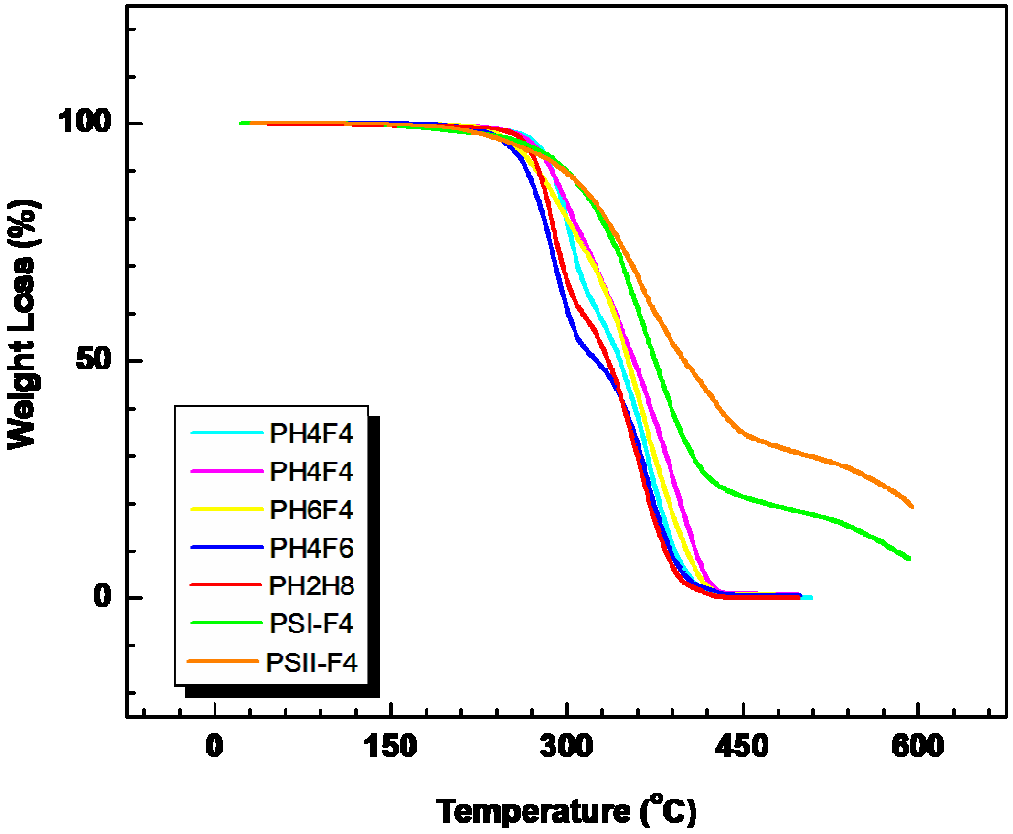

Figure 2.5 TGA thermograms of the fluorinated polymers PH4F4, PH4F4, PH6F4, PH4F6, PH2F8, PSI-F4 and PSII-F4.

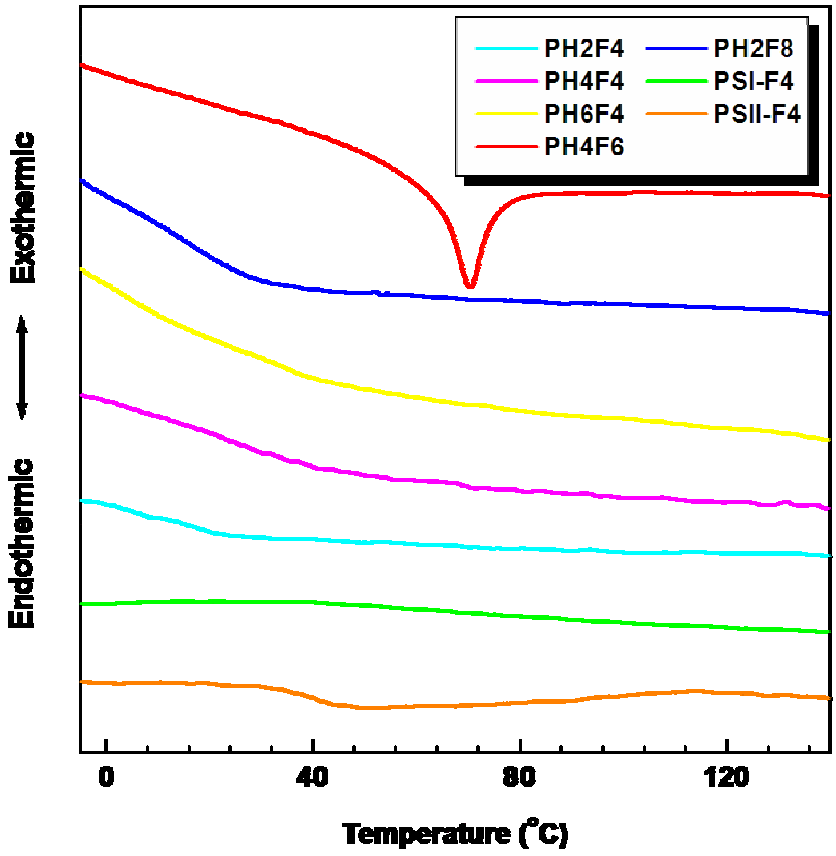

Figure 2.6 DSC spectra of all the fluorinated polymers PH2F4, PH4F4, PH6F4, PH4F6, PH2F8, PSI-F4 and PSII-F4.

polyacrylate homopolymers with four fluorocarbons of the side chains.[77] However, no such transitions were observed by (Figure 2.6). In this case, the relaxation of long polymer backbones might have screened the phase transition behaviour of the side chains. The thermal properties of these polymers will be further investigated by the relaxation behaviors of analog semifluorinated alcohols and discussed later in this part.

II-4.2 Wetting properties

The wetting properties of our polymers were characterized by contact angle measurements. Static contact angle measurements were performed with water, hexadecane, diiodidemethane and a series of n-alcohols with various surface tensions. The surface tensions were quantified using two methods, Zisman analysis and Owen-Wendt-Fowkes analysis. Dynamic tensiometry measurements were performed with water and hexadecane and analyzed with Wilhelmy Plate method.

II-4.2.1 Static contact angle

The repellency is defined as the limited wetting under the static conditions, which is directly reflected in the performance of static contact angle measurements. Figure 2.7 shows the static contact angles of the C4 methacylates against water and hexadecane. The water static contact angle of the C4 methacrylates was 110^{o}, independent of the methylene spacer length of the side chains. The hexadecane contact angles of C4 methacrylates slightly decreased from 68^{o} to 65^{o} with increasing methylene spacer length. C4 styrene with a benzyl group as the spacer exhibited a contact angles of 109^{o} and 60^{o}, against water and hexadecane, which was not shown in Figure 2.7. Polymer PH2F8 and PH4F6 whose side chains have the

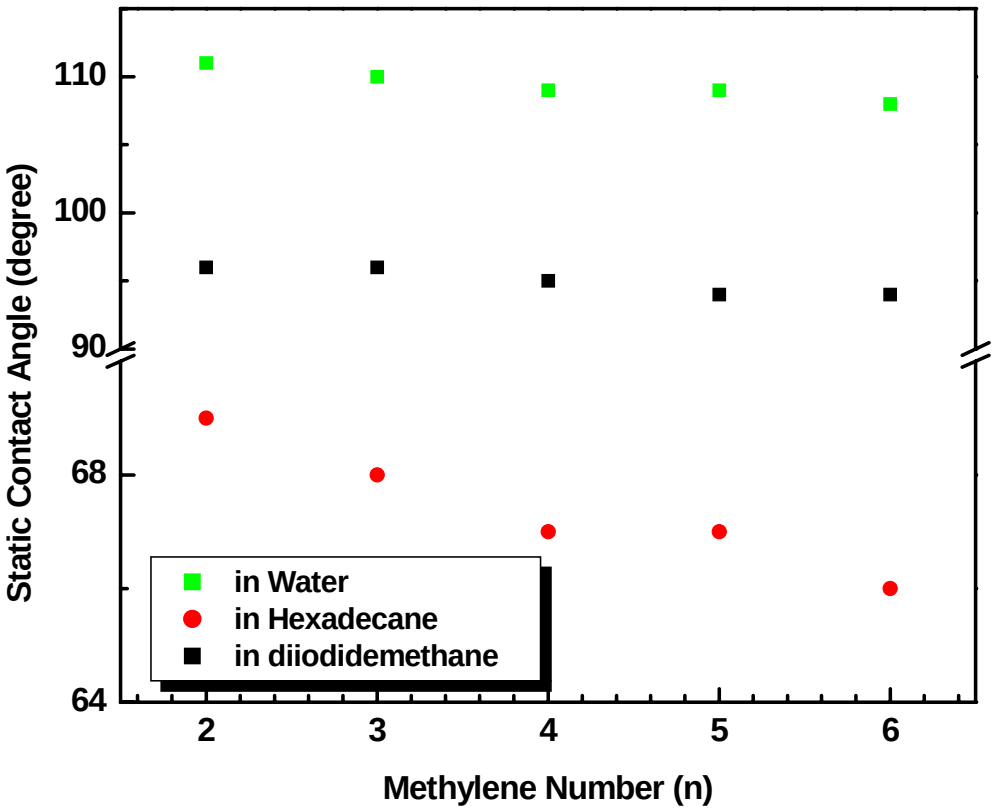

Figure 2.7 Dependence of the contact angles on the methylene spacer length of the C4 methacrylates side chains in water, hexadecane and diiodidemethane.

same total carbon number as that of PH6F4, however, were found to display higher contact angles against water (~ 120^{o}) and hexadecane (~ 80^{o}).[68,75] This suggests that polymer surface properties are strongly depended on fluorine content of side chains.

II-4.2.2 Surface tension

The hydrophobic and oleophobic properties of the materials were determined by the surface tension. Two methods were used to predict the chemical nature and surface tensions of the resistant materials, Zisman analysis and Owen-Wendt-Fowkes method.

By measuring contact angles (θ) of a homolog series of liquids on low-energy surfaces, a typical Zisman plot was plotted as cos(θ) values versus the surface tensions of the liquids. The linear plot was then extrapolated approximately to the value of cos(θ) = 1 to obtain the critical surface tension. A series of homolog alcohols were chosen as the test liquid of Zisman analysis to measure the critical surface tension (γ_c). The critical surface tensions of C4 methacrylates increased slightly from 13 to 15 mN / m with the increasing length of methylene spacers (Figure 2.8). These surface energies were significantly lower than silicone based repellents (~22 mN/m) and even lower than that of Teflon (18 mN/m).[78] The C4 styrene exhibited a higher γ_c of 18 mN / m due to the higher content of hydrocarbon of the side chains. The critical surface tension results agreed with the observations of static contact angles of these fluorinated polymethacrylates. All polymers are considered to be hydrophobic and oleophobic, since their critical surface tensions are well below that of water (72.8 mN /m, 25 ^{o}C) and hydrocarbon oil (20-30 mN / m). It can be concluded that side chains with four fluorocarbons are long enough to provide resistance to both water and oil. The γ_c values of polymethyacrylates PH2F8 and PH4F6 were reported to be 10 mN / m and 12 mN /m,

respectively, by Stöhr and coworkers.[79] Considering the polymers with ten carbons as pendant side chains (PH6F4, PH2F8 and PH4F6), the values of γ_c decreased with the increasing fluorine content the side chain. Substitution of two CF_2 groups by two CH_2 groups more than doubles the values of γ_c.

The surface properties are generally determined by the chemical composition and construction of the exposed solid surfaces. For the comb-like polymers, the wetting properties of the polymers are strongly dependent on the packing and segregation of side chains on topmost surface region.[8] The surface tension of constituent $–CF_3$ group is the lowest known (~ 6 mN / m). Hence, the surface covered with the closely packed$–CF_3$ groups exhibits the lowest critical surface tension.[6,80,81] Fluorinated polymers with long perfluorinated alkyl side chains such as polymer PH2F8 can undergo side chain crystallization as a result of the inter-side-chain interactions of the perfluoro groups. The side chains of these polymers were forced to pack tightly on the topmost surface, providing a dense layer of $–CF_3$ groups to repel liquid. Hence, they exhibited excellent repellency to water and oil.[68,75,76,81] However, for C4 materials without side chain crystallization, the perfluorinated alkyl groups distributed randomly on the surface with a loose packing of the $–CF_3$, thus resulting in the higher critical surface tensions. On the other hand, the introduction of larger hydrocarbon spacers increased free space between the side chains to some extent, so that increased the possibility of wetting and penetration of liquids.

The free surface energies (γ_s) of the polymers were measured using water and hexadecane as the testing liquids. According to Owen-Wendt-Fowkes methods, the free surface energy is the sum of the dispersion contribution (γ_s^d) and the polar component contribution (γ_s^p). By measuring the contact angles of polymers against two different liquids,

γ_s can be calculated through equation

$$1+\cos(\theta)=2\left(\frac{(\gamma_s^d\gamma_l^d)^{0.5}}{\gamma_l}\right)+2\left(\frac{(\gamma_s^p\gamma_l^p)^{0.5}}{\gamma_l}\right) \quad (2.1)$$

where θ is the static contact angle; γ_l is the surface tension of a liquid; γ_l^d and γ_l^p are the dispersion component and the polar component of the liquid surface tension, respectively. The results of free surface energy for polymers are summarized in Table 2.6. The value of γ_s for C4 methacrylates was 11 – 13 mN / m, lower than the results from Zisman analysis. However, these two surface tensions reasonably agree. The difference might be the result of the curvature of Zisman plots due to the incompatibility between the fluorinated surfaces and alcohols.

The length of methylene spacer also exhibited weak influence on the free surface energy, consistent with observations of the critical surface tension. The polar component surface energy, resulting from hydrogen bonding interactions, was about 16-19% of the total free surface energy and so made an important contribution to the surface behavior of C4 methacrlylates. Polymer PH2F8 displayed much lower values of γ_s^p from polar component contribution, suggesting the weak interaction between polymer surface and liquids. It is interesting to note that there was no polar component contribution to free surface energies of C4 styrene. The possible explanation is that the absence of carboxyl groups of styrene based materials. The oxygen moieties on the topmost surface of polymethacrylares determined the strength of hydrogen bonding interactions, upon contacting with polar liquids.

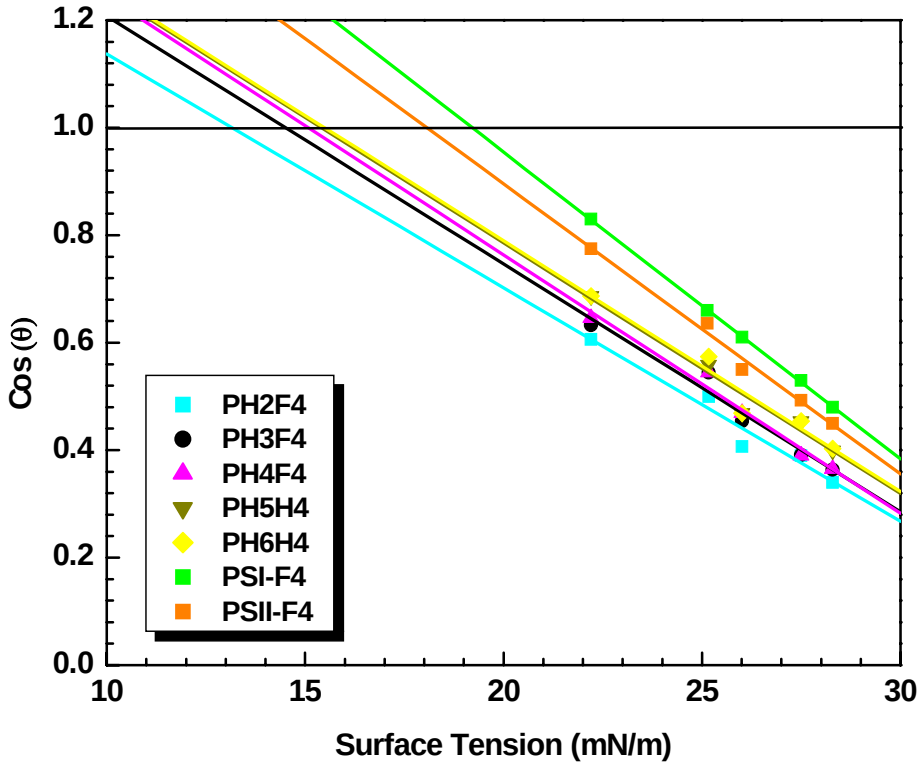

Figure 2.8 Zisman analyses of C4 polymers PH2F4, PH3F4, PH4F4, PH5F4, PH6F4, PSI-F4 and PSII-F4.

Table 2.6 Summary of the critical surface tensions and free surface energies of the fluorinated polymers.

Polymers	γ_c	γ_s	γ_s^d	γ_s^h
PH2F4	13.2	11.1	9.1	2.0
PH4F4	14.2	11.8	9.4	2.4
PH6F4	15.1	12.2	10.0	2.2
PH4F6	-	9.8	8.6	1.2
PH2F8	-	8.8	8.1	0.7
PSI-F4	18.1	17.6	17.5	0.1
PSII-F4	18.3	17.3	17.3	0

II-4.2.2 Dynamic contact angle

As shown in Figure 2.9, dynamic contact angle measurements were performed using water and hexadecane as the testing liquids. The water advancing contact angles of C4 methacylates slightly increased with the decreasing length of methylene spacers. The weak influence of the methylene spacer on the advancing contact angles was consistent with the results from static measurements. This indicates that the advancing performance is only related to the initial state of the surface organization. However, the receding contact angles against water decreased rapidly when the number of the methylene spacer increased to six. Therefore, the contact angle hysteresis, expressed as the difference between advancing and receding contact angles, also increased by 10 degrees. As expected, the polymer (PH2F8) bearing eight perfluorocarbon in side chains displayed the lowest hysteresis. Figure 2.10 shows the dynamic performance of the polymers in hexadecane. The methylene spacer displayed no effects on the contact angles hystersis of C4 methacrylates. However, the contact angle hysteresis started to decrease dramatically when the side chains contained eight perfluorocarbon groups.

The hysteresis is regarded as the movement of the front liquid line on the solid surface.[69,70] The parameters which effect contact angle hystersis include surface roughness, heterogeneity, reorientation and mobility.[70] AFM observations of the testing film surfaces revealed roughness as 0.5 nm (Rms) which was considered to have no effect on the contact angles measurements. In addition, there was no difference in morphology of the films observed before and after dynamic contact angle measurements. Hence, the liquid film presented after the contact liquid line had receded was responsible for the observed contact angle hysteresis. The contribution of reorientation and mobility of the side chains was

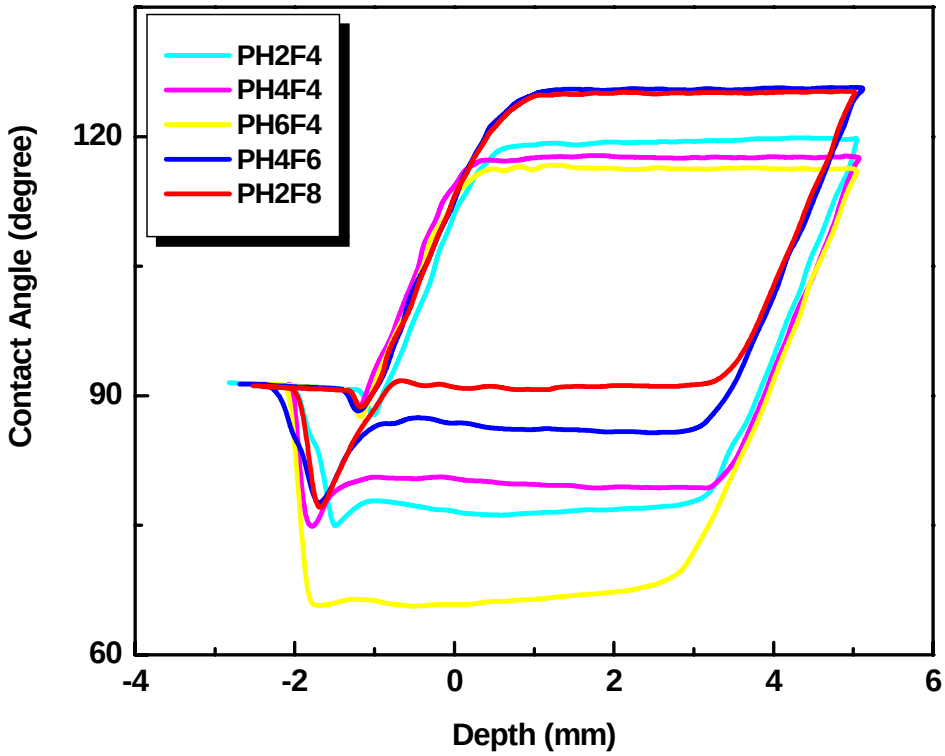

Figure 2.9 Dynamic contact angles of the methacrylate polymers PH2F4, PH4F4, PH6F4, PH4F6 and PH2F8 in water.

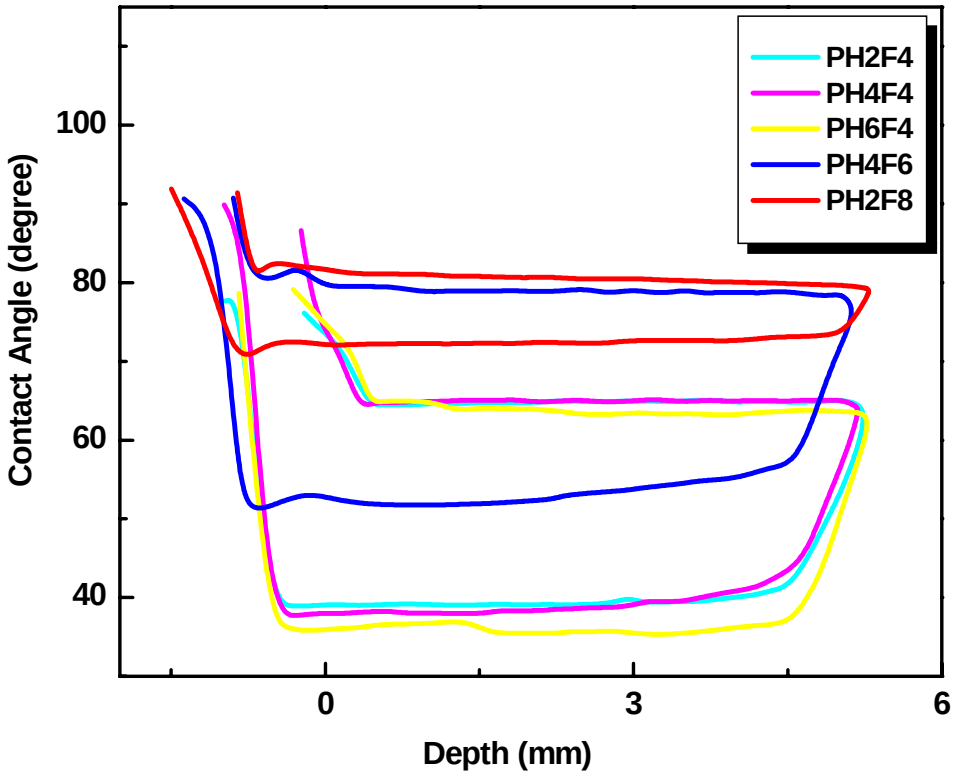

Figure 2.10 Dynamic contact angles of the methacrylate polymers PH2F4, PH4F4, PH6F4, PH4F6 and PH2F8 in hexadecane.

expected in this case. The side chains of C4 methyacrlates were comprised of both oleophilic fluoroalkyl groups and oleophobic spacers. The mobility of the random distributed perfluoroalkyl groups enables the reorientation of the side chains after the receding liquid line, favoring exposure of the hydrocarbon spacers to interact with the liquid. However, the existence of the side chain crystallization for PH2F8[81] prohibited the movements of the perfluoro groups to provide resistance to the liquid wetting, thus result in a extremely low hysteresis both in water and oil. These explanations also support the observation of phase transitions in DSC spectra, arising from the side chain crystallization.

Figure 2.11 and 2.12 showed the dynamic contact angles against water and hexadecane for the C4 styrene (PSI-F4 and PSII-F4). Compared to C4 methacylates, C4 styrene demonstrated slightly lower water advancing contact angles. However, the high water receding contact angles of C4 styrene lead to a significantly low hysteresis by 20 degrees. This value was much lower than that of PH2F8 as shown in Figure 2.9, indicating that, to some extent, the introduction of the bulky phenyl rings into the side chains instead of methylene groups constricted the mobility and reorientation of the side chains. Additionally, the interactions between the solid surface and the polar solvent, water, were much weaker of C4 styrene for the absence of carboxyl groups, compared to that of C4 methacrylates. The zero polar component contribution to the free surface energy suggests no hydrogen bonding exist between the polymer surface and water because of the eliminations of the carboxyl groups. The hysteresis of C4 methacrylates in hexadecane was between that of PSII-F4 and PSI-F4. It seems that the higher flexible ether linkage of the spacer of PSII-F4 favored the reorientation of the surface groups after the receding liquid line.

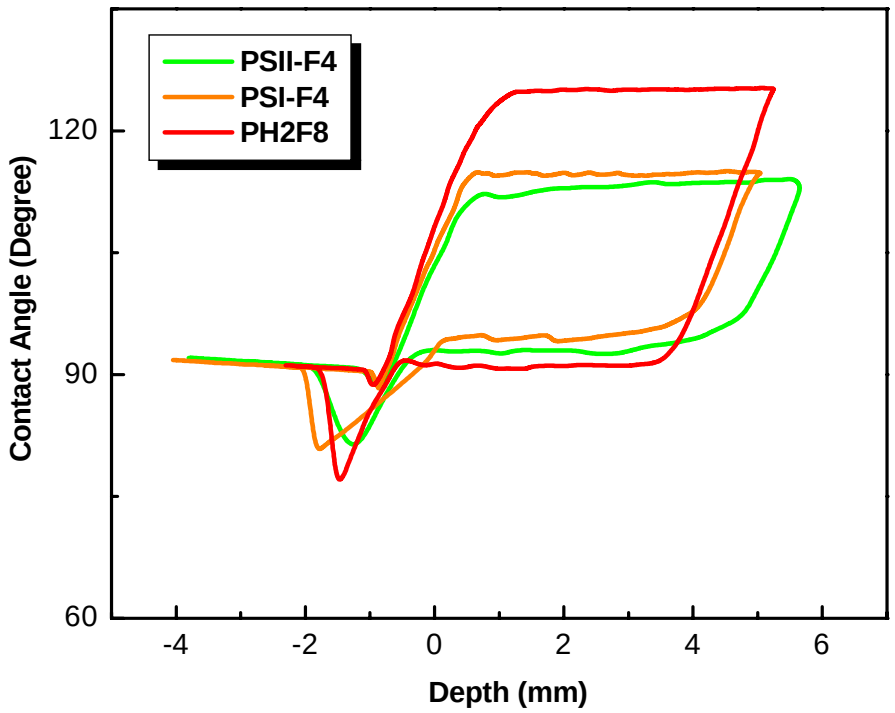

Figure 2.11 Dynamic contact angles of C4 styrene polymers PSI-F4 and PSII-F4 in water (PH46 inserted as the comparison).

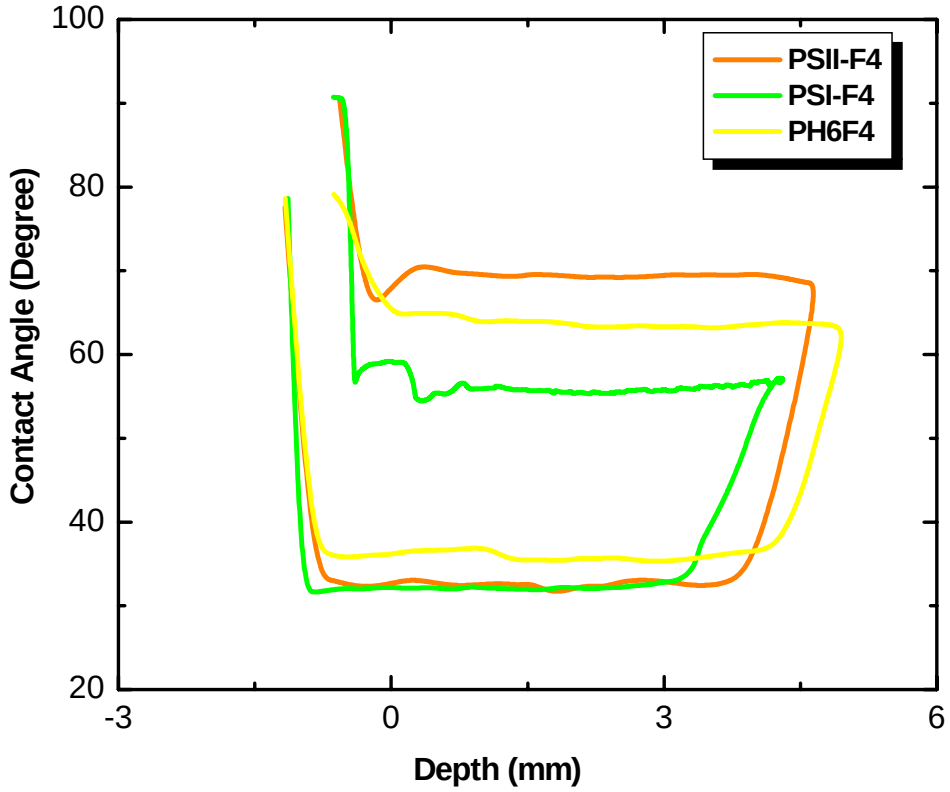

Figure 2.12 Dynamic contact angles of C4 styrene polymers PSI-F4 and PSII-F4 in hexadecane (PH46 inserted as the comparison).

II-4.3 Surface orientation

II-4.3.1 NEXAFS experiments

The segregation and orientation of side chains on the uppermost surface region of polymer films were investigated in collaboration with Jan Ganzer by near edge X-ray absorption fines structure (NEXAFS) experiments. NEXAFS is a powerful tool to analyze the surface construction of materials, especially semifluorinated polymers. The measurements of the electron intensity in NEXAFS spectra enables the identification of the chemical bonds and their relative population density within the samples.[74,82]

NEXAFS experiments were carried out at three different orientations ($\theta = 20^o, 50^o, 90^o$) of the polymer samples with respect to the X-ray beam. The resulting partial electron yield (PEY) NEXAFS signals were normalized and provided information of the orientation of the pendant side chains on the surface. Figure 2.13 showed PEY (upper part) signals of the carbon K-edge NEXAFS from the sample PH2F4. The overlapped intensities from three angles in Figure 2.13 exhibited the element population density of C, F and O in different orientations. Several characteristic peaks corresponding to the $1s \rightarrow \sigma^*$ transitions were demonstrated in PEY NEXAFS spectra in Figure 2.13, including C-H bond (E = 288.7 eV), C-F bond (E = 292.8 eV) and C-C bond (E = 295.7 eV). Moreover, the signal PEY spectra at E = 285.2 eV is corresponded to the $1s \rightarrow \pi^*$ transitions of C=O bond of methacrylates or C=C bond of the phenyl rings in this case. The difference PEY NEXAFS spectra (lower part in Figure 2.13) were obtained by subtracting the PEY NEXAFS signal measured at $\theta = 20^o$ (edge) from that at $\theta = 90^o$ (topmost). They were considered to be the direct indications of the angular dependence of the intensities for transitions of $1s \rightarrow \sigma^*_{C-F}$ and $1s \rightarrow \sigma^*_{C-C}$. Generally, the difference PEY NEXAFS spectrum is a good measure of the orientation. The

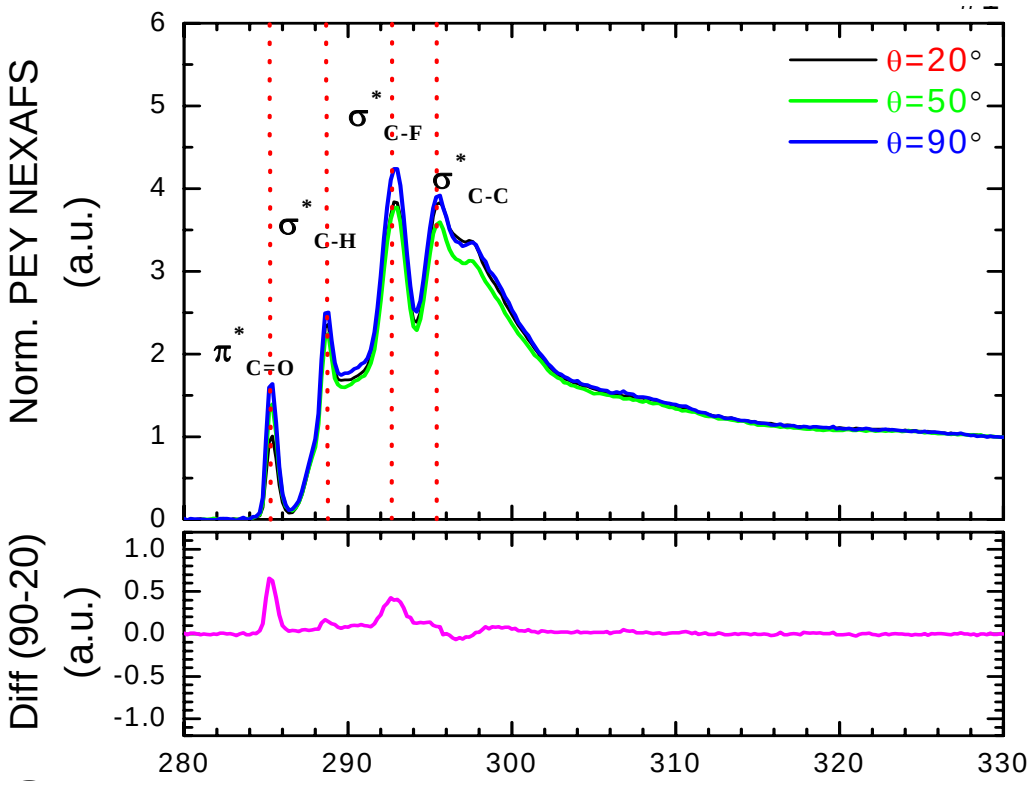

Figure 2.13 PEY signals and differential PEY signals of the carbon K-edge NEXAFS for sample PH2F4.

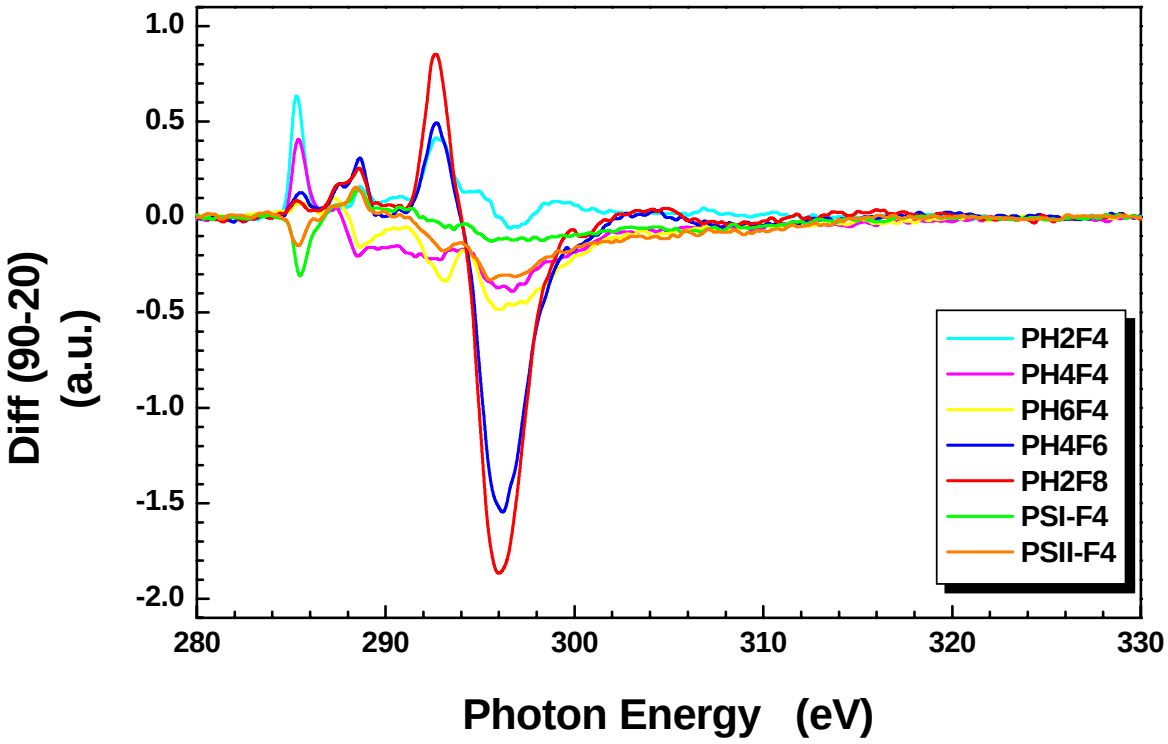

Figure 2.14 The difference PEY NEXAFS spectra from the polymer samples PH4F4, PH4F4, PH6F4, PH4F6, PH2F8, PSI-F4 and PSII-F4, by subtracting the signals at $\theta = 20^{o}$ from that at $\theta = 90^{o}$.

difference PEY NEXAFS spectra of C4 material, polymers PH2F8 and PH4F6 were summarized in Figure 2.14. For an ordered surface of semifluorinated polymers, when the detection angle θ increased, the intensity corresponded to the C-F bond transitions increased while that of the C-C bonds decreased.[74,83,84] The intensities for the 1s→ σ^*_{C-F} transitions and the 1s→ σ^*_{C-C} transitions for C4 methacrylates were found to be independent of the variations of detection angles, suggesting no orientations of perfluoro parts presented on the topmost surfaces. The length of methylene spacers exhibited weak influence on the C-F bond transition intensity of C4 methacrylates. The peaks associated with the transition of 1s→ σ^*_{C-F} decreased with the increase of the methylene spacer length, indicating less population of fluorine moiety on the topmost region (θ = 90^o). This confirmed the dependence of the surface tensions on the length of the methylene spacers. On the other hand, the semi-crystallization polymer PH2F8 showed the best orientation and organization of side chains, according to the angular dependence of intensities from C-H and C-C bonds. NEXAFS spectra of PH4F6 showed the similar fashion of intensity transitions to PF2F8, indicating order structure of the side chains presented on the topmost surface even without side chain crystallization. This agreed with the observations of Ganzer et al. that at least six perfluoroalkyl groups were needed to form an ordered segregation structure.[73]

It is interesting to note that the C=O bonds of polymers PH2F4 and PH4F4 might orientate roughly perpendicular to the substrate, according to the variations of C=O signals. Moreover, the intensity associated to the 1s→ π^* transition of C=O decrease with the increasing length of methylene spacers, until C=O signals vanished for polymer PH6F4. This suggested that the increasing population of CH_2 spacers prevented the exposure of C=O groups on the topmost region. In the case of PH2F8 and PH4F6, the weak intensity from

C=O bond was due to the shielding from the dense population of $–CF_3$ groups resulted from the side chain crystallization.

The NEXAFS spectra of C4 styrene (PSI-F4 and PII-F4) displayed no side chain orientation with the introduction of a phenyl ring. However, the intensity corresponding to C=C bond apparently varied with the different detection angles, indicating that the phenyl ring might take an orientation roughly parallel to the substrate surfaces. This special surface construction with low mobility of bulky spacers might be part of the reasons for low hysteresis in water.

NEXAFS spectroscopy also provided a relative measurement of the concentration of the fluorine content on the surface. In Figure 2.15, the difference between the preedge (E = 680 eV) and postedge (E = 730 eV) signals in the PEY spectra at the fluorine K-edge were displayed and considered as a indication of the concentration of fluorine per area of the incident beam in the sample.[85] Figure 2.16 summarized the PEY NEXAFS spectra collected at 50^o. It was found that all the polymer surfaces were rich in fluorine, illustrated by the high contrast between preedge intensity and postedge intensity. The fluorine moiety on the surface increased with increasing the fluoroalkyl number, while decreased with the methylene number. The PSI-F4 surface showed the lowest fluorine density on the surface. All the results were in good agreement with the observations from contact angle and surface tension measurements.

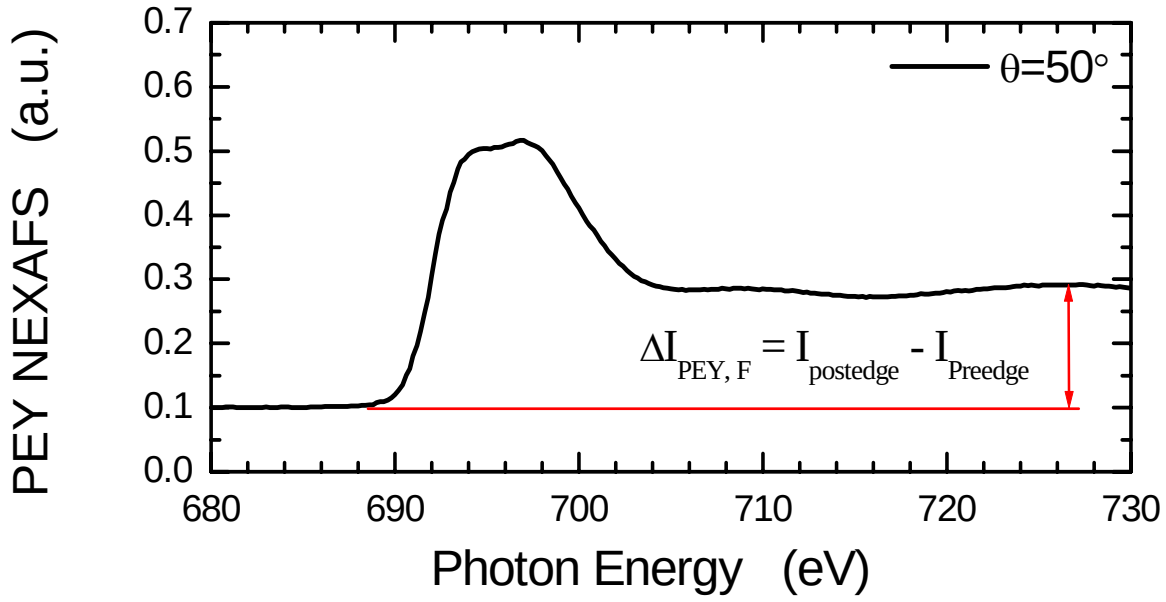

Figure 2.15 Fluorine K-edge PEY NEXAFS spectra from sample PH2F6 collected at $\theta = 50^{o}$.

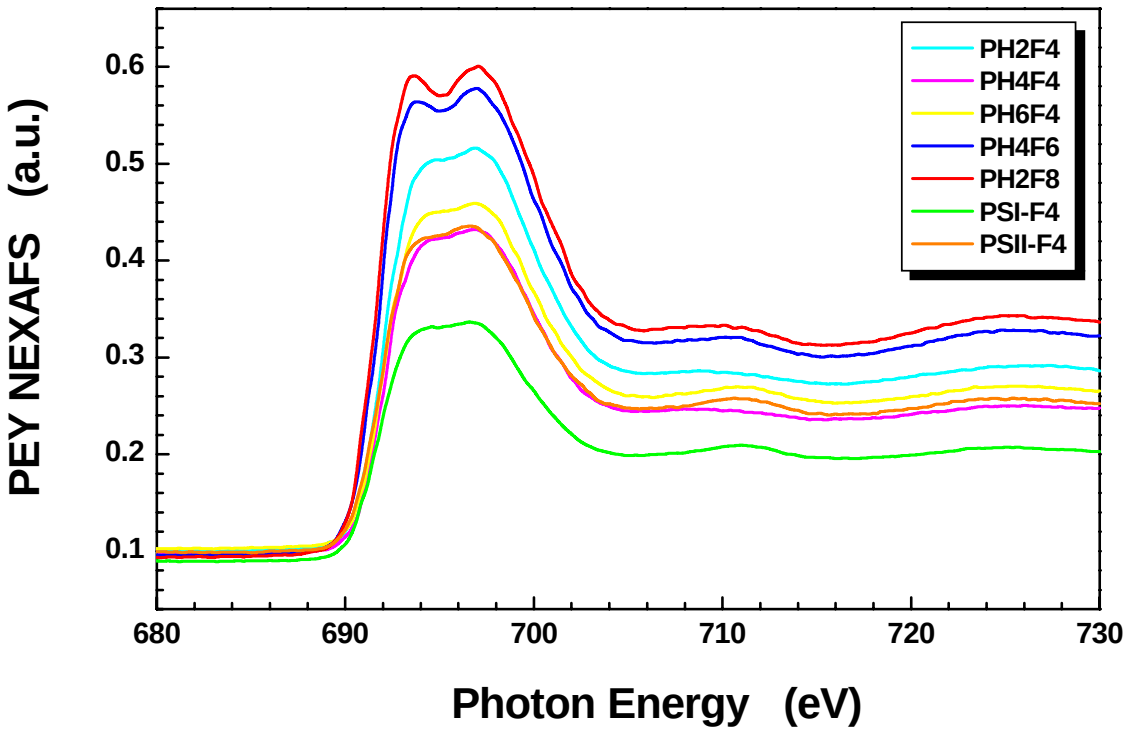

Figure 2.16 Overlap of fluorine K-edge PEY NEXAFS spectra for the polymers PH4F4, PH4F4, PH6F4, PH4F6, PH2F8, PSI-F4 and PSII-F4, collected at $\theta = 50^{o}$.

II-4.3.2 Fluorinated alcohols

A semifluorinated alkyl chain could be regarded as a miniblock oligomer, because the pefluorocarbon segment (CF_2) is strongly immiscible with its hydrocarbon analog. The stiff perfluoroalkyl groups adapt a helical structure due to electrosteric repulsion of fluorine atoms in the relative 1,3-positions of the crystalline state.[86,87] This helical structure of perfluroalkyl groups determines the length of side chains needed to initiate the side chain crystallization. In Figure 2.14, it was obvious that surface properties of polymers strongly depended on length of “hard” segment (fluoromethylene groups). In addition, the content of “soft” segment (methylene spacer) affects the segregation of the side chains in a way by varying the enthalpy to disorder the highly orientated liquid crystal structure of the semifluroinated compounds.[88] The influence of methylene groups and fluroalkyl groups on behaviors of the side chain were further investigated by DSC experiments of the fluorinated alcohols. These alcohols were used to synthesis the methacrylates monomers to provide different fluorinated side chains .[89]

In general, liquid crystals such as the semifluorinated alcohols display four distinct phase regions upon heating: crystal, smectic B (S_B), smectic A (S_A), and isotropic (I). Depending on the different content of the fluroalkyl groups and methylene groups, either S_A, S_B or I phases existed.[89,90] The highly ordered smetic B mesophase is a solid-solid transition[91], also presented in thermographs of semifluorinated alkanes[92,93]. The melting peak was associated with phase transitions from S_B to S_A or crystal to S_A.

The ordered construction of semifluroinated segments of the polymers and the thermal behavior of fluorinated alcohols were determined by the architecture of the mesogen, the number of CF_2 groups and CH_2 groups. As shown in Figure 2.17, the DSC spectra of all fluorinated alcohols demonstrated four phase transitions as the typical liquid crystal. Upon

heating, a crystallization peak of $C_4F_9(CH_2)_4OH$ was presented at lower temperature than the melting peak, indicating the reorganization of the crystal phase. The thermograph of $C_6F_{13}(CH_2)_2OH$ showed two melting peaks, associated with two possible crystalline phases. The thermographs of $C_4F_9(CH_2)_2OH$ was not complete due to the fast volatizing under higher temperature. In general, the melting temperature of the semifluorinated alcohols increased with the increasing length of methylene groups or perfluoroalkyl group. All the melting temperatures for the partially fluorinated alcohols were below zero, except for $C_8F_{17}(CH_2)_2OH$. The molecules of $C_8F_{17}(CH_2)_2OH$ even displayed a melting temperature as high as 45 ^oC. Therefore, only the smetic B phase of $C_8F_{17}(CH_2)_2OH$ was thermally stabile at higher temperatures.

For semifluorinated alcohols with less than six perfluoromethylene, only S_A phases existed at higher temperatures. And the exposed perfluoro groups possessed a high mobility due to the high degree of freedom from S_A liquid phases. A surface in S_A phase region will reconstruct and reorientate after the liquid recedes, resulting in the high contact angle hysteresis. In contrast, semifluorinated chains with more than eight fluromethylene which had a highly ordered S_B phase can form a nearly uniform close packing of $–CF_3$ on the topmost surface region. Hence, polymers with $C_8F_{17}(CH_2)_2–$ mesogen provides high resistance to water and oil, along with a low hysteresis. This demonatrated that the high thermal stability of S_B phase of these alcohols was the key factor leading to the side chains crystallization. Kramer and coworker also studied the unique mesophase S_B in fluorinated block polymers and attributed the high stability of this phase to high enthalpy needed for destroying the ordered structure.[94]

The mixing temperature for the transitions from S_B to I is regarded as an indication of

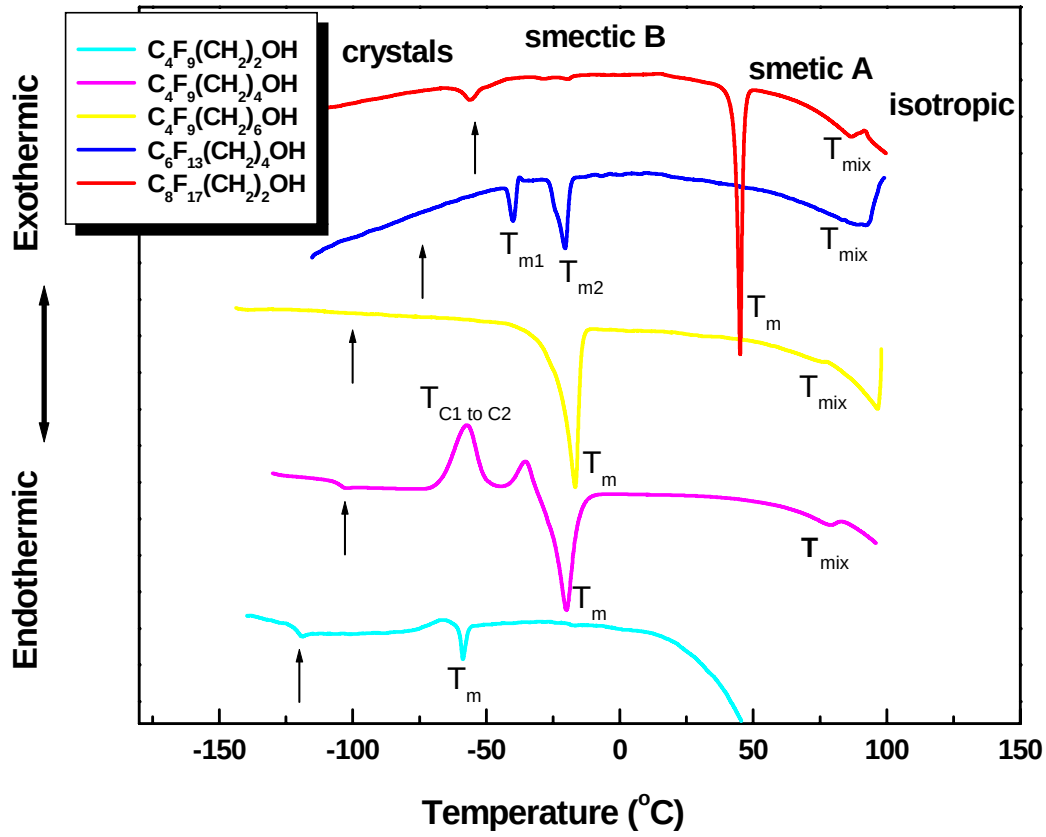

Figure 2.17 DSC thermographs of different semifluorinated alcohols $C_4F_9(CH_2)_2OH$, $C_4F_9(CH_2)_4OH$, $C_4F_9(CH_2)_6OH$, $C_6F_{13}(CH_2)_4OH$ and $C_8F_{17}(CH_2)_2OH$.

the vanishing of microphase separations between hydrocarbon regions and fluorocarbon regions.[77] As illustrated in Figure 2.17, the increase of methylene or fluoroalkyl repeating units slightly enhanced the microphase separation process, due to the increase of the enthalpy for mixing of fluorinated domains and hydrocarbon domains.

II-5 Conclusions and future directions

Short chain perfluorinated carboxylic and sulfonic acids containing a chain of four or less perfluorinated carbon atoms do not bioaccumulate. In order to find environmentally benign and nontoxic alternative fluoropolymers to avoid the challenges associated with PFOA, new fluorinated polymers containing perfluorobutyl side chains have been successfully prepared starting from perfuorobutyl iodide. Structures of the monomers and polymers have been confirmed by ^{1}H and ^{19}F NMR.

All the C4 polymers were hydrophobic and oleophobic with low free surface energies ranging from 10 to 18 mN / m. The static contact angles of C4 materials were 106 - 110^{o} against water, and 60 - 70^{o} against hexadecane, respectively. The contact angle hysteresis of C4 methacrylates was 40 degree in both water and hexadecane. The C4 styrene displayed a much lower hysteresis of 20 degree.

The surface properties of the polymers could be controlled by varying the “spacer” of the side chains, which were functional groups between the polymer backbones and the perfluorinated parts of the side chains. The major results for the relationship between compositions of side chains and surface properties of C4 materials can be summarized as follows.

1) The methylene spacers of C4 materials displayed weak influence on the surface

properties. Spacers as long as six methylene groups were not long enough to undergo side chain crystallization. On the uppermost surface of the C4 methacrylates, the $–CF_3$ groups distributed randomly and re-orientated after receding liquid lines.

2) The introduction of phenyl ring as the spacer improved of dynamic performance in water. These bulky groups interfered with the movement and reconstruction of the side chains. In addition, the low hysteresis of C4 styrene could be attributed to the absence of the –C=O groups, which avoided the formation hydrogen bonding with polar solvents such as water.

3) Varying the length of the perfluoroalky units and hydrocarbon units of semifluorinated alcohols gave rise to different liquid crystallization phases. The surface properties of the polymers synthesized with these alcohols were determined by thermal stability of the smetic B phase of the alcohols.

The synthesis and characterizations of new non-biopersistent materials in this chapter laid the ground work for many future directions.

1) The surface orientation was only observed under the dry state. The reorientation of the wet polymer surfaces after the receding liquid could be observed by XPS or NEXAFS equipped with a cold stage. This observation will help us to better understand the influence of the bulky phenyl ring spacer.

2) The textile treating agents are most of fluorinated copolymers with side chain cross-linking agents. [37] The introduction of the side chain crosslinker as the second or third co-monomers would help to immobilize the perfluoro groups on the surface and improve the dynamic performance in liquid, in addition to

benefit the durability of the textile.

3) The new monomers can be designed and synthesized based on the current results of C4 polymers with methylene spacers or phenyl ring spacers. For example, two tentative schemes are proposed here in order to increasing the fluorine moiety of the polymer side chains.

(A) Different telomers

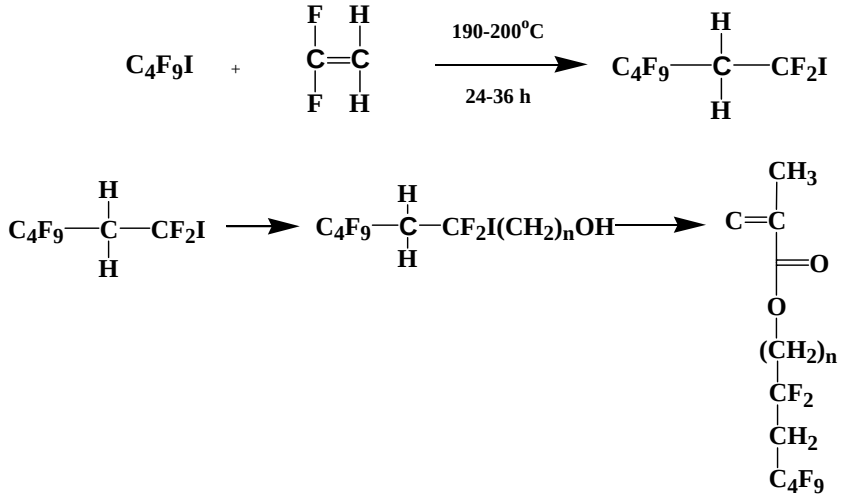

The fluorine content of the side chains increases, though the largest perfluorocarbon number of side chains is still lower than four.

(B) Styrene based monomer

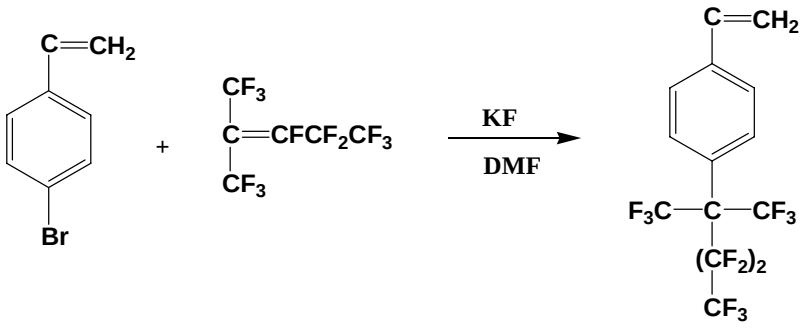

The branching of the fluorinated side chains will increase the population of $-CF_3$ groups on the polymer surfaces.

II-6 References

(1) Kissa, E. *Functional Finishes, Part B, Handbook of Fiber Science and Technology*; Marcel Dekker: New York, 1984; Vol. II.

(2) Zisman, W. A. *Contact Angle, Wettability, and Adhesion*; American Chemical Society: Washington DC, 1964; Vol. 43.

(3) Owens, D. K.; Wendt, R. C. *Journal of Applied Polymer Science* **1969**, *13*, 174.

(4) Fowkes, F. M. *Journal of Physical Chemistry* **1962**, *66*, 382.

(5) Fowkes, F. M. *Journal of Physical Chemistry* **1963**, *67*, 2538.

(6) Bernett, M. K.; Zisman, W. A. *Journal of Physical Chemistry* **1960**, *64*, 1292.

(7) Bernett, M. K.; Zisman, W. A. *Journal of Physical Chemistry* **1962**, *66*, 1207.

(8) Owens, M. J. *Comments of Inorganic Chmistry* **1988**, *7*, 195.

(9) Kissa, E. *Fluorinated Surfactants and Repellents*; Marcel Dekker: New York, 2001.

(10) Safrin, E. G.; Zisman, W. A. *Journal of Physical Chemistry* **1962**, *66*, 740.

(11) Parsons, R. E. t. D.: U. S. Patent 3,234, 294, 1962.

(12) Parsons, R. E. t. D.: US Patent 3132,185, 1964.

(13) Renner, R. *Environmental Science and Technology* **2005**, *39*, 56A-57A.

(14) Renner, R. *Environmental Science and Technology* **2001**, *35*, 154 A-160A.

(15) Ellis, D. A.; Martin, J. W.; Silva, A. O. d.; Mabury, S. A.; Hurley, M. D.; Andersen, M. P. S.; Wallington, T. J. *Envrionmental Science and Technology* **2004**, *38*, 3316-3321.

(16) Renner, R. *Environmental Science and Technology* **2006**, *40*, 2083.

(17) Dinglasan-Panlilio, M. J. A.; Mabury, S. A. *Environmental Science and Technology* **2006**, *40*, 1447-1453.

(18) Renner, R. *Environmental Science and Technology* **2005**, *39*, 56A.

(19) Kannan, K.; Perrotta, E.; Thomas, N. J. *Environmental Science and Technology* **2006**, *40*, 4916-4921.

(20) akata, H.; Kannan, K.; Nasu, T. C.; Hyeon-Seo;; Sinclair, E.; Takemura, A. *Environmental Science and Technology* **2006**, *40*, 4916-4921.

(21) So, M. K.; Yamashita, N.; Taniyasu, S.; Jiang, Q.; Giesy, J. P.; Chen, K.; Lam, P. K. S. *Environmental Science and Technology* **2006**, *40*, 2924-2929.

(22) Rostkowski, P.; Yamashita, N.; So, I. M. K.; Taniyasu, S.; Lam, P. K. S.; Falandysz, J.; Lee, K. T.; Kim, S. K.; Khim, J. S.; Im, S. H.; Newsted, J. L.; Jones, P. D.; Kannan, K.; Giesy, J. P. *Environmental Science and Technology* **2006**, *25*, 2374-2380.

(23) Daoud, W. A.; Xin, J. H.; Tao, X. *Journal of the American Ceramic Society* **2004**, *87*, 1782-1784.

(24) Grajeck, E. J.; Peterson, W. H. *Textile Research Journal* **1962**, *32*, 320.

(25) Yoerger, W. E.; McCabe, J. M.; Wright, J. F.: US 3859090 19750107, 1975; p 14.

(26) Pentz, L.: US 4070152 19780124, 1978.

(27) Koda, Y.; Ona, I.; Takeda, A.: US 4417024 A 19831122, 1983; p 5.

(28) Waratani, K.; Saito, Y.; Seki, M.; Asakawa, S.: JP 01143621 A2 19890606 Heisei., 1989; p 4.

(29) Ono, I.; Uehara, H.; Ichinohe, S.: Jpn. Kokai Tokkyo Koho JP 06271679 A2 19940927 Heisei., 1994; p 7.

(30) Kobayashi, H.; Masatomi, T.: Jpn. Kokai Tokkyo Koho JP 09151357 A2 19970610 Heisei., 1997; p 7.

(31) Mignani, G.; Olier, P.; Priou, C.: PCT Int. Appl.WO 2000000559 A1 20000106, 2000; p 44.

(32) Sato, K.; Yamaya, M.; Asai, M.; Matsumura, K.: EP 1178071 A2 20020206, 2002; p 14.

(33) Scheirs, J. *Modern Fluoropolymers*; John Wiley & Sons, Ltd.: New York, 1997.

(34) Sianesi, D.; Pasetti, A.; Fontanelli, R.; Bernardi, G. C.; Caporiccio, G. *Chim. Ind.* **1973**, *55*, 208-221.

(35) Priola, A.; Bongiovanni, R.; Malucelli, G.; Pillicino, A.; Tonelli, C.; Simeone, G. *Macromol. Chem. Phys.* **1997**, *198*, 1893-1907.

(36) Jhon, M. S. *Advances in Chemical Physics* **2004**, *129*, 1-70.

(37) Yarbrough, J. C.; Rolland, J. P.; DeSimone, J. M.; Callow, M.; Finlay, J. A.; Callow, J. A. *Macromolecules* **2006**, *39*, 2521-2528.

(38) Rolland, J. P.; Dam, R. M. V.; Schorzman, D. A.; Quake, S. R.; DeSimone, J. M. *J. Am. Chem. Soc.* **2004**, *126*, 2322-2323.

(39) Rolland, J. P.; Hagberg, E. C.; Denison, G. M.; Carter, K. R.; DeSimone, J. M. *Angew. Chem. Int. Ed.* **2004**, *43*, 5796-5799.

(40) Messori, M.; Toselli, M.; Pilati, F.; Fabbri, P.; Pasquali, L.; Montecchi, M.; Nammarone, S.; Tonelli, C. *European Coatings* **2005**, *81*, 4-13.

(41) Barhlott, W.; Neinhuis, C. *Planta* **1997**, *202*, 1-8.

(42) Otten, A.; Herminghaus, S. *Langmuir* **2004**, *20*, 2405-2408.

(43) Patankar, N. A. *Langmuir* **2004**, *20*, 8209-8213.

(44) Marmur, A. *Langmuir* **2004**, *20*, 3517-3519.

(45) Oner, D.; McCarthy, T. J. *Langmuir* **2000**, *16*, 7777-7782.

(46) Chen, W.; Fadeev, A. Y.; Hsieh, M. C.; Oner, D.; Youngblood, J.; McCarthy, T. J. *Langmuir* **1999**, *15*, 3395-3399.

(47) Krupenkin, T. N.; Taylor, J. A.; Schneider, T. M.; Yang, S. *Langmuir* **2004**, *20*, 3824-3827.

(48) Quere, D.; Lafuma, A.; Bico, J. *Nanotechnology* **2003**, *14*, 1109-1112.

(49) Callies, M.; Quere, D. *Soft Matter* **2005**, *1*, 55-61.

(50) Quere, D. *Nature Mater.* **2005**, *1*, 14-15.

(51) Gao, L.; McCarthy, T. J. *Langmuir* **2006**, *22*, 5998-6000.

(52) Lei Zhang; Zhilian Zhou; Bin Cheng; Joseph M. DeSimone; Samulski, E. T. *Langmuir* **2006**, *22*, 8576-8580.

(53) Dams, R. In *14th European Symposium on Fluorine Chemistry*: Poznan, Poland, 2004; pp paper c-O-07.

(54) Huang, W. *Journal of Fluorine Chemistry* **1992**, *58*, 1-8.

(55) Huang, X.; Long, Z.; Chen, Q. *Journal of Fluorine Chemistry* **2001**, *111*, 107-113.

(56) Xiao, F.; Wu, F.; Shen, Y.; Zhou, L. *Journal of Fluorine Chemistry* **2005**, *126*, 63-67.

(57) Brace, N. O.; Van Elswyk, E. *Journal of Organic Chemistry* **1976**, *41*, 766-771.

(58) Leebrick, J. R.; Ramsden, H. E. *Journal of Organic Chemistry* **1958**, *23*, 953-956.

(59) Banks, A. R.; Fibiger, R. F.; Jones, T. *Journal of Organic Chemistry* **1977**, *42*, 3965-3966.

(60) Audenaert, F.; Elst, P. J. v. d.; Rolly, D. G.: EP 1 493 761 A1, 2005; p 24.

(61) Kostov, G.; Ameduri, B.; Boutevin, B. *Journal of Fluorine Chemistry* **2002**, *114*, 171-176.

(62) Guo, X.; Chen, Q. *Journal of Fluorine Chemistry* **1999**, *93*, 81-86.

(63) Wu, F.; Huang, W. *Journal of Fluorine Chemistry* **2001**, *110*, 59-61.

(64) Plenkiewicz, H.; Dmowski, W.; Lipinski, M. *Journal of Fluorine Chemistry* **2001**, *111*, 227-232.

(65) Dmowski, W.; Ignatowska, J. *Journal of Fluorine Chemistry* **2003**, *123*, 37-42.

(66) Dmowski, W.; Ignatowska, J.; Piasecka-Maciejewska, K. *Journal of Fluorine Chemistry* **2004**, *125*, 1147-1151.

(67) Guyot, B.; Ameduri, B.; Boutevin, B. *Journal of Fluorine Chemistry* **1995**, *74*, 233-240.

(68) Tsibouklis, J.; Graham, P.; Eaton, P. J.; Smith, J. R.; Nevell, T. G.; Smart, J. D.; Ewen, R. J. *Macromolecules* **2000**, *33*, 8460-8465.

(69) Lam, C. N. C.; Kim, N.; Hui, D. K., D. Y.; Hair, M. L. *Colloids and Surfaces A: Physicochemical and Engineering Aspects* **2001**, *189*, 265-278.

(70) Chibowski, E. *Advanced in Colloid and Interface Science* **2003**, *103*, 149-172.

(71) Johnson, R. E.; Dettre, R. H. *Surfactant Science*; Marcel Dekket: New York, 1997.

(72) Adamson, A. W.; Gast, A. P. *Physical Chemistry of Surfaces*; John Wiley and Sons: New York, 1993; Vol. 49.

(73) Genzer, J.; Sivaniah, E.; Kramer, E. J.; Wang, J.; Xiang, M.; Char, K.; Ober, C. K.; Bubeck, R. A.; Fischer, D. A.; Graupe, M.; Colorado Jr., R.; Shmakova, O. E.; Lee, T. R. *Macromolecules* **2000**, *33*, 6068-6077.

(74) Fischer, D. A.; Efimenko, K.; Bhat, R. R.; Sambasivan, S.; Genzer, J. *Macromolecular Rapid Communications* **2004**, *25*, 141-149.

(75) Saidi, S.; Guittard, F.; Guimon, C.; Geribaldi, S. *Journal of Polymer Science: Part A: Polymer Chemistry* **2005**, *43*, 3737-3747.

(76) Shimizu, T.; Tanaka, Y.; Kutsumizu, S.; Yano, S. *Macromolecules* **1993**, *26*, 6694-6696.

(77) Roussel, F.; Saidi, S.; Guittard, F.; Geribaldi, S. *The European Physical Journal E* **2002**, *8*, 283-288.

(78) Rossier, J.; Reymond, F.; Michel, P. E. *Electrophoresis* **2002**, *23*, 858-867.

(79) Luning, J.; Yoon, D. Y.; Stohr, J. *Journal of Electron Spectroscopy and Related Phenomena* **2001**, *121*, 265-279.

(80) Lau, Y. W.; Burns, C. M. *Journal of Polymer Science, Physical Edition* **1974**, *12*, 431.

(81) Honda, K.; Morita, M.; Otsuka, H.; Takahara, A. *Macromolecules* **2005**, *38*, 5699-5705.

(82) Hayakawa, T.; Wang, J.; Xiang, M.; Li, X.; Ueda, M.; Ober, C. K.; Genzer, J.; Sivaniah, E.; Kramer, E. J.; Fischer, D. A. *Macromolecules* **2000**, *33*, 8012-8019.

(83) Genzer, J.; Sivaniah, E.; Kramer, E. J.; Wang, J.; Korner, H.; Xiang, M.; Char, K.; Ober, C. K.; DeKoven, B. M.; Bubeck, R. A.; Chaudhury, M. K.; Sambasivan, S.; Fischer, D. A. *Macromolecules* **2000**, *33*, 1882-1887.

(84) Genzer, J.; Efimenko, K.; Fischer, D. A. *Langmuir* **2002**, *18*, 9307-9311.

(85) Stohr, J. *NEXAFS Spectrascopy*; Springer-Verlag: Berling, 1992.

(86) Bunn, C. W.; Howells, E. R. *Nature* **1954**, *174*, 549.

(87) Kirsch, P. *Fluoroorganic chemistry*; Wiley-VCH: Weinheim, Germany, 2004.

(88) Wang, J.; Ober, C. K. *Macromolecules* **1997**, *30*, 7560-7567.

(89) Vilalta, P. M.; Weiss, R. G. *Liquid Crystals* **1992**, *12*, 531-544.

(90) McGrath, K. J.; Weiss, R. G. *Journal of Physical Chemistry* **1993**, *97*, 11115-11121.

(91) Rabolt, J. F.; Russell, T. P.; Siemens, R.; Twieg, R. J.; Farmer, B. In *American Chemical Society, Division of Polymer Chemistry*; Polymer Preprints, 1986; p 1135.

(92) Mahler, W.; Guillon, D.; Skoulios, A. *Molecular Crystals and Liqud Crystals Letter* **1985**, *2*, 111.

(93) Viney, C.; Twieg, R. J.; Russell, T. P.; Depero, L. E. *Liquid Crystals* **1989**, *168*, 63.

(94) Wang, J.; Mao, G.; Ober, C. K.; Kramer, E. J. *Macromolecules* **1997**, *30*, 1906-1914.